JET-P(96)51

Many Authors

JET Papers presented at the 16th International Atomic Energy Agency Fusion Energy Conference (Montreal, Canada, 7-11 October 1996)

FEATURES OF JET PLASMA BEHAVIOUR IN TWO DIFFERENT DIVERTOR CONFIGURATIONS

The JET Team[1]
(presented by J Jacquinot)

JET Joint Undertaking,
Abingdon, Oxfordshire,
United Kingdom.

Abstract

Two pumped divertors have been installed and tested in JET under ITER relevant conditions. A closed divertor is found to increase the particle and impurity exhaust rate in agreement with code modelling. Excellent power handling is demonstrated allowing high current discharges with record stored energy (15 MJ) and quasi steady-state discharges with high fusion triple product (4×10^{20} m^{-3} s keV). The ITERH93-P confinement scaling law is confirmed over a broad range and a more favourable β scaling is found. No hysteresis is found in the H-mode power threshold. A data base of highly radiating discharges including impurity seeding describes the relationship between radiated power, impurity concentration and density.

First results of high performance with optimised magnetic shear are presented. Strong internal confinement barriers develop despite the relatively small input of toroidal momentum and particle fuelling from ICRH and NBI.

1. INTRODUCTION - JET, A FLEXIBLE FACILITY

The JET Joint Undertaking is an organisation involving the participation of 15 European countries with central funding from EURATOM. The JET machine [1] was designed with the essential objectives of obtaining and studying plasmas in conditions and dimensions approaching those required in a fusion power plant. In order to pursue new objectives, JET has been extended to the end of 1999 to make essential contributions to a viable divertor concept for ITER and carry out D/T experiments in an ITER-like configuration.

JET has considerable flexibility that allows the study of many different modes of operation. It can match ITER geometry and dimensionless parameters (except the normalised Larmor radius, ρ^*) and can study the effect of large variations around the ITER values. JET has operated at 6 MA in H-mode [2]. D/T plasmas were studied for the first time in 1991 [3]. In preparing for the forthcoming D/T phase (DTE1) to be carried out in early 1997, a closed circuit gas handling system is being commissioned with 3 g of tritium which will be increased to 10 g for the experiments. Remote handling of in-vessel components is an integral part of the programme and will be used for a divertor target exchange after DTE1.

JET has a coherent divertor programme which includes divertor model validation. The main thrust of the programme is to operate successively a series of single-null divertor configurations (Section 2) with increasing "closure", ie the fraction of recycled neutrals escaping from the divertor region is increasingly smaller. Retaining the neutrals in the divertor region leads to a higher density and lower temperature divertor plasma for a given scrape-off layer (SOL) power and

[1] See Appendix

mid-plane separatrix density. The pumping in the divertor region is therefore made easier. Target sputtering could be reduced (unless chemical sputtering is dominant) and the retention of impurities could be enhanced [4]. However, ELMs (Edge Localised Modes) could defeat some of the favourable features of closed divertors by producing strong interactions with plasma facing components outside the target plates.

The divertor programme includes the successive testing of three pumped divertors between 1994 and 1998 with the following sequence :

- in 1994-1995, Mk I: an open divertor requiring sweeping the heat load in the divertor region;
- in 1996-1997, Mk IIA: a moderately closed divertor with a large wetted area. This divertor can accommodate up to 40MW for 8s without sweeping. In Mk IIA, operation is possible on both the horizontal and vertical target plates. Mk IIA is compared with Mk I in Fig. 1; and
- in 1997-1998, Mk II GB: a closed gas box divertor configuration to be installed by remote handling after DTE1.

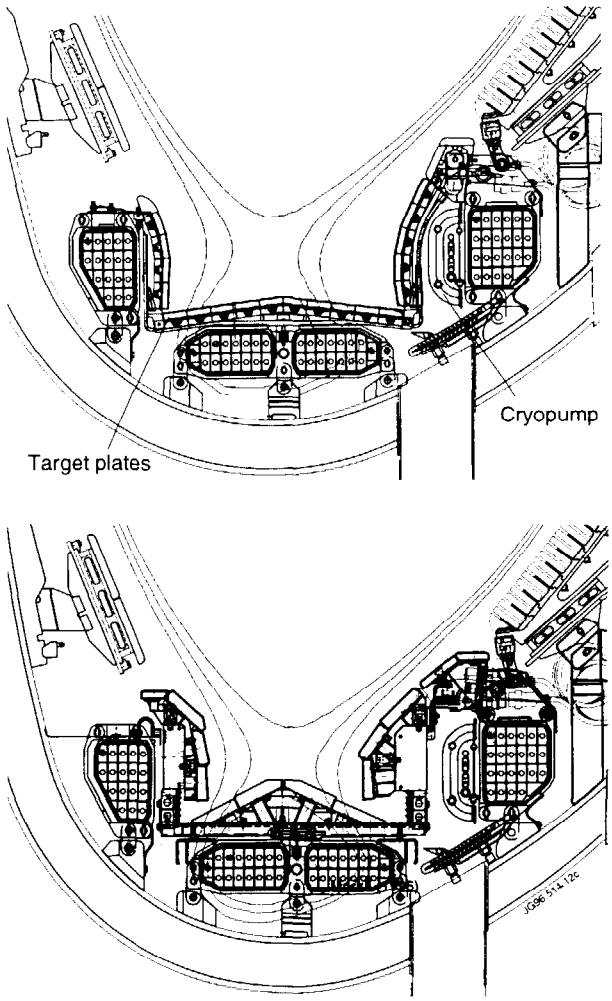

Fig.1 A view of the poloidal cross-section of the Mk I (top) and Mk IIA (bottom) pumped divertors.

Parameter	
Plasma minor radius, a (m)	0.95
Plasma half height, b (m)	1.75
Plasma major radius, geometrical centre, R_0 (m)	2.85
Plasma Volume (m^3)	85
Plasma aspect ratio, R_0/a	3.0
Plasma elongation, b/a	1.85
Toroidal magnetic field (at R_0), $B_{TO}(T)$	3.6
Flat top pulse length, t(s)	10 to 25
Plasma current, I_p (MA)	6.0
Transformer flux, f (Wb)	42
Neutral Beam power at 80 keV and 140 keV, (MW)	21
Ion Cyclotron power at 25 to 55 MHz, (MW)	17
Lower Hybrid power at 3.7 GHz, (MW)	7

TABLE I: JET parameters for Mk I and Mk II divertor experiments

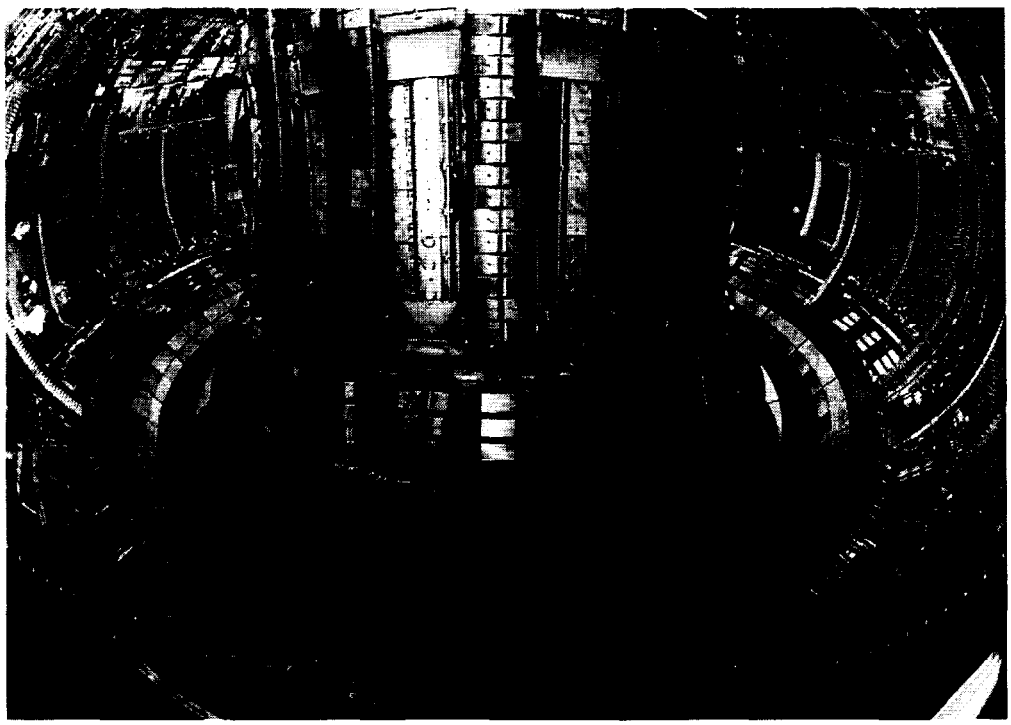

Fig.2 The interior of the modified JET in 1996 showing several important in-vessel components: four ICRH antennae each on the right and left, adjacent lower hybrid launcher on the right, a part of the saddle coils on the inner wall and the Mk IIA divertor on the floor.

The parameters of the JET tokamak are given in Table I. A view of the in-vessel components of JET at the restart of operation in 1996 is given in Fig.2 where some of the components such as the divertor target plates, ion cyclotron

resonance heating (ICRH) antennas and lower hybrid current drive (LHCD) launcher can be seen. The core and divertor plasma parameters are measured with an extensive set of instruments [5]. Specific Toroidal Alfvén Eigenmode (TAE) studies have been carried out [6] by exciting these modes using either in-vessel saddle coils or ICRF beat waves created by energising two antennas with a precisely controlled frequency difference. A new and entirely digital real time plasma position and shape control system [7] has been implemented providing greatly increased flexibility and accuracy. The JET control and data acquisition system is based on a network of dedicated minicomputers (in UNIX environment) which provide centralised control, monitoring and data acquisition on CAMAC and VME standards.

The support of the Vacuum Vessel has been fitted with hydraulic restraints in order to limit vessel displacements, in particular with regard to large sideways forces [8]. New instrumentation is available for measuring halo currents, forces applied to the vessel and the corresponding displacements.

Long pulse operation and scenario optimisation rely on the continuous development of the non-inductive current drive capability of JET which is based mainly on the LHCD system (3 MA has been driven) but also on the fast waves launched from the phased 4-strap ICRH antennas and the quasi-tangential neutral beam lines.

2. DIVERTOR PHYSICS ASPECTS

2.1 JET divertor configurations

X-point tiles fixed directly to the vacuum vessel were used in 1989-91 for H-mode studies in which the target to X-point distance was very small (< 10 cm). As a result, the screening effect of the divertor was mediocre at low divertor densities and a fraction of the impurity atoms sputtered from the target plates could go directly into the main plasma. Furthermore, the divertor plasma was not fully opaque to impurity and hydrogenic neutrals. This was partly beneficial since neutrals could re-enter the SOL well upstream and increase the flow over a significant part of the SOL [2]. However, these neutrals also led to increased impurity influxes by charge exchanged neutral sputtering. The duration of high performance discharges was often limited, ultimately, by a strong influx of carbon impurities, the so-called "carbon bloom". Energies of only about 15 MJ could be conducted to the target plates.

The relatively open Mk I divertor and in-vessel cryopump were installed for JET operation during 1994-95 (Fig.1). For high power handling, the magnetic configuration was swept (4 Hz) horizontally with the help of the in-vessel divertor coils. This allowed energies in excess of 180 MJ (CFC-tiles) and 120 MJ (beryllium tiles) to be conducted to the tiles without significant sublimation or melting occurring [2]. The carbon blooms which previously terminated high performance discharges were avoided. Operation with plasma currents up to 6 MA was possible, the plasma stored energy reached 13.5 MJ and the maximum D-D neutron rate was 4.7×10^{16}/s. A range of divertor physics experiments was conducted with high power (up to 32 MW) and steady-state H-mode plasmas with a radiative divertor using N_2 as the seeded impurity were studied.

The Mk IIA divertor presently used in JET is a moderately closed divertor consisting of a continuous water-cooled divertor structure about 6 m in diameter and weighing about 7 tonnes. It was installed to an alignment accuracy of 1 mm and its replacement is compatible with remote handling. The increased wetted area leads to a power handling capability which is a factor of 3 - 5 better than Mk I. Operation is carried out on both the horizontal and vertical target plates, permitting a comparison of results on impurity retention and neutral recycling, and on the orientation of the target plates both with and without pumping

provided by the cryogenic pump. An extensive experimental campaign has been carried out with this divertor with plasma currents up to 5 MA and energies up to 150 MJ have been accommodated by Mk IIA without producing excessive impurity influxes. A number of configurations such as Standard Fat, Super Fat, High Flux Expansion, Vertical Plate and High X-point (to simulate Gas-Box type) configurations have been used with low (0.18) and high (0.32) triangularity plasmas.

2.2 Regimes of divertor operation

2.2.1 The low recycling regime is characterised by a low temperature gradient (target-upstream), reduced particle flows to the target and low density in the divertor and is required by scenarios providing the highest fusion performance (albeit transiently). The performance increases as the duration of the ELM-free period is increased by reducing the recycling (extensive wall conditioning, use of the cryopump, and use of target plate material such as beryllium and/or beryllium evaporation).

2.2.2 The high recycling regime is characterised by a high density at the target and a high parallel flow of ions to the target helps to retain impurities in the divertor by friction. The radiated power fraction is moderate and it is mostly confined to a narrow region close to the target. This could lead to a high power density at the target and excessive erosion. ITER has therefore also considered a "gas box" design [9] in which the radiation losses in the divertor are enhanced and the exhaust power is distributed over a larger sidewall area of a deep divertor via charge exchange and radiation losses. The target geometry is tailored to enhance this effect and the divertor is relatively closed. Hydrogenic and impurity neutrals are required to recirculate within the divertor region and the loss of these neutrals to the main chamber is minimised with the help of the divertor cryopump. However, flows from the main plasma to the X-point are reduced and this may adversely affect impurity control.

Code calculations at JET and elsewhere show that hydrogenic plasmas cannot radiate sufficiently for the plasma to be extinguished before reaching the target. To achieve this "fully detached" regime, in which the energy reaching the target is negligible, impurity seeding is needed to increase the radiative losses. In experiments at JET with Mk I and Mk IIA, detached plasmas obtained by seeding N_2 in the divertor region have been obtained with up to 80 % of the power being radiated [10]. The plasma then becomes detached as evidenced from the ion saturation current characteristics measured by Langmuir probes in the divertor region. The plasma remains stable, but the continued increase in radiation causes the radiation peak to move from the target plates to the X-point and leads ultimately to a radiative collapse in which the whole plasma surface radiates.

2.3 Differences in performance of Mk I and Mk IIA

2.3.1 Detachment is defined to occur when the ion flux (ion saturation current measured by Langmuir probes) to the target starts to decrease when the density is increased by gas fuelling. In agreement with code calculations, it is found [11] that detachment in L-mode occurs at a factor of 2 lower density in Mk IIA than in Mk I because the increased closure in Mk IIA permits a higher divertor density for the same mid-plane density. H-mode data has not been obtained as the probe characteristics are strongly perturbed by the ELMs.

2.3.2 Neutral particle compression. The loss of hydrogenic and impurity neutrals from the divertor into the main chamber increases the neutral pressure in the main chamber and adversely affects the H-mode power threshold, deteriorates H-mode confinement, and increases the release of impurities from the main

chamber walls by charge exchanged neutral sputtering. Neutral particle retention in the divertor (or closure of the divertor) is important and is generally expressed as a compression ratio between the neutral particle fluxes in the divertor and the main chamber using calibrated hot-ion cathode gauges and D_α measurements. It is found that the compression ratio is higher by a factor of 2 - 2.5 in Mk IIA than Mk I. Particle removal with the cryopump is similarly increased. This result has been confirmed by the measurement of the decay time of injected Neon which is found to be a factor 2 to 4 greater in Mk I (Fig.3).

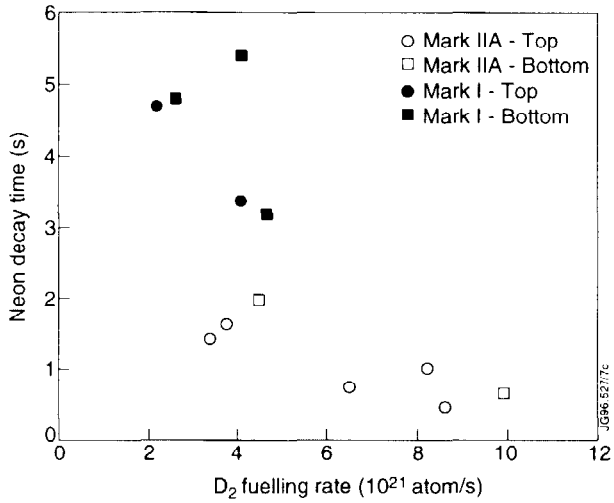

Fig. 3 A comparison of neon decay time as a function of D_2 fuelling rate in Mk I and Mk IIA divertor in neon puff experiments. Top and bottom refer to D_2 fuelling in the main chamber and in divertor respectively.

2.4 Modelling

The multifluid plasma code EDGE2D/U coupled to the Monte Carlo neutral particle code NIMBUS has been used at JET to simulate and compare the modelled and experimentally measured divertor performance. The codes calculate the distribution of deuterium and impurity density, temperature and flow, and other quantities corresponding to measurements such as the ion saturation current density (measured by probes at the divertor target), D_α and bremsstrahlung radiation signals, and the impurity and deuterium radiation power densities. The basic equations include classical (collisional) parallel (along the magnetic field lines) plasma transport for electrons, hydrogenic and impurity ions. Anomalous transport across the field lines is described by a simple prescription in which the transport coefficients are specified and generally taken constant across the SOL. The modelling of divertor plasmas has made good progress during the last few years, but there is still no satisfactory modelling of ELMy H-mode plasmas. The difficulty arises principally from the very large variations in density during and after an ELM and in periods between ELMs. Although between ELMs, the magnetic geometry is well defined, it can be strongly perturbed during the ELM itself. Modelling of long ELM-free H-modes as well as grassy ELMs in radiative H-mode plasmas has been successful since the variation in plasma parameters does not change appreciably on the short time scale.

Generally the modelling of tokamak plasmas treats the edge and core plasma separately, which often leads to artificial boundary conditions between the two regions. At JET, the transport codes describing the plasma core (JETTO) and the plasma edge (EDGE2D/U-NIMBUS) have been coupled using transport

coefficients and fluxes which allow self-consistent modelling [12]. A pinch term is found to be required in the edge transport to simulate the observed narrow SOL. This has allowed an ELM-free hot-ion H-mode to be modelled self-consistently and the results are given in Fig.4.

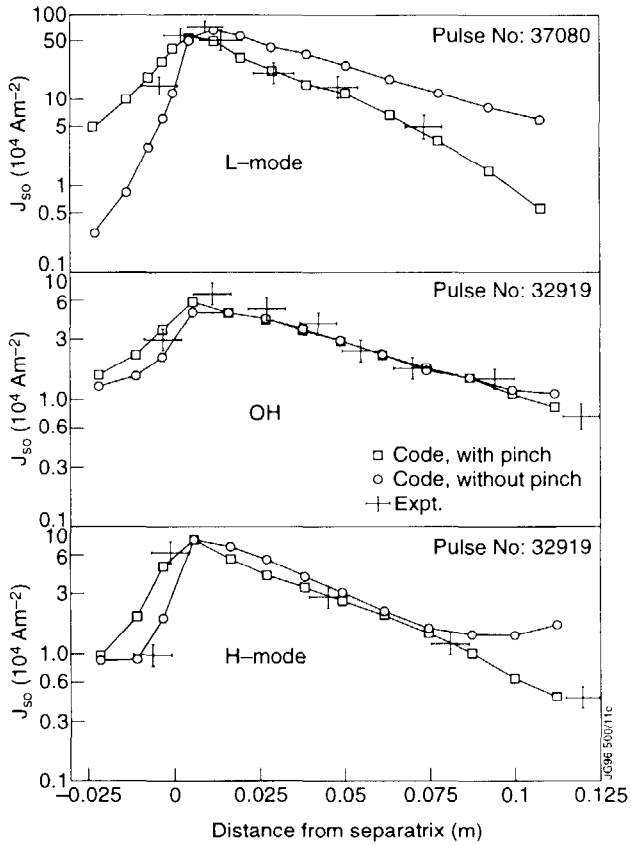

Fig.4 Measured ion saturation current density versus distance from the separatrix in the Mk IIA divertor in L-mode, OH and H-mode discharges is compared with code calculations with and without a pinch term.

An example of a JET L-mode discharge modelled with EDGE2D/U-NIMBUS is shown in Fig.5 [13]. The electron temperature and pressure drop is reproduced by the calculations which include radiation losses in the divertor and SOL.

3. CONFINEMENT ISSUES

3.1 ITER similarity experiments

The prediction of energy confinement in ITER is based on a confinement scaling (ITERH93-P) derived from a multi-machine data base of H-mode discharges. There is a need to confirm this scaling and improve its accuracy by conducting experiments in which dimensionless parameters describing the plasma are varied around ITER values. The most relevant variables are (i) normalised Larmor radius ρ^*, (ii) normalised collisionality ν^* and (iii) normalised plasma pressure β. The ITERH93-P scaling has been written in the dimensionless form as follows [14]:

$$B\,\tau_{ITERH93\text{-}P} \propto \rho^{*\,-2.7}\,\nu^{*\,-0.28}\,\beta^{-1.2} \qquad (1)$$

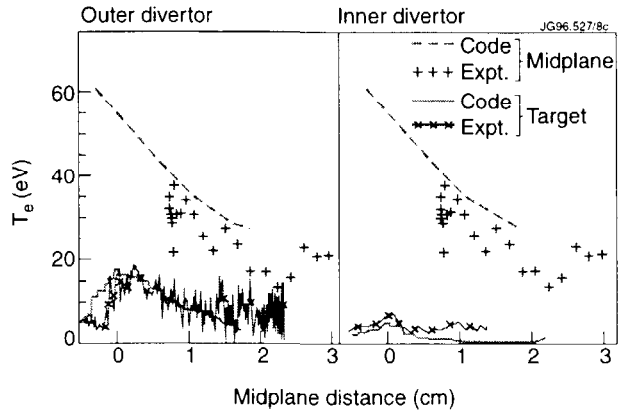

Fig.5 Measured and code calculated electron temperature profiles in the mid-plane and the divertor target for the inner and outer legs of the divertor in an L-mode discharge as a function of distance from the separatrix at the outer mid-plane.

where the parameters ρ^*, ν^* and β are defined in terms of their average values. Recently, careful experiments have been carried out in JET in which each of the three parameters was changed while keeping the other two fixed. Moreover, the power level was significantly above the H-mode threshold and producing type I discrete ELMs. It is concluded (Fig.6) that the dependence on ρ^* (close to gyro-Bohm) and ν^* is correctly described in the ITERH93-P scaling but the dependence on β is found to be very weak ie $\beta^{-0.05}$. It is suspected that the ITERH93-P scaling is based on data which includes some taken too close to the MHD β-limit. This new result on β scaling is more favourable and, if confirmed by other experiments, would increase the ITER confinement at ignition by 10 to 15 %.

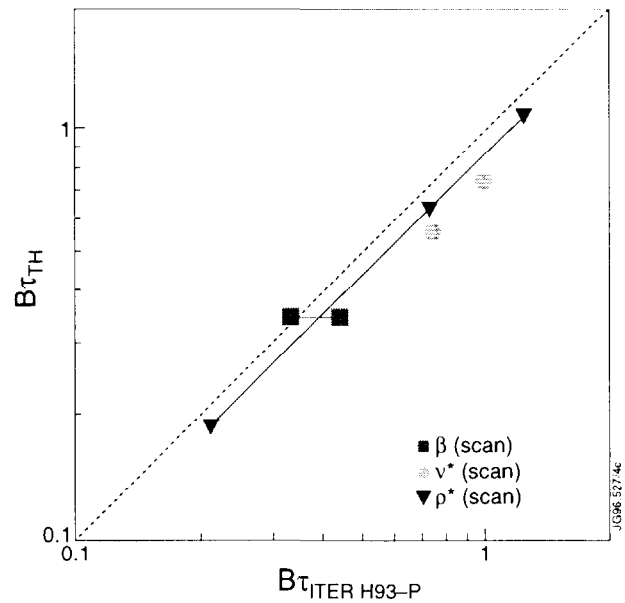

Fig.6 Normalised confinement time $B\,\tau_{th}$ is plotted as a function of $B\,\tau_{ITERH93\text{-}P}$ scaling for ρ^*, ν^* and β-scans. B represents the cyclotron frequency.

3.2 H-mode threshold

Existing H-mode threshold scalings have large data dispersion leading to uncertainty in the threshold: P_{th} = 50 - 200 MW in ITER at a density of

5 x 10^{19} m^{-3}. As the power threshold decreases with density, it is considered to enter the H-mode at low density (2-3 x 10^{19} m^{-3}) and then to increase the density progressively as the α-particle heating increases. The input power has to be somewhat higher than the power threshold, otherwise the confinement is insufficient. ITER ignition scenarios also depend on a possible hysteresis between H to L and L to H transitions. Although there is evidence of hysteresis in ELM-free H-modes, more recent experiments in JET [14] in ELMy H-modes indicate that there is essentially no hysteresis. This behaviour might be different in JET because of the high temperature walls and high pumping which are very effective at controlling recycling. The data on threshold power in Mk IIA can be described by $P_{th} \sim 0.3\ n_{20}\ B\ R^{2.5}$ (x 10^{20} m^{-3} T $m^{2.5}$) but data dispersion is still large, indicating that other aspects will have to be included for an appropriate description of the scaling. The threshold power was found to be independent of the type of additional heating (NBI or ICRH).

3.3 Effect of plasma configuration

The ELM behaviour in JET depends on plasma shape (triangularity), divertor magnetic configuration (high or low flux expansion), neutral recycling in the divertor and in the main chamber, and gas fuelling at the edge. High flux expansion with high triangularity, low recycling and no edge fuelling produces long ELM-free periods during which the confinement time increases continuously to 1.2 - 1.5 times ITERH93-P scaling. Figure 7 shows that, in steady-state discharges with constant power and fuelling, the ELM frequency decreases with increasing triangularity; on the other hand, the energy confinement appears to be independent of triangularity [11].

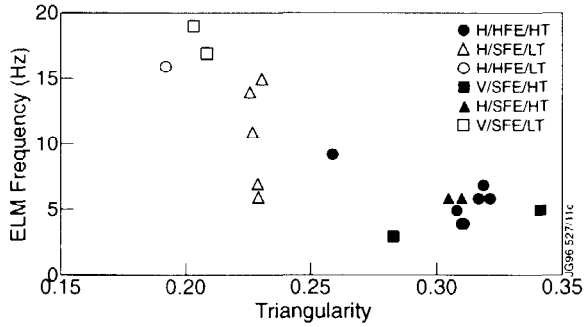

Fig.7 ELM frequency versus plasma triangularity for 2.5 MA, 2.5 T discharges with 12 MW beam power. The notation for the plasma equilibria A/B/C indicates target orientation (H = horizontal, V = vertical), flux expansion (HFE = high, SFE = standard) and triangularity (HT = high, LT = low) respectively.

3.4 Highly radiative ELMy H-modes

Highly radiative plasmas reduce the heat load to the divertor target plates avoiding excessive erosion of the target. An example of a highly radiative divertor discharge [2] which was heated at a power level of 32 MW (17 MW of NBI and 15 MW of ICRH) is shown in Fig.8. Such a discharge was obtained by nitrogen injection to enhance radiation and indeed the radiated power fraction reached 70 % of the total input power. The density reaches steady-state and the H-mode quality factor relative to ITER89-P scaling is about 1.5.

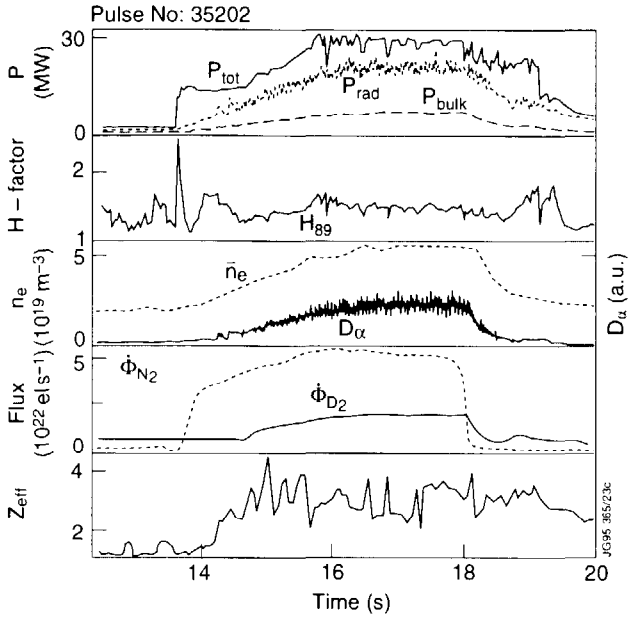

Fig.8 Time traces of an H-mode discharge with 30 MW of combined ICRF and NB heating and more than 70 % of the power is exhausted by radiation from seeded nitrogen.

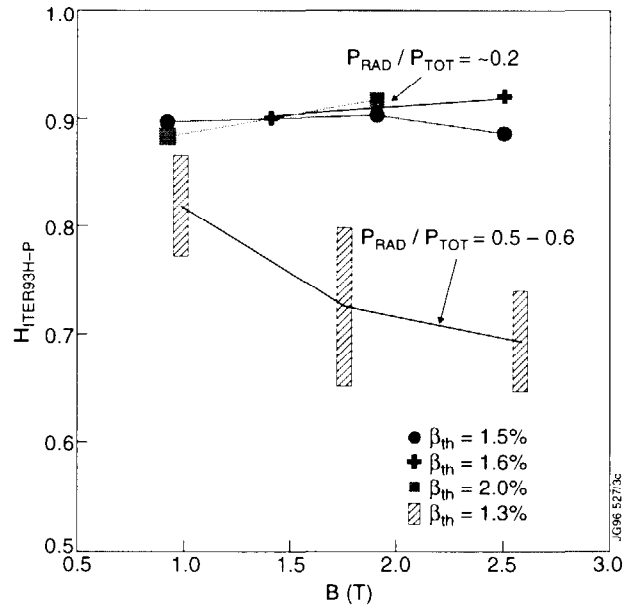

Fig.9 Confinement (normalised to ITERH93-P) versus toroidal field B in discharges with low and high radiated power fractions. Confinement degrades with radiation and loses gyro-Bohm scaling.

The confinement quality degrades progressively with increasing radiation and impurity concentrations in the main plasma can be high if the plasma density is too low. When the radiated power fraction is larger than 0.5, the confinement scaling is seen to become worse than gyro-Bohm scaling (Fig.9, [15]). A multi-machine size scaling for Z_{eff} in radiating divertor plasmas has been established so that a value for ITER can be predicted. The data from various divertor tokamaks

world-wide is included with the proviso that discharges have a radiated power fraction larger than 50 %. The following scaling best represents the data [16]:

$$Z_{eff} = 1 + 5.6\ P_R\ Z^{0.19} / (< n_e >^{1.95}\ S^{1.03}) \qquad (2)$$

where P_R (MW) is the radiated power, S (m^2) is the plasma surface area, $< n_e >$ (10^{20} m^{-3}) is the line averaged density and Z is the atomic number of the seeded impurity. The Z_{eff} data obtained with the Mk I and Mk IIA divertors of JET are plotted as a function of this scaling as shown in Fig.10. The value of Z_{eff} predicted for ITER in such highly radiating discharges (85 %) and $< n_e > = 1.2 \times 10^{20}$ m^{-3} would be about 1.6. According to this scaling, ITER would have a tolerable impurity level. There is a clear need to increase the data set with data obtained in other divertor configurations.

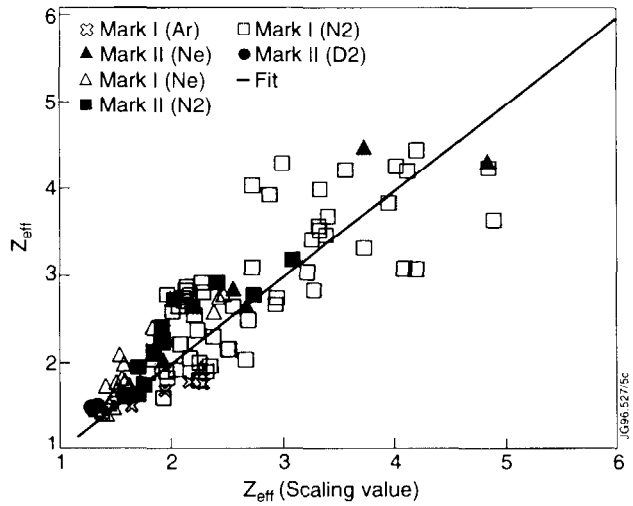

Fig.10 Measured effective charge (Z_{eff}) versus the scaling of Eq.(2) for a number of JET discharges in Mk I and Mk IIA with seeded impurity gas as indicated. The solid line is a fit to the data.

4. ENERGETIC PARTICLE EFFECTS

Alpha particles will be the dominant power source in ITER. Therefore, the confinement of the energetic α-particles and the impact on plasma performance are important issues. Moreover, any uncontrolled loss of α-particles either by collective instabilities such as Toroidal Alfvén Eigenmodes (TAE) or ripple induced losses could have serious consequences for the first wall.

4.1 TAE excitation

Global Alfvén eigenmodes can be excited by energetic particles such as fusion born α-particles, injected neutral beam ions or fast-ions accelerated by ICRH. In a reactor, the destabilisation of these modes can lead to a spatial redistribution or an enhanced loss of α-particles with the result that they may not fully heat the plasma. There are a variety of effects which can dampen the modes and both the driving and damping effects must be evaluated to assess the linear stability. External excitation of the modes has been done in two ways: (i) by saddle-coils mounted inside the vacuum vessel and (ii) by beat waves generated by two ICRH antennas run master-slave at slightly different frequencies (100 - 200 kHz at 50 MHz). A coherent detection of AEs in the magnetic, electron cyclotron emission or reflectometry diagnostics provides a means of determining

their damping rates. Measurements are made in the presence of a varying fast particle drive, such as 140 keV deuterium NBI, in order to resolve the differences in damping and driving rates of the mode. A feedback loop acting on the frequency of the exciter is used to track chosen eigenmodes during the discharge. Figure 11 shows such a real-time tracking of AEs [17] over a period of 2.5 s in which the frequency of the exciter oscillates around the mode frequency and provides a means of determining the damping rate as a function of time. Values of $\gamma / \omega = 0.55$ - 0.59 % are found, compared to the theoretical estimates of about 1 %. The application of high power NB heating appears first to dampen the n = 1 mode but later the phase resolved measurements by several MHD coils indicate that higher order modes up to n = ±20 start to grow at the AE frequency. These modes are routinely observed during hot ion H-modes with 140 keV NBI with $V_{||} = V_A / 3$ and could be responsible for limiting the fusion performance. Kinetic TAEs have been identified. Ballooning AEs have also been observed.

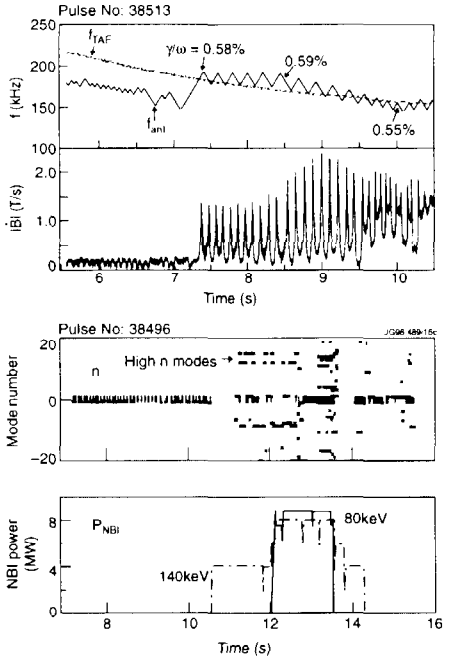

Fig.11 Tracking during the ohmic phase of TAEs (n = 1) excited by the saddle coils and high-n modes driven unstable at $V_A/3$ by high power 140 keV NB heating.

4.2 Confinement of fast ions

Ion cyclotron minority heating has been used previously in JET to produce 1 - 1.5 MeV He^3 ions with an energy content up to 2 - 2.5 MJ corresponding to almost 40 - 50 % of the total plasma energy of such discharges [18]. The suprathermal ion energy could be described by classical slowing down of the fast ions. Further studies have been carried out of central ICRF heating at the third harmonic of deuterium in JET where suprathermal effects are dominant and a very energetic tail is expected to develop that does not cut off until 4 MeV when the ion orbits reach the limiters. The deuterium neutron rate in these discharges is observed to reach a high value of 9 x 10^{15}/s due to the energetic deuterium tail. These results were well reproduced by PION code calculations, giving confidence in the understanding of the production and confinement of energetic tails [19].

4.3 Ripple experiments

The effect of toroidal field ripple on plasma behaviour and fast particle losses was studied with the Mk I divertor. The ripple was varied in the ITER relevant range of 0.1 to 2 %. Ripple induced losses of thermal and high energy particles (125 keV neutral beam ions and 1 MeV tritons) were less than 1 % and were consistent with theoretical estimates. However, the observed losses of particles of intermediate energy (thermal to tens of keV) were higher than predicted [2]. The slowing down of rotation due to ripple was also a notable result of these experiments.

5. HIGH PERFORMANCE AND STEADY STATE REGIMES

In preparing for the D/T phase, JET is pursuing two scenarios for high fusion performance: (i) hot-ion H-mode and (ii) optimised shear mode. Good fusion performance is also achieved in steady-state at high current (5 MA) in a regime directly relevant to ITER.

5.1 Hot ion H-mode

Traditionally "hot ion H-mode" refers to operation with strong neutral beam heating of a low electron density target plasma, with high triangularity (0.25) and high flux expansion in the divertor. Central NB power deposition and central fuelling produces a moderately peaked density profile. The neutral beam predominantly heats the ions and T_i exceeds T_e considerably (> 2 - 2.5) over the inner half of the plasma radius. The high performance lasts for about 2 s and is terminated either brutally or softly ("roll over") by a complex and largely unexplained event [20] involving (i) sawteeth or other internal MHD phenomena occurring in the central region, (ii) "outer-modes" occurring in the body of the plasma and (iii) "giant" ELMs at the plasma edge. The outer modes have now been identified by detailed soft X-ray measurements as ideal kink modes [20] and giant ELMs appear when the ballooning instability criterion is satisfied. The rollover in performance could be linked to the excitation of TAEs (Section 4.1) where the TAE resonance condition $V_{||} = V_A / 3$ for the 140 keV neutral beam is satisfied. Code calculations suggest that, at the resonance condition, sufficient beam ion redistribution within the plasma could account for the degradation in performance.

LHCD has been used to eliminate the sawteeth and to soften the effect of the outer modes but the performance is still limited at a normalised $\beta_N \approx 1.8$ well below the Troyon limit ($\beta_N = 2.8$). More recently, ICRH has been applied to hot ion H-modes [21]. The effect of the ICRH is shown in Fig.12. The addition of 6 MW of ICRH improves the rate of rise of the neutron rate, increases the stored energy by about 5 MJ and T_e by about 30 %. Therefore good confinement is maintained even when the power input to the electrons is substantially increased. A stored energy of up to 14 MJ was obtained with combined heating. Power step-down experiments allow the highest Q to be reached.

5.2 Discharges with optimised shear

Weak or reversed magnetic shear has been associated with improved core confinement since the JET experiments with deep pellet injection (PEP mode [22]). MHD instabilities like ballooning, resistive tearing and internal MHD modes are then stabilised provided that low rational values of q are avoided. Shear of plasma rotation (plasma flows) has also been shown by theory to stabilise microinstabilities involved in anomalous transport. In such a situation, an internal transport barrier can be established and the resulting steep ion temperature gradient produces more rotation shear.

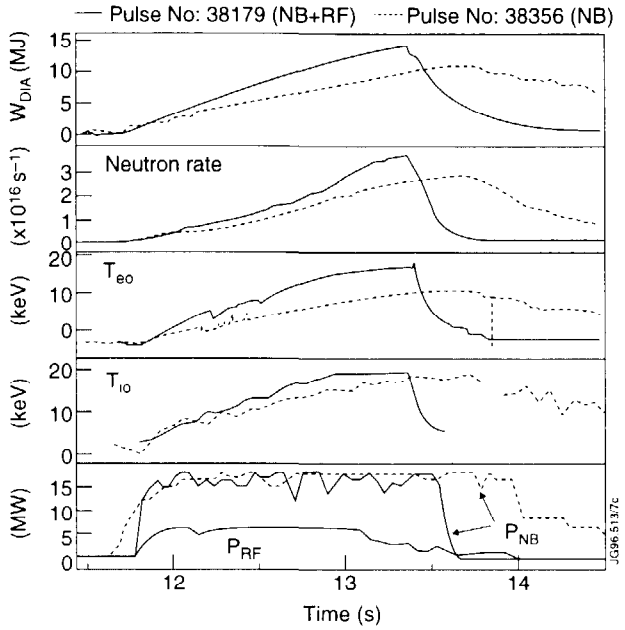

Fig.12 Time traces of NB heated hot ion H-modes with and without ICRH.

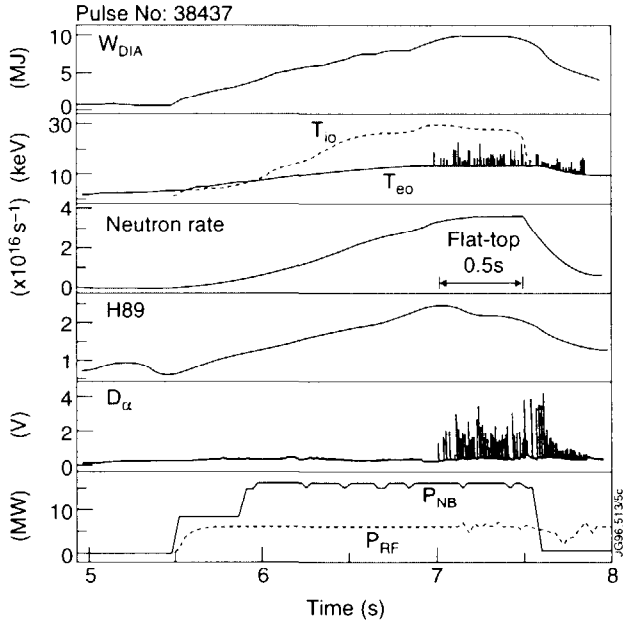

Fig.13 Time traces of a combined (NB + ICRF) heating optimised shear discharge giving enhanced core confinement. H89 refers to an improvement of confinement over the ITER89-P (L-mode) scaling.

In JET, optimised shear experiments [23] are carried out immediately after the current rise phase of the discharge where advantage is taken of the natural delay in the current diffusion to the plasma centre as the current is ramped up. The current diffusion can be further delayed by electron heating by ICRH. The target plasma has q > 1 everywhere. Neutral beams and ICRH are injected at optimised times in the low target plasma density. An example of time traces of such a high performance discharge is shown in Fig.13 where the maximum

neutron rate of 3.4 x 10^{16} /s is flat for ~ 0.5 s, the stored energy is 9.4 MJ and the peak T_e and T_i are 14 keV and 28 keV respectively. The q profile obtained from a combination of EFIT equilibrium code and Faraday rotation measurements shows that the magnetic shear in the core is weak and slightly positive just before and during the heating. Figures 14 and 15 compare the profiles of T_i, pressure P and rotation ω in the above two high performance modes. The internal confinement barrier corresponds to r/a ~ 0.55. The shear in plasma rotation is large at this location.

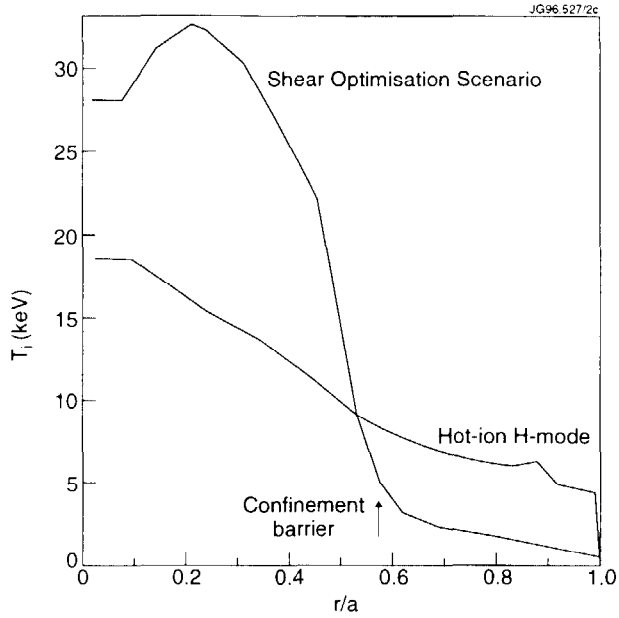

Fig.14 A comparison of typical ion temperature profiles in a hot ion H-mode and an optimised shear discharge.

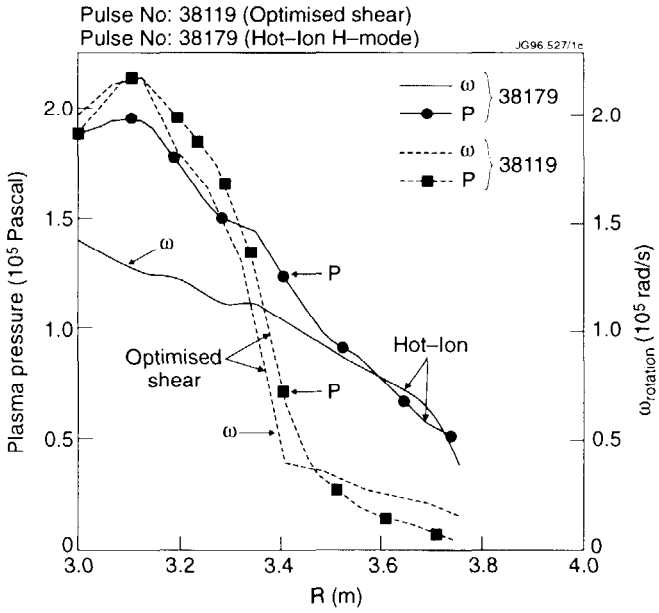

Fig.15 Profiles of total plasma pressure and poloidal rotation frequency in a hot ion H-mode and an optimised shear discharge.

5.3 High current plasmas and approach to steady-state

The combined advantages of the high power handling of Mk IIA, the divertor cryopump and the high recycling conditions established in the divertor enable the production of long pulse steady-state H-modes. ELMy H-modes of 20s duration at 2 MA were achieved in Mk I [24]. Recently, this regime has been extended to higher plasma currents (4.7 MA) and higher input powers with combined ICRH and NB heating. An example of a discharge at 4.7 MA is given in Fig.16 where a fusion triple product of 4 x 10^{20} (m^{-3} s keV) is maintained for 1.5s. This constitutes substantial progress from the best steady-state performance presented [24] at the 1994 IAEA Conference (2.65 x 10^{20} m^{-3} s keV). At higher power (28 MW), the plasma stored energy reached a new world record of 15 MJ. However, steady-state was not achieved in this case. The reasons for this are not clear. It should be noted that in these high current discharges the plasma density increases over several seconds and it is more difficult to maintain the input power above the H-mode power threshold.

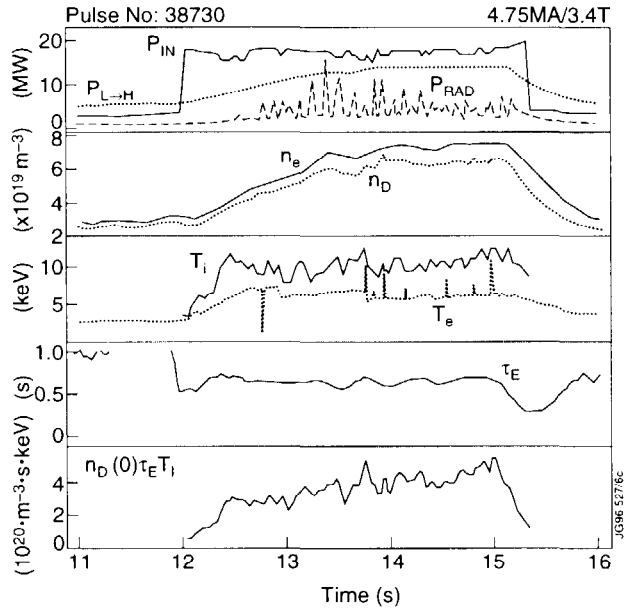

Fig.16 Time traces of a high power 4.7 MA discharge where the fusion triple product reaches a value of 4 x 10^{20} m^{-3} s keV. $P_{L\rightarrow H} \propto nBS$ represents an L- to H-mode threshold power scaling.

6. JET FUTURE PROGRAMME

In the present Mk IIA configuration the conductance of the "by-pass leak" between the divertor and the main torus chamber is comparable to the pumping rate of the cryopumps. These leaks reduce the neutral pressure in the divertor and increase it in the main chamber. They could contribute to the pollution of the main plasma and adversely affect the evaluation of the divertor performance such as the effect of pumping, gas fuelling at different locations within the divertor and seeding of N_2 impurity. The conductance will be reduced by a factor of 5 after a machine intervention in October 1996 to close the larger gaps.

Another divertor configuration is scheduled to be investigated in JET during 1997/98: the so-called Gas Box configuration which will simulate the presently chosen configuration for ITER. It has a large open region close to the target and a narrower entrance. The X-point is high to achieve the longest

divertor leg length adjacent to the region of free recirculation of neutrals from the target while minimising the escape of neutrals to the main chamber. Operation with Mk II GB would emphasise the divertor SOL plasma being extinguished (detached) before the target plates are reached. The target configuration can be changed from vertical to horizontal targets by removing parts of the tiles. The target tiles and the tile carriers are both fabricated from CFC and will be installed in JET by remote handling just after the DTE1 experiments.

D/T operation (DTE1) is planned to start on JET in early 1997. The effect of tritium on energy confinement and H-mode threshold will be assessed for the first time in an ITER-like divertor configuration. These experiments are also aimed at demonstrating long-pulse fusion power production with expected fusion power output in the range of 10 MW for several confinement times. A second period of high performance D/T operation (DTE2) is scheduled to take place in 1999. It will take advantage of a preceding period for optimising the operating modes and the in-vessel configuration. This period of D/T operation will also provide a full scale test of the technology of processing tritium in conjunction with an operating tokamak and the experiments will address α-particle heating and associated effects.

7. DISCUSSION AND CONCLUSIONS

JET has conducted a wide range of experiments in both an open and moderately closed divertor configuration. The issues of confinement quality, plasma purity and divertor operating conditions have been addressed and are reported in ten papers at this Conference. The excellent power handling of the Mk IIA divertor has been demonstrated and has allowed new performance developments including a record plasma energy of 15 MJ and a high fusion triple product in high current steady-state discharges.

Modelling of the particle and power exhaust in the divertor has progressed and describes the observations well, with the notable exception of discharges with large ELMs which are not presently taken into account accurately.

Long pulse ITER dimensionless conditions and type I ELMs satisfy the ITER confinement requirements. The ITERH93-P confinement scaling is confirmed over a broad range of parameters but the scaling with β is found to be more favourable. If this is confirmed on other experiments, the confinement time predicted for ITER should increase by about 10 to 15 %.

Confinement degrades in highly radiating discharges and Z_{eff} can be large in impurity seeded discharges at low density. Plasma purity is better at high density and a data base quantifies the expected plasma purity in ITER.

In addition to the hot ion H-mode, a second high performance regime has been developed in JET. It is based on optimising the plasma current profile. With low central magnetic shear and $q > 1$ everywhere in the plasma, internal confinement barriers are observed above a power threshold which is presently about 17 MW. This regime appears similar to that obtained with identical geometry in DIII-D. It is significant that the confinement barrier appears in JET despite a lower fuelling and toroidal momentum input in JET than in DIII-D.

D/T experiments will start in early 1997. The experiment will address the effect of tritium on energy confinement and H-mode threshold in an ITER-like divertor configuration.

ACKNOWLEDGEMENTS

The JET team wishes to acknowledge the collaborations with the European Institutions which were essential to the progress made throughout this research. The optimised shear experiments reported here were conducted in collaboration

with the DIII-D team (General Atomics, USA). The author wishes to thank Dr V Bhatnagar for the preparation and editing of this paper.

REFERENCES

[1] JET TEAM (presented by P.H. Rebut), in Plasma Physics and Controlled Fusion Research 1990 (Proc. 13th Int. Conf. Washington, 1990), Vol. 1, IAEA, Vienna (1991) 27.
[2] JET TEAM, Plasma Phys. Control. Fusion **37** (1995) A3.
[3] JET TEAM, Nucl. Fusion **32** (1992) 187.
[4] VLASES, G.C. and SIMONINI, R., in Controlled Fusion and Plasma Physics (Proc. 18th Eur. Conf. Berlin, 1991) Vol. 15C, part III, European Physical Society, Geneva (1991) 221.
[5] STOTT, P., paper presented at Fusion Technology 1996 (Proc. 19th Symp. (SOFT), Lisbon, 1996).
[6] FASOLI, A. et al., Nucl. Fusion **35** (1995) 1485.
[7] PUPPIN, S. et al., paper presented at Fusion Technology 1996 (Proc. 19th Symp. (SOFT), Lisbon, 1996).
[8] JET TEAM (presented by A. Tanga), IAEA-CN-64/AP1-18, this Conference.
[9] REBUT, P.H. et al., Fusion Eng. and Design **22** (1993) 7.
[10] JET TEAM, Plasma Phys. Control. Fusion **37** (1995) A227.
[11] JET TEAM (presented by G. Vlases), IAEA-CN-64/A4-1, this Conference.
[12] JET TEAM (presented by A. Taroni), IAEA-CN-64/D3-3, ibid.
[13] LOARTE, A., paper presented at 12th Int. Conf. on Plasma Surface Interactions, St. Raphael, France, 1996 (to be published in J. Nucl. Mater.).
[14] JET TEAM (presented by J.G. Cordey), IAEA-CN-64/A2-1, this Conference.
[15] JET TEAM (presented by D. Stork), IAEA-CN-64/A1-1, ibid.
[16] MATTHEWS, G.F. et al., paper presented at 12th Int. Conf. on Plasma Surface Interactions, St. Raphael, France, 1996 (to be published in J. Nucl. Mater.).
[17] JET TEAM (presented by D.F.H. Start), IAEA-CN-64/A2-6, this Conference.
[18] JACQUINOT, J. et al., Fusion Technology **21** (1992) 2254.
[19] N'GUYEN, F. et al., in Controlled Fusion and Plasma Physics (Proc. 22nd Eur. Conf. Bournemouth, 1995) Vol. 19C, part II, European Physical Society, Geneva (1995) 353.
[20] JET TEAM (presented by P.R. Thomas), IAEA-CN-64/A3-2, this Conference.
[21] JET TEAM (presented by P. Lomas), IAEA-CN-64/A1-5, ibid.
[22] HUGON, M. et al., Nucl. Fusion **32** (1992) 33.
[23] JET TEAM (presented by C. Gormezano), IAEA-CN-64/A5-5, this Conference.
[24] JET TEAM (presented by D. Stork), in Plasma Physics and Controlled Fusion Research 1994 (Proc. 15th Int. Conf. Seville, 1994), Vol. 1, IAEA, Vienna (1995) 51.

Appendix I

THE JET TEAM

JET Joint Undertaking, Abingdon, Oxon, OX14 3EA, U.K.

J.M. Adams[1], P. Ageladarakis, S.Ali-Arshad, B. Alper, H. Altmann, P. Andrew, N. Bainbridge, P. Bak[12], B.Balet, Y. Baranov[8], P. Barker, R. Barnsley[2], M. Baronian, K. Barth, D.V. Bartlett, A.C. Bell, E. Bertolini, V. Bhatnagar, A.J. Bickley, H. Bindslev, K. Blackler, D. Bond, T. Bonicelli, D. Borba, M. Brandon, P. Breger, H. Brelen, P. Brennan, W.J. Brewerton, M.L. Browne, T. Budd, A. Burt, P. Burton, T. Businaro, M. Buzio, C. Caldwell-Nichols, D.J. Campbell, D. Campling, P. Card, G. Celentano, C.D. Challis, A.V. Chankin, A. Cherubini, D. Chiron, J. Christiansen, P. Chuilon, D. Ciric, R. Claesen, H.E. Clarke, S. Clement, J.P. Coad, U. Cocilovo[10], I. Coffey[7], G. Conway[17], S. Cooper, J.G. Cordey, G. Corrigan, G. Cottrell, M. Cox[7], P. Crawley, R. Cusack, N. Davies, S.J. Davies, J.J. Davis, M. de Benedetti, H. de Esch, J. de Haas, E. Deksnis, N, Deliyanakis, E. di Marchi, A. Dines, S.L. Dmitrenko, J. Dobbing, N. Dolgetta, S.E. Dorling, P.G. Doyle, H. Duquenoy, A.M. Edwards[7], A.W. Edwards, J. Egedal, J. Ehrenberg, A. Ekedahl[11], T. Elevant[11], J. Ellis, M. Endler[13], S.K. Erents[7], L.G. Eriksson, H. Falter, J.W. Farthing, A. Fasoli[18], B. Fechner, M. Fichmüller, B. Fischer, G. Fishpool, C. Froger, K. Fullard, M. Gadeberg, L. Galbiati, E. Gauthier[3], R. Giannella, A. Gibson, R.D. Gill, D. Godden, A. Gondhalekar, M. Goniche[5], D. Goodall[7], C. Gormezano, C. Gowers, J. Graham, K. Guenther, R. Guirlet[3], H. Guo[22], A. Haigh, B. Haist[4], C.J. Hancock, P.J. Harbour, N.C. Hawkes[7], N.P. Hawkes[1], J.L. Hemmerich, T. Hender[7], J. Hoekzema, L. Horton, J. How, A. Howman, M. Huart, T.P. Hughes, F. Hurd, G. Huysmans, A. Hwang, C. Ibbott, C. Ingesson[15], B. Ingram, M. Irving, J. Jacquinot, H. Jaeckel, P. Jaeckel, J.F. Jaeger, O.N. Jarvis, F. Jensen, M. Johnson, E.M. Jones, L.P.D.F. Jones, T.T.C. Jones, J-F. Junger, F. Junique, A. Kaye, B.E. Keen, M. Keilhacker, W. Kerner, N.G. Kidd, Q.A. King, S. Knipe, R. Konig, J.G. Krom, H. Kubo[19], P. Kupschus, P. Lamalle[14], R. Lässer, J.R. Last, L. Lauro-Taroni, K. Lawson[7], M. Lennholm, J. Lingertat, A. Loarte, P.J. Lomas, M. Loughlin, T. Lovegrove, C. Lowry, A.C. Maas[15], B. Macklin, C.F. Maggi[16], M. Mantsinen[5], V. Marchese, F. Marcus, J. Mart, D. Martin, T. Martin, G. Matthews, H. McBryan, G. McCormick[13], G. McCracken, P.A. McCullen, A. Meigs, P. Miele, F. Milani, J. Mills, R. Mohanti, R. Monk, P. Morgan, D. Muir, G. Murphy, F. Nave[21], G. Newbert, P. Nielsen, P. Noll, W. Obert, D. O'Brien, E. Oord, R. Ostrom, M. Ottaviani, S. Papastergiou, V.V. Parail, R. Parkinson, W. Parsons, B. Patel, A. Paynter, A. Peacock, N. Peacock[7], R.J.H. Pearce, C. Perry, M.A. Pick, J. Plancoulaine, O. Pogutse, L. Porte, R. Prentice, S. Puppin, G. Radford[9], T. Raimondi, R. Reichle, V. Riccardo, E. Righi, F. Rimini, A. Rolfe, A. Rookes[17], R.T. Ross, A. Rossi, L. Rossi, G. Sadler, G. Saibene, M. Salisbury[12], A. Santagiustina, F. Sartori, R. Sartori, R. Saunders, P. Schild, M. Schmid, V. Schmidt, B. Schokker[15], B. Schunke, M. Scibile, S.M. Scott, S. Sharapov, A. Sibley, R. Simonini, A.C.C. Sips, P. Smeulders, O. Smith[12], P. Smith, R. Smith, F. Söldner, J. Spence, E. Springmann, M. Stamp, P. Stangeby[20], D.F. Start, D. Stork, P.E. Stott, P. Stubberfield, D. Summers, L. Svensson, P. Svensson, A. Tabasso[12], M. Tabellini, J. Tait, A. Tanga, A. Taroni, C. Terella, P.R. Thomas, K. Thomsen, B. Tubbing, Y. Ul'Haq[12], A. Vadgama, P. van Belle, R. van der Linden, G. Vlases, M. von Hellermann, T. Wade, R. Walton, D. Ward, M.L. Watkins, N. Watkins[1], M.J. Watson, J. Wesson, M. Wheatley, D. Wilson, T. Winkel, C. Woodward, D. Young, I.D. Young, Q. Yu[6], F. Zannelli, K-D. Zastrow, W. Zhang[12], N. Zornig, W. Zwingmann.

PERMANENT ADDRESSES

1. UKAEA, Harwell, Didcot, Oxon, UK.
2. University of Leicester, Leicester, UK.
3. CEA, Cadarache, France.
4. KFA, Jülich, Germany.
5. Helsinki University of Technology, Espoo, Finland.
6. Institute of Plasma Physics, Hefei, P R of China.
7. UKAEA Culham Laboratory, Abingdon, Oxon, UK.
8. A.F. Ioffe Institute, St. Petersburg, Russia.
9. Institute of Mathematics, University of Oxford, UK.
10. ENEA, CRE Frascati, Roma, Italy.
11. Royal Institute of Technology, Stockholm, Sweden.
12. Imperial College, University of London, UK.
13. Max Planck Institut für Plasmaphysik, Garching, Germany.
14. Plasma Physics Laboratory, ERM-KMS, Brussels, Belgium.
15. FOM Instituut voor Plasmafysica, Nieuwegein, The Netherlands.
16. Dipartimento di Fisica, University of Milan, Milano, Italy.
17. University of Saskatchewan, Saskatoon, Canada.
18. EPFL, Lausanne, Switzerland.
19. JAERI, Tokyo, Japan.
20. Institute for Aerospace Studies, University of Toronto, Canada.
21. LNETI, Savacem, Portugal.
22. INRS-Energieet Materiaux, Univ. du Quebec, Canada.

At July, 1996

OPTIMISATION OF JET STEADY-STATE ELMY DISCHARGES WITH ITER-RELEVANT DIVERTOR CONDITIONS

The JET Team[1]
(Presented by D Stork)

JET Joint Undertaking,
Abingdon, Oxfordshire,
United Kingdom.

Abstract

Experiments with the JET Mark IIA divertor involving optimisation of performance with gas fuelling are discussed. The development of plasmas in the Mark IIA configuration at high current ($\geq$ 4.5MA) and low q ($q_{95} \leq 2.6$) is presented. The results of a preliminary experiment to study the dimensionless (ρ^* and ν^*) scaling of energy confinement in impurity-seeded plasmas with high radiated power are discussed. It is found that the energy confinement is not consistent with gyro-Bohm scaling and does not follow the ITERH93-P scaling law for ELM-free plasmas.

1. INTRODUCTION

JET is now in the middle of a programme designed to investigate the effect of divertor geometry on plasma performance. The configurations studied so far are the Mark I (Fig.1(a)) and the Mark IIA (Fig.1(b)). This series will conclude with an ITER-specific "Gas Box" (Mark IIGB) in 1997/98. The programme follows a progressively more closed series of configurations. Each of the divertors uses a cryopump with a nominal pumping speed (deuterium) of $240 m^3 \cdot s^{-1}$.

Optimisation of plasma performance in steady-state ELMy H-mode discharges in the Mark IIA divertor has concentrated on the effect of changes in plasma configuration and fuelling. Changes in bulk plasma parameters (such as plasma triangularity) and in divertor closure-related parameters (such as magnetic flux expansion at the target) are covered in a related paper [1] which also addresses the behaviour of type I ELMs in the Mark IIA. The changes in plasma performance due to main species (D_2) fuelling are discussed in Section 2 below.

The steady-state ELMy H-mode is a candidate for production of high performance (in terms of stored energy and fusion yield) plasmas in the forthcoming deuterium-tritium experiments in JET (DTE1) scheduled for early 1997. The optimisation of this regime at high current ($\geq$ 4.5MA) and full field ($3.4 \geq B_T \geq 3.1$T) in JET involves plasma operation at low values of q ($q_{95} < 2.6$) where experimental input would provide useful information for ITER operation. The status of this work is described in Section 3.

The highly-radiating impurity-seeded divertor plasmas which were first studied in JET in the Mark I campaign [2] have been the subject of further study in Mark IIA [1]. An important issue is whether the confinement quality of these discharges, which is barely acceptable for ITER [1,2] is maintained as the dimensionless variables (ρ^* and ν^*) are increased towards the ITER range. Investigations into this topic in Mark IIA are described in Section 4.

[1] See Appendix to IAEA-CN-64/O1-4, The JET Team (presented by J Jacquinot).

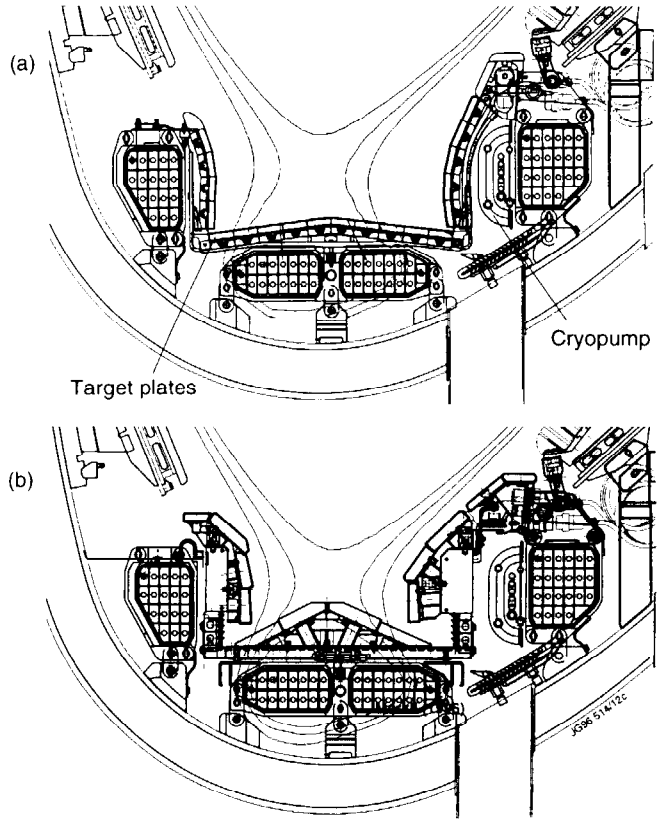

Fig.1 JET divertor geometries. (a) Mark I divertor (1994/95) (b) Mark IIA divertor(1996).

2. DIVERTOR PLASMA BEHAVIOUR WITH FUELLING VARIATIONS

2.1 Discharges with fuelling only from neutral beams

As with the Mark I divertor [3], steady-state discharges with Type I ELMs are routinely achieved in the Mark IIA divertor. The "natural" behaviour of discharges which are not fuelled by added gas, but only sustained by neutral beams and the input from edge recycling, has been extensively studied [1]. This natural behaviour can be summarised as follows:

- the type I ELMy H-modes have a similar confinement to Mark I plasmas with confinement enhancement (H_{93}) relative to the ITERH93-P ELM-free H-mode scaling of $0.9 \leq H_{93} \leq 1.1$ at plasma currents from 2.5-3.5MA;
- the discharges reach a steady-state density which for a fixed plasma configuration scales as

$$\langle n_e \rangle \propto \left(I_p \cdot P_{nbi}\right)^{0.5} / \pi a^2$$

  similar to the behaviour in Mark I but with a 15% lower density for similar configurations [4];
- the discharges have similar low fraction of radiated power (around 20% of input power) and moderate Z_{eff} (1.5-2.5). Z_{eff} is highest in discharges with higher triangularity, principally because of the reduced ELM frequency in such discharges [1]. Carbon is the predominant impurity.

2.2 Discharges with external deuterium gas fuelling

Heavy D_2 gas puffing (up to ~ 5 10^{22} atoms s^{-1}) has been applied to all the Mark IIA plasma configurations. The fuelling efficiency is lower than in Mark I. This is partly due to the fact that the rate of pumping in Mark IIA is higher than in Mark I [1], the Mark IIA geometry behaving as a moderate slot divertor by trapping the returning neutrals near the pumping ports.

The fuelling efficiency is found to be independent of the location of the gas feed. Fuelling in the upper vessel; in the private region; in the outboard midplane and at the inner and outer strike zones, all achieve the same asymptotic density for a given fuelling rate, plasma current and configuration.

As the fuelling is increased, the ELM frequency rises and the confinement begins to degrade [1]. The confinement degradation is correlated with an increase in the outer midplane pressure or outer midplane recycling, which rise due to the imperfect closure of the Mark IIA configuration. The same global behaviour was observed in Mark I [3,5]. The plasma density increases at first as fuelling is increased (Fig.2(a)) but eventually a maximum density is reached beyond which a further density rise is impeded because the ELMing rate continues to increase with increased fuelling and density is expelled. The maximum density is not accompanied by any dramatic fall in confinement (Fig.2(b)) which continues to decline slowly. The density limit appears to be related to poor fuelling efficiency as ionised neutrals are unable to convect into the plasma against the increasing ELM frequency. The limit is not associated with a disruptive or radiative collapse.

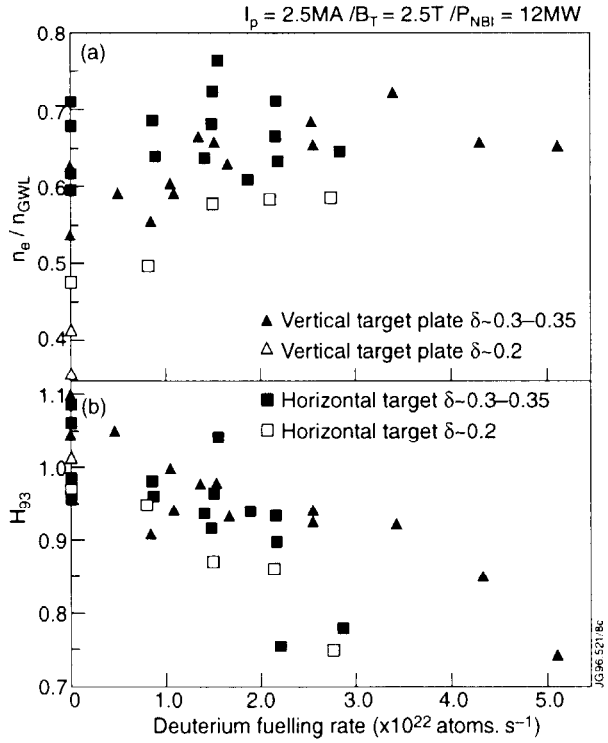

Fig.2 (a) Plasma density achieved (as a fraction of the Greenwald limit) against deuterium gas fuelling in the various Mark IIA configurations. (b) Confinement enhancement relative to the ITERH93-P scaling law (H_{93}) as a function of deuterium gas fuelling for the discharges in (a).

For all configurations, the plasmas with Vertical Target (VT) strike zone positions are most tolerant to high fuelling rates. They are able to maintain their

confinement at higher values of fuelling, and reach their maximum density at higher fuelling rates (Fig.2). Thus they sustain a higher radiated power fraction with a less strongly deteriorated confinement. The radiated power fractions in a fuelling scan on VT plasmas at 2.5MA/2.5T with fixed beam power are shown in Fig.3(a). The radiated power reaches ~ 45% of the input power and the increase in radiation with fuelling comes entirely from the divertor region. In a reactor plasma this would be beneficial for target loading and erosion. The plasma purity also increases steadily in this scan (Fig.3(b)) partly offsetting the decline in H_{93}.

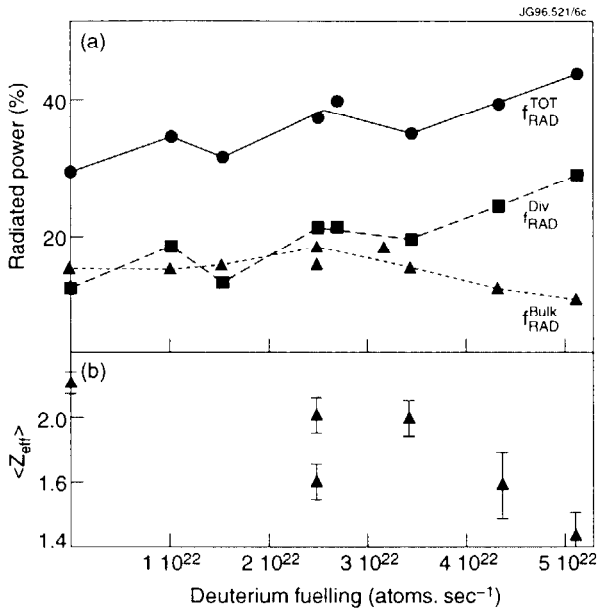

Fig.3 (a) Radiated power as a function of deuterium gas fuelling for the Vertical Target, higher triangularity discharges from the dataset in Fig.2. (Ip=2.5MA; B_T=2.5T; P_{nbi}=12MW). (b) Z_{eff} as a function of deuterium fuelling for the dataset of Fig.3(a).

The density limit in the Mark IIA configuration lies close to the Greenwald limit (Fig.4(a)). In contrast, with Mark I it was possible to exceed the Greenwald limit at low current (Fig.4(b)). There appears to be a trend towards a lower density limit as the divertor geometry becomes more closed. In the pre-1992 JET configuration with its open divertor, the Greenwald limit could be exceeded over a much larger range of I_p.

3. CONFINEMENT IN STEADY-STATE ELMY H-MODES AT HIGH CURRENT AND LOW q

ELMy H-modes lasting up to 10 energy confinement times have been obtained in diverted plasmas at plasma currents ≥ 4.5MA. An example of such a discharge is shown in Fig.5. Operation above 4.5MA in JET requires low q_{95} (≤ 2.5) as the toroidal field is presently limited to 3.4T. Thus optimisation of these plasmas is addressing a regime of particular interest to ITER.

It is found that energy confinement enhancement (H_{93}) does not degrade at low q in JET relative to the ITERH93-P law, but H_{93} in discharges with combined high current and low q (q_{95} ~ 2.4-2.5) is about 10% down on the mean values achieved at lower Ip. The energy confinement of ELMy H-modes with steady ELMy conditions lasting > $3\cdot\tau_E$ is shown in Fig.6 where H_{93} is plotted against q_{95}. The discharges above 4.5MA have a restricted triangularity range ($0.2 < \delta < 0.23$).

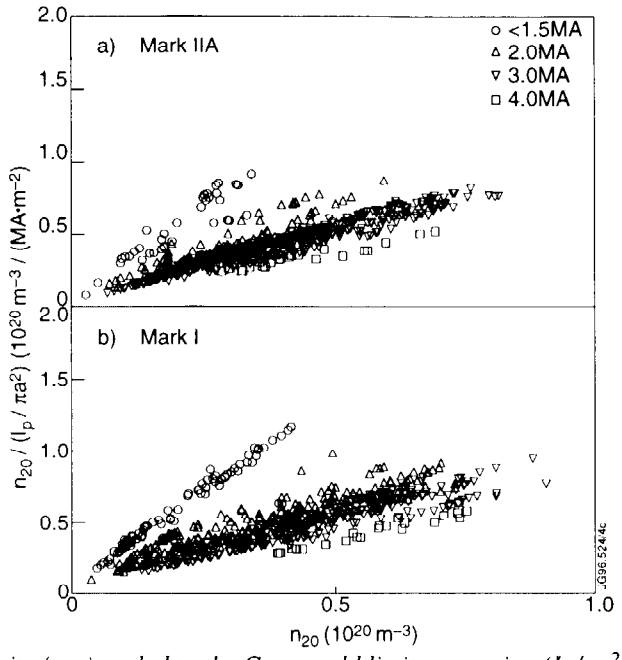

Fig.4 Plasma density (n_{20}) scaled to the Greenwald limit expression ($Ip/\pi a^2$) as a function of density and current for (a) Mark IIA plasmas; (b) Mark I plasmas.

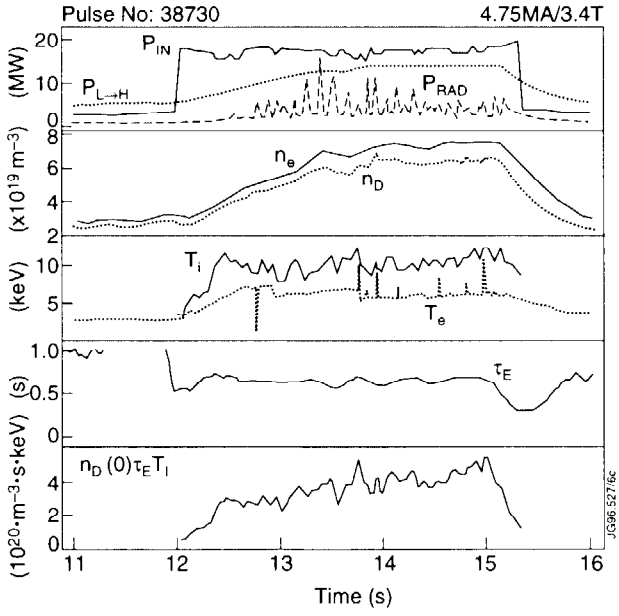

Fig.5 Time evolution of a steady-state type I ELMy H-mode at high current and low q (q_{95}~2.5).

Although good confinement can be achieved at low q, a significant number (~ 50%) of the ELMy H-modes produced at low q show a deterioration in confinement from one of two mechanisms.

i) Discharges with q_{95} ~ 2.4 are prone to the appearance of large n=2 MHD activity which, whilst the ELMy H-mode steady-state is maintained, leads to a loss of confinement by 10-15%. Examples of the steady-state confinement deterioration obtained are marked in Fig.6. It can be seen that

this is a low q rather than a high current phenomenon. These modes were present only rarely in Mark I. The nature of their appearance in Mark IIA is not yet understood, but the causal link with lack of confinement is clear.

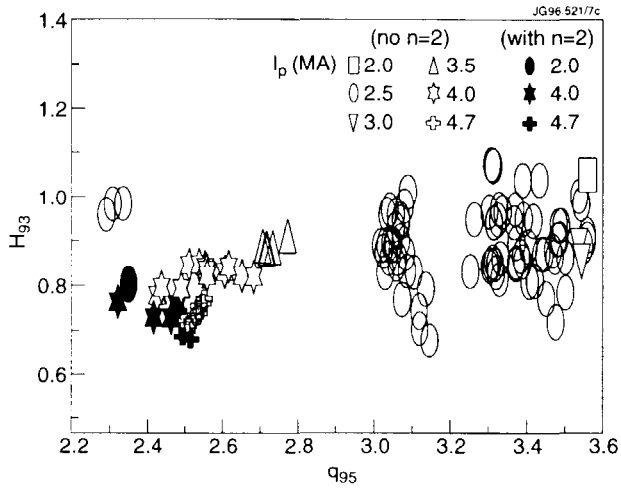

Fig.6 H_{93} as a function of q_{95} for steady-state ($\tau_H > 3 \cdot \tau_E$) ELMy H-modes. The solid symbols indicate discharges accompanied by strong n=2 MHD activity.

ii) Many discharges at $q_{95} < 2.6$ and $I_p > 4.0$MA suffer H-L transitions which occur randomly, frequently after many energy confinement times. A few of these discharges have input powers which are close to the L-H power threshold when bulk radiated power is subtracted. For the rest, the reverse transition occurs spontaneously and is accompanied by impurity influx and often by a slowly rotating or locked n=1 mode. These are generally thought to be effects of the loss of confinement rather than the causes. It is possible, at this early stage in the high current development, that the vessel has not been conditioned sufficiently for reproducible behaviour at high current and power.

Up to 25MW of combined heating power (17MW NBI and 8MW ICRF) has been coupled into JET plasmas at 4.7MA and 3.4T. The fusion triple product $n_D(o) \cdot \tau_E \cdot T_i(o)$ has reached ~ $4 \cdot 10^{20} m^{-3} \cdot s \cdot keV$ for three energy confinement times. Such plasmas would give a fusion amplification factor in D-T plasmas ($Q_{D\text{-}T}$) of around 0.25.

4. CONFINEMENT SCALING WITH DIMENSIONLESS PARAMETERS IN RADIATIVE DIVERTOR DISCHARGES

The scaling of energy confinement in discharges with a high fraction (> 50%) of radiated power, seeded by N_2 gas, has been studied in a series of plasmas which are dimensionally similar, except for the variation in normalised ion Larmor radius (ρ^*) and collisionality (ν^*). The aim of these experiments was to ascertain whether these ITER-relevant discharges are consistent with a gyro-Bohm scaling [6] such as ITERH93-P.

The time development of these H-mode discharges at 1MA/1T, 1.8MA/1.8T and 2.6MA/2.6T is shown in Fig.7. The discharges had the same q_{95} (=3.1), triangularity (δ ~ 0.3), minor radius, elongation and were all seeded by a mixture of N_2 and D_2 gas such that they reached a radiated power fraction ~ 60%. It can also be seen that they attained the same Z_{eff} of about 3.5. The input powers were adjusted such that the same thermal β_T was obtained (~ 1.3%). This involved scaling the input powers approximately as B^2. Due to the difficulty in adjusting the plasma density, ν^* was not kept constant from shot to shot, but varied by a

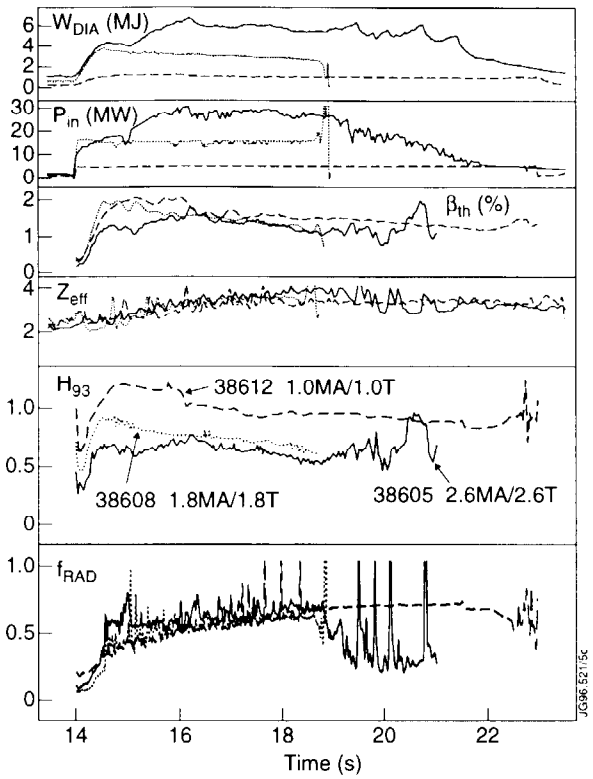

Fig.7 Comparative time evolution of stored energy; input power, thermal β; Z_{eff}; H_{93} and radiated power fraction for three discharges in the (ρ^*,ν^*) scan of radiative divertor plasmas.

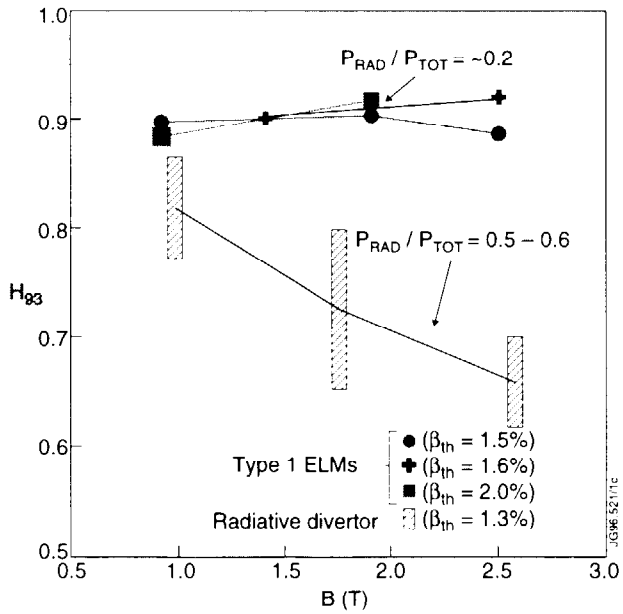

Fig.8 H_{93} as a function of toroidal field for the JET radiative divertor plasmas at similar (β, q, δ, κ, a, Z_{eff}, f_{RAD}). Also plotted are the type I ELMy H-modes from the ρ^* scan in JET (see [6]).

factor ~ 1.7. Since the collisionality scaling of ITERH93-P (gyro-Bohm like) and Bohm like scalings such as ITER89P are similar (~ $\nu^{*-0.3}$) the dataset should be capable of distinguishing the ρ^* scaling. The variation in ρ^* across the dataset is close to a factor 2.

It can be seen from the plot of H_{93} as a function of toroidal field in Fig.8 that confinement progressively decays relative to ITERH93-P as B increases. This is in contrast to the type I ELMy H-mode discharges in JET, which satisfy gyro-Bohm ρ^* scaling [6].

This data suggests that the radiative discharges are not consistent with a gyro-Bohm scaling law. Note also the tendency (Fig.8) for the confinement to approach the type I ELMy discharges at low toroidal field (higher ρ^*).

5. CONCLUSIONS

The scaling of density with power and current in ELMy H-modes in the Mark IIA divertor without added gas fuelling is similar to that seen in Mark I.

With gas fuelling, confinement progressively degrades from equality with the ITERH93-P scaling law. This degradation may be due to interaction caused by increased midplane pressure and recycling which occurs at high gas fuelling due to bypass leaks from the divertor region.

The vertical target plasmas are most tolerant of gas fuelling, maintaining their confinement to higher fuelling rates and producing radiative power fractions of 40-50% with good plasma purity.

There is a maximum density for gas fuelling in any particular plasma configuration. As fuelling rates are increased further the plasma density declines. It has not yet been possible to exceed the Greenwald limit in Mark IIA although operation close to this limit has been possible. The density limit appears to be an inability to maintain fuelling efficiency because of increased ELM activity. JET data supports the conclusion that the density limit becomes lower as divertor closure improves.

Confinement does not degrade relative to the ITERH93-P scaling law at low q in steady-state ELMy discharges. There is a slight degradation at high current but this may be due to insufficient conditioning at high current and power. Low q discharges are more susceptible to n=2 MHD activity in Mark IIA than in Mark I. There is also a significant increase in the number of low q, high current discharges with unexplained reverse H→L transitions.

The confinement scaling in JET radiative divertor ELMy H-modes at constant shape, q and β is not consistent with a gyro-Bohm scaling such as ITERH93-P. Further work is needed on truly dimensionless discharges in this regime to determine the precise dependence on ρ^*.

6. REFERENCES

[1] THE JET TEAM (presented by G. Vlases), IAEA-CN-64/A4-1, this Conference.

[2] THE JET TEAM (presented by G. F. Matthews), Plasma Phys. and Control. Fus. **37**, 227 (1995).

[3] STORK, D. et al., in Controlled Fusion and Plasma Phys. (Proc. 22nd Eur. Conf. Bournemouth, 1995) Vol. 19C Part II (1995) 125.

[4] THE JET TEAM (presented by L.D.Horton), paper presented at 23rd Eur. Conf. Kiev, 1996 (to be published in Plasma Phys. Control. Fusion).

[5] SAIBENE, G. et al., to be published in J. Nucl. Mater. (Proc. 12th Int. Conf. on Plasma Surface Interactions, St Raphael, 1996).

[6] The JET TEAM (presented by J. G. Cordey), IAEA-CN-64/AP1-2, this Conference.

HIGH FUSION PERFORMANCE ELM-FREE H-MODES AND THE APPROACH TO STEADY OPERATION

The JET Team[1]
(Presented by PJ Lomas)

JET Joint Undertaking,
Abingdon, Oxfordshire,
United Kingdom.

Abstract

The highest fusion yield in JET has been obtained in the hot ion H-mode regime. This paper reports progress in fusion performance in this regime. Since the last IAEA conference the fusion performance on the MKI pumped divertor has been doubled, with D-D neutron rates up to 4.65 10^{16}n/s demonstrated, equivalent to $Q_{DT} \sim 1$, similar to the PTE-1 series. More recently a more closed divertor MKII has been installed, and the new results will be described.

1. BASIC FEATURES OF THE REGIME

Figure 1 shows a typical hot ion H-mode plasma obtained with the new MKII divertor. After formation of the X-point the density is allowed to pump out to ~$1x10^{19}m^{-3}$ before the application of high power neutral beam (NB) heating. After a period of threshold ELMs the plasma becomes ELM-free, during which time both stored energy and D-D neutron rate increase steadily. The ion temperature, on the other hand, reaches a maximum and then declines somewhat as the density continues to increase. The loss power, P_{NB}-dW/dt-P_{SH} (where P_{SH} corresponds to the calculated shine through power), increases with time as does the stored energy, indicating approximately constant confinement time. The high performance phase is limited in this case by beam switch off followed 50ms later by a giant ELM and sawtooth (coincident to within 100μs). These and other limitations to performance are discussed in [1].

The duration of the ELM free phase is similar on both MKI and MKII for similar core plasma shapes, edge shear, $S_{95} \gtrsim 3.5$, triangularity, $\delta \gtrsim 0.3$. Higher triangularity configurations have been tested up to $\delta \sim 0.6$, $S_{95} \sim 4.0$ at 2.5MA but have not demonstrated any significant improvement in confinement quality. Configurations with low edge shear $S_{95} \lesssim 3$ and low triangularity $\delta \lesssim 0.2$ show repetitive giant ELM's with frequencies $\gtrsim 5Hz$.

Given the similarities in plasma behaviour in MKI and MKII it is not surprising that the fusion performance of the NB only data is also similar at the same beam power and shows the same strong scaling with NB power as illustrated in Fig.2. Thus far, for technical reasons, the NB power on MKII has been limited to <17MW, but this deficiency is being corrected, and this is expected to restore the MKI performance later this year. Note also that steady neutron yields can be maintained for about 1s by step-down of the beam power to the level of the loss power in the preceding transient phase.

---

[1] See Appendix to IAEA-CN-64/O1-4, The JET Team (presented by J Jacquinot).

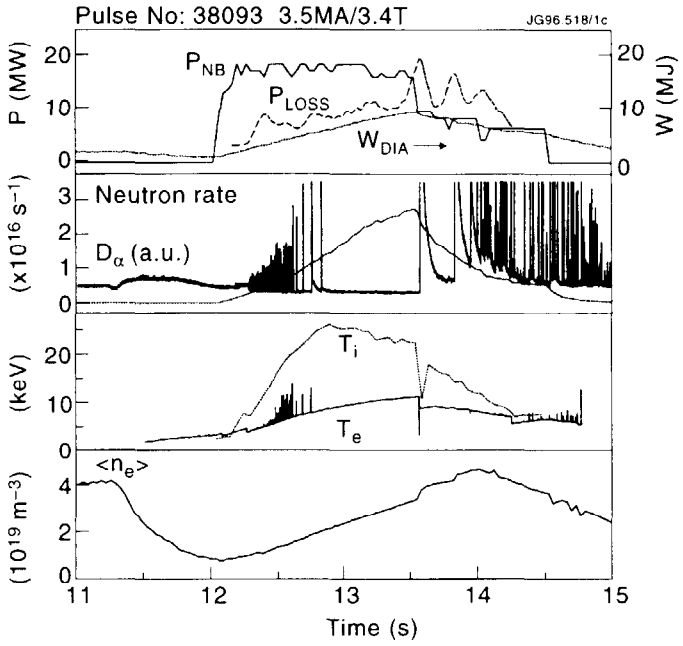

Fig.1 Typical time traces for an hot ion plasma showing neutral beam power P_{NB}, loss power P_{Loss} (see text), diamagnetic stored energy W_{DIA}, D-D neutron rate, D_α, ion and electron temperatures T_i and T_e and volume averaged density <n_e>.

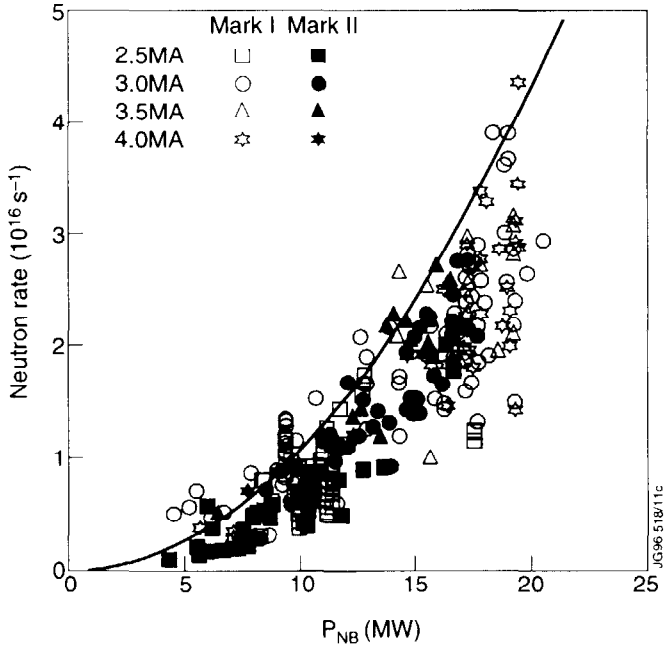

Fig.2 Neutron rate plotted against total neutral beam power. Open symbols refer to MKI and closed symbols refer to MKII. The shape of the symbols indicate plasma current: squares 2.5MA, circles 3MA, triangles 3.5MA and stars 4MA.

2. THE TRANSPORT BARRIER

A model has been developed [2] which accounts for many of the features observed in JET ELM-free H-modes. The model assumes:- (1) transport inside the barrier region is given by ion neo-classical together with anomalous terms including both Bohm (global) and gyro-Bohm terms, (2) transport coefficients within the transport barrier $D \sim \chi_i \sim \chi_e \sim \chi_i^{neocl}$ are given by the ion neo-classical diffusivity and (3) the width of the transport barrier is given by the ion poloidal banana width $\Delta \sim \sqrt{\varepsilon}\rho_{\theta i}$. Note that the Bohm terms dominate the transport in the outer regions of the plasma up to the transport barrier and the gyro-Bohm terms dominate the central confinement.

With these assumptions it is possible to construct a complete set of transport equations for n_e, T_e, T_i and J which can be solved self consistently. A single free parameter remains which can be the edge density (or alternatively the net recycling coefficient) which is adjusted to match the observed density evolution. When applied to hot ion plasmas the time evolution of plasma parameters and profiles are well reproduced. In particular, the initial linear rise in stored energy is well described, and is followed by a progressive saturation which the model suggests is due to the density rise. The model describes accurately the evolution of power step-down pulses and the effect of strong gas puffing, and can account qualitatively for the temporary degradation of confinement following a sawtooth crash. The code predicts the time when ballooning modes become unstable which is consistent with the experimentally observed appearance of giant ELM's as shown in Fig.3. Indeed, this confirms, in a very satisfying manner, that the transport is close to ion neo-classical in the barrier region because an increase in transport would lead to ballooning modes always being stable.

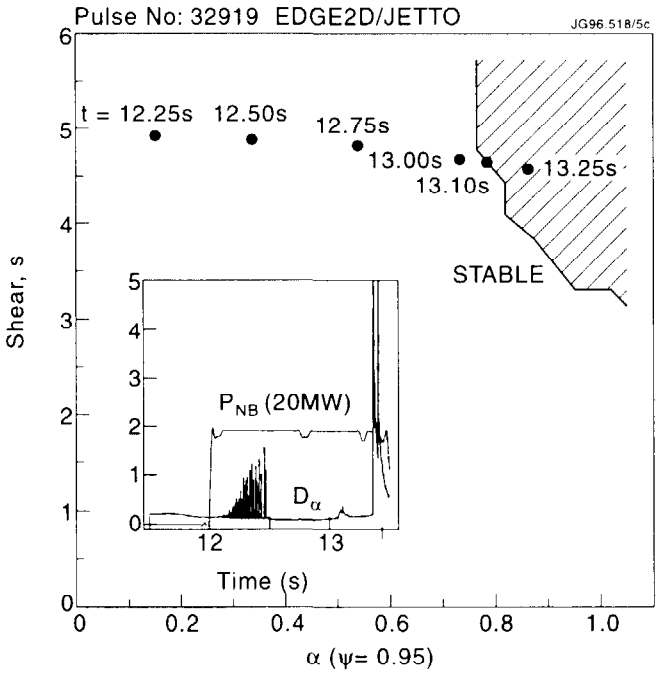

Fig.3 Trajectory of the model simulation of pulse 32919 in the S-α (shear versus normalised pressure gradient) diagram. The ballooning unstable region is shown shaded. Ballooning instability is predicted at 13.1 s which should be compared with the ELM time of 13.4 s shown in the inset.

Measurements of both ion and electron temperature profiles across the transport barrier are shown in Fig.4(a). The transport barrier is most clearly defined in the electron temperature data and this width is plotted against the best fit in Fig.4(b). Note that this result does not conform to the expected scaling $T_i^{1/2}/I_p$. Further analysis is in progress which may resolve these discrepancies, but it may be necessary to include more physics elements such as the penetration depth of cold neutrals. The first attempt to self consistently compute the scrape-off layer (SOL) and core transport together with neutral penetration is described in [3].

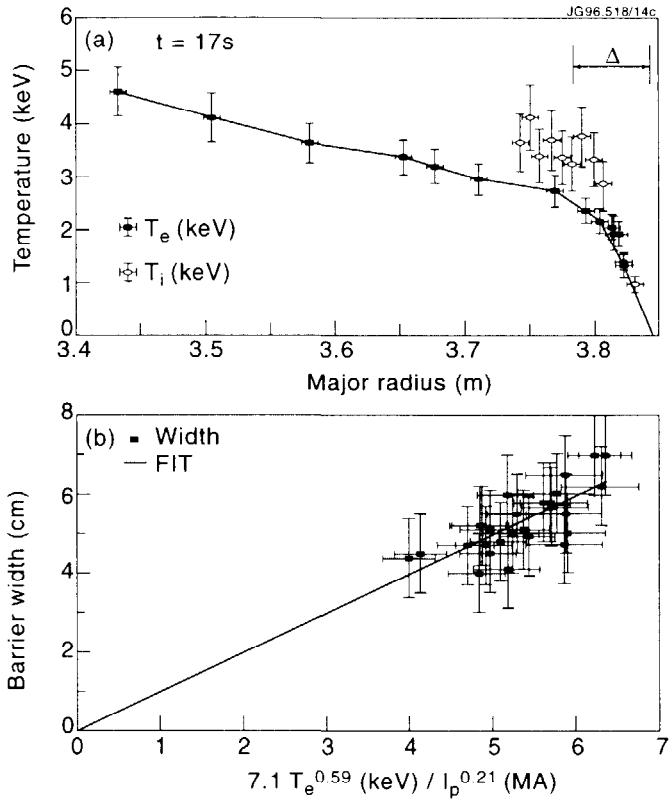

Fig.4 (a) Ion and electron temperature profiles for pulse 37444 (2.6MA/2.54T) from which the transport barrier width Δ is determined. (b) barrier width against fitted dependence on temperature and plasma current. Note the weak dependence on I_p.

3. THE ROLE OF RECYCLING

It was already described at the last IAEA conference [4] how the main chamber recycling plays an important role influencing both ELM-free period and performance. Simulations with the model described above confirm this sensitivity. The distribution of the D_α light clearly shows the brightest signals from the divertor strike zones but reveals some contribution from the inboard (small major radius) plasma edge.

Measurements of Zeeman split D_α on a horizontal chord indicates approximately 4 times the light from the small major radius side of the plasma compared to the large major radius side.

In order to quantify the relative contribution of recycling in the main chamber compared to the divertor a selective hydrogen loading experiment was performed. The measured H/H+D fraction determined from vertical chord H_α and D_α is shown in Fig.5 as a function of pulse number for 4 sequences of pulses repeated on two successive days.

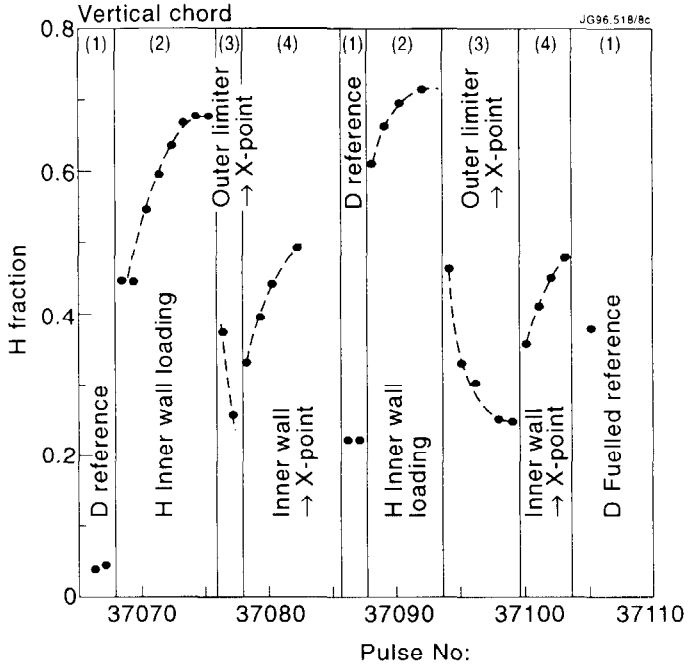

Fig.5 Ratio of H/H+D from H_α, D_α light measured on a vertical chord for a series of pulses from the selective hydrogen loading experiment (see text). Where the plasma pulse includes both limiter and X-point phases the measurement is taken during the deuterium beam fuelled H-mode in the X-point phase. The figure shows two cycles of experiments 37066-37084 and 37086 - 37105 repeated on successive days.

The sequence of pulses are as follows (as labelled on Fig.5). (1) reference pulse with deuterium gas fuelled inner limiter phase followed by deuterium beam fuelled H-mode, (2) inner wall limited pulses with hydrogen gas fuelling (3) pulses with deuterium gas fuelled outboard limiter phase followed by deuterium beam fuelled H-mode (4) pulses with hydrogen gas fuelled inner wall limiter phase followed by deuterium fuelled H-mode. For clarity the data points in Fig.5 represent the X-point phase when there is more than one phase. Generally the hydrogen concentration is low during the outboard limiter phases of sequences (1) and (3). The H/H+D ratio during the inner wall hydrogen loading pulses (2) behaves in a similar manner to previous isotope exchange experiments [5]. Note that sequence (3) has no direct contact with the inner wall and its inventory of hydrogen, and yet the X-point phase starts with an high concentration of hydrogen which decreases pulse by pulse. In sequence (4), where the hydrogen concentration is topped up during the inner wall phase, the concentration during the X-point phase increases pulse by pulse. These results demonstrate that there is significant exchange, during the H-mode phase only, of hydrogen from the inner wall to the divertor target and of deuterium from the divertor target to the inner wall. Thus a significant fraction (0.25 - 0.5) of the recycled particles originate

from the inner wall, demonstrating the importance of the main chamber recycling during diverted H-modes.

The more closed MKII divertor was predicted to increase the pressure of neutrals in the diverted region and hence increase pumping. The data in Fig.6 clearly shows the increase in pumping during ELM-free H-modes in MKII compared with MKI. Indeed in MKII the density rise during the ELM-free H-modes is reduced by ~ 30% such that it is necessary to add gas to optimise the fusion yield (minimise NB shine through losses and Z_{eff}). At low gas puff there is a clear net source of particles from either walls or target whereas at sufficiently high gas flow these surfaces provide a net pump. Alternatively these results can be thought of as a decrease in gas fuelling efficiency (from ~ 50% to $\leq$ 10%). This strong divertor pumping has reduced the need for extensive conditioning for access to the hot ion regime and increased the reproducibility of the performance achieved but has not, as yet, significantly improved the performance or confinement quality.

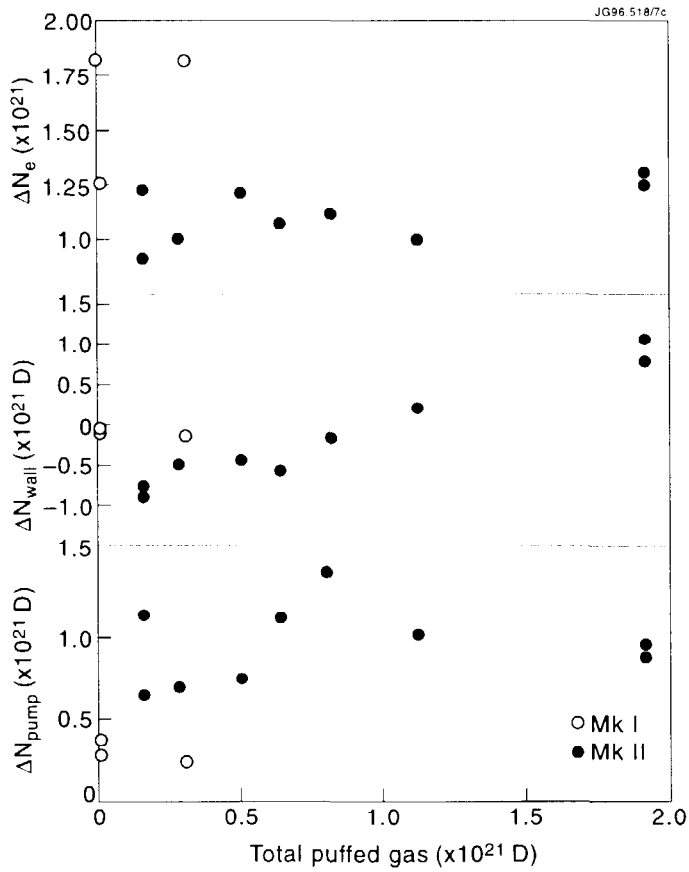

Fig.6 Particle balance over the first second of neutral beam heating for a series of ELM free H-modes. The change in plasma particle inventory, wall inventory and pump inventory are shown as a function of total gas puffed in the same interval. Open symbols refer to MKI and closed symbols refer to MKII. The neutral beams inject 17MW and 1.4 10^{21} particles per second.

4. COMBINED HEATING

Ion cyclotron resonance heating (ICRH) has been coupled in conjunction with NB heating to produce ELM-free H-modes with combined heating (NBRF). The coupling resistance falls during the ELM-free H-mode from about 2Ω to 1.5Ω. Nevertheless, it has been possible to couple up to 9.5MW. Together with NB a total power up to 25MW has been applied for plasma currents up to 3.8MA generating stored energies up to 14MJ. The diamagnetic energy confinement time $\tau = W_{dia}/(P_{NB} + P_{RF} - dW/dt)$ is about 1 s in these cases, similar to the NB only cases, suggesting no strong effect according to different proportions of electron and ion heating.

Figure 7 compares high D-D yield pulses at similar NB power with and without 6.5MW of ICRH resonant on axis with hydrogen and second harmonic deuterium. The increase in stored energy, D-D neutron yield, ion and electron temperatures are clear, and the shorter ELM-free phase is as expected. The high energy neutral particle analyser clearly shows the generation of a deuteron tail with energies up to 1MeV, as expected from PION code calculations. Neutron accounting using kinetic data suggest increased neutron production from both thermonuclear and non-thermal reactions. With added hydrogen or mixed

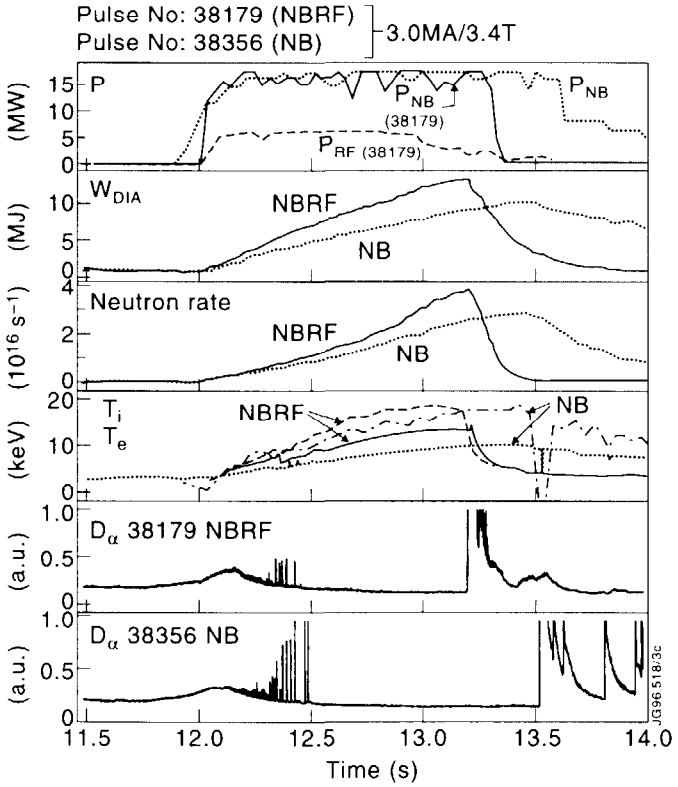

Fig.7 Typical time traces comparing NB only (38356) and combined heating NBRF (38179). The traces shown are input powers, P_{NB}, and P_{RF}, diagmagnetic stored energy W_{DIA}, neutron rates, ion and electron temperatures and D_α

frequency (multiple resonance position) ICRH the observed tail can be smaller by an order of magnitude and yet still the D-D neutron rate is increased over and above the NB only cases. These results suggest a useful increase in fusion yield when ICRH is applied to DT plasmas, but it is too early to make quantitative predictions.

5. DT EXPECTATIONS

The best NB only plasma in MKI has demonstrated $n_D(0)\tau_E T_i(0) \sim 8.8\times10^{20}$ and TRANSP analysis indicates $Q_{DT}^{equiv} \sim 1$ (with the definition in [6]). High performance can be sustained for about 1 s by stepping down the NB power to about the loss power and in such cases $Q_{DT}^{equiv} > 0.8$ for 1s. Similar results are expected with MkII when the full beam power is restored later in 1996.

These extrapolations assume that 50:50 D:T mix can be achieved. By operation of the tritium beams at full power and the deuterium beams at reduced power 20 MW can be delivered with comparable deuterium and tritium fluxes. Provided that the core is dominated by beam fuelling a 60:40 mix should be readily achievable. Contributions to the core D-T mix from recycling could be offset by tritium beam prefuelling or gas puffing. Operation of the deuterium beams at full power would deliver ≃ 23MW and would be expected to increase the D-T neutron yield by up to 30% provided that the shortfall in tritium fuelling can be made up (by gas puffing or prefuelling).

6. CONCLUSIONS

The behaviour of the hot ion ELM-free H-mode regime is reassuringly similar in the MKI and MKII divertor. Improved pumping has reduced the characteristic density rise and increased operational flexibility, but has not as yet led to any significant improvement in performance. Similar high fusion performance, as already demonstrated on MKI, is expected on MKII when the neutral beam power is restored. Improved performance has been demonstrated with the addition of ICRH power to the hot ion ELM-free regime. The transport model continues to describe the main features of this regime and recently detailed edge temperature measurements have been made which should enable a refinement of the physics of the transport barrier.

Last, but not least, the rapid progress so far achieved with the MKII divertor shows great promise for the forthcoming DT experiments.

REFERENCES

[1] THE JET TEAM (presented by P. R. Thomas), IAEA-CN-64/A3-2, this Conference.

[2] BAK, P., et al., Nucl. Fusion **36** (1996) 321.

[3] THE JET TEAM (presented by A. Taroni), IAEA-CN-64/D3-3, this Conference.

[4] THE JET TEAM (presented by P. J. Lomas) in Plasma Physics and Controlled Nuclear Fusion Research 1994 (Proc. 15th Int. Conf. Seville, 1994) Vol. 1, IAEA, Vienna (1996) 211.

[5] HORTON, L.D., et al., J. Nucl. Mater. **196-198** (1992) 139.

[6] BALET, B., et al., Nucl. Fusion **33** (1993) 1345.

ENERGY CONFINEMENT AND H-MODE POWER THRESHOLD SCALING IN JET WITH ITER DIMENSIONLESS PARAMETERS

The JET Team[1]
(Presented by J G Cordey)

JET Joint Undertaking,
Abingdon, Oxfordshire,
United Kingdom.

Abstract

An account is given of recent experiments carried out on JET to determine the scaling of the L-H and H-L power threshold and the dependence of the energy confinement on the dimensionless parameters ρ^*, ν^* and β.

1. INTRODUCTION

In JET a series of ELMy H-mode experiments has been undertaken in which the values of the dimensionless physics parameters are close to ITER values. Two physics aspects have been studied. The first, described in Section 2, is the scaling of the H-mode power threshold where, in addition to the previously reported work on the L-H transition [1] also the H-L back transition is studied. In particular, it is found that there is little hysteresis in the two threshold powers. In the second series of experiments, described in Section 3, the dependence of the confinement scaling upon the dimensionless parameters, ρ^* (larmor radius $\equiv T^{1/2}/Ba$) , ν^* (collisionality $\equiv na/T^2$) and β ($\equiv nT/B^2$) is examined in turn. The dependence of energy confinement with the parameter ρ^* is obtained for a larger range of ρ^* and at higher β's than studied previously [2],[3]. The dependence of τ_E is again found to be close to gyro-Bohm and in agreement with the ITERH93-P [4] scaling expression which is being used to predict the ITER confinement time. A similar behaviour was first found on DIII-D for low q ELMy H-modes [5]. The dependence of τ_E with ν^*, the collisionality, is also found to be in agreement with the ITERH93-P expression, whilst the scaling with β is found to be very weak in contrast to the strong scaling with β of ITERH93-P. The reasons for this discrepancy and the implications of the results of Sections 2 and 3 are discussed in Section 4.

2. H-MODE THRESHOLD SCALING STUDIES

The studies reported in reference [1] have continued in the same ITER like JET geometry R = 2.9m, a = 0.92m, κ = 1.7, $q_{\psi 95}$ = 3.2, δ = 0.2. The current and toroidal fields ranged from 0.83MA/0.83T to 3MA/3T. The scaling of L-H power threshold with density and toroidal field was found to be the same in the Mk IIA divertor as that of the Mk I divertor. However the range of density and field has been increased particularly at the low density end. The data obtained in Mk IIA is shown in Fig.1 versus one of the dimensionally correct forms of the threshold scaling used by F. Ryter and the ITER data base group [6]. As in Mk I there is a departure from linearity of the threshold with density at both low and high densities. However, at the low density end there is no increase in the threshold power at very low densities seen in some machines. Several different geometrical configurations have also been assessed and it has been found that there is no significant change in the threshold.

[1] See Appendix to IAEA-CN-64/O1-4, The JET Team (presented by J Jacquinot).

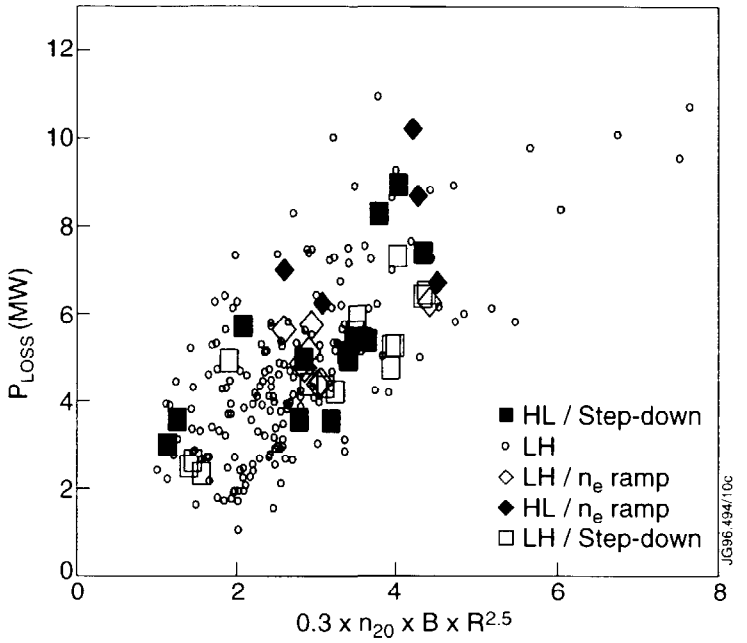

Fig.1 The loss power P_{input} - $\dot{w}$ versus $0.3\, n_{20} B R^{2.5}$ ($\times 10^{20}$ m^{-3} T $m^{2.5}$). The open symbols are for the L-H transition and the solid symbols are for the H-L transition, the rectangles are the power step down experiments, the diamonds are for the density ramp experiments, and the circles are power staircase experiments.

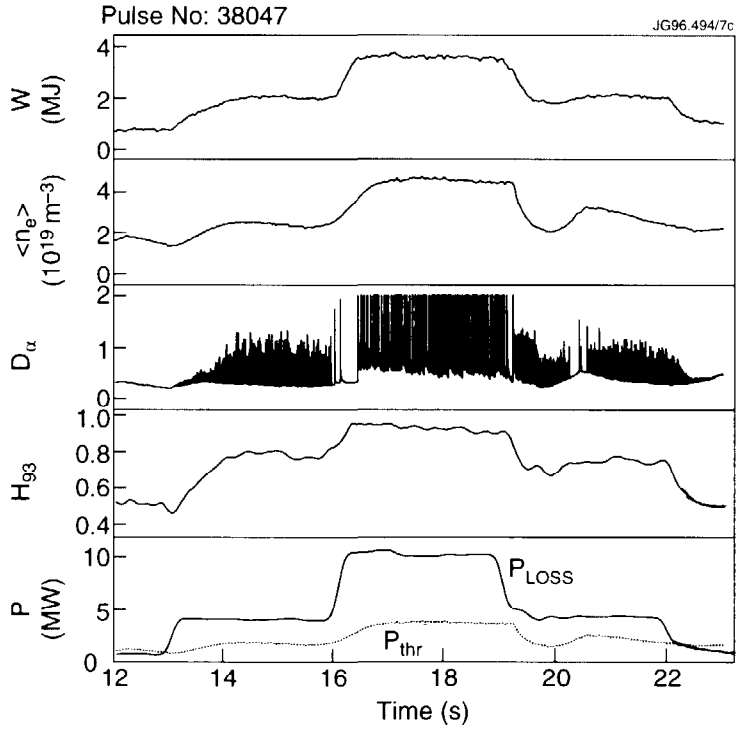

Fig. 2 Time traces of total stored energy, volume averaged density, D_α, H_{93} factor, and P_{loss} and the threshold power P_{thr} where the same expression as in Fig.1 was used.

Two types of experiments have been performed on the H-L back transition: (a) power step-down experiments and (b) density ramp experiments. An example of a power step-down pulse is shown in Fig.2. The NBI input power level was varied in three steps. Soon after the onset of the first 4MW step, the D_α signal indicates the presence of an H-mode by the very high frequency transition ELMs (>100 Hz). One second after the start of the heating, the stored energy and density reach steady values and the confinement enhancement factor H_{93} relative to ITERH93-P has a value ~0.8. At t =16s the power is further increased to 10MW, and as a result the character of the ELMs changes to the type I with a frequency ~20 Hz. During this period H_{93} increases to 0.95. After a steady state is achieved the power is switched down to the starting value (4MW) and the nature of the ELMs then changes back to the transition type. As a consequence, H_{93} drops to around 0.8. Finally, when the NBI power is switched off the H-mode is lost at a similar loss power to that which was required to achieve the L-H transition.

Thus there is no hysteresis in the L-H/H-L threshold in these step-down pulses. The same is found to be the case for the density ramp experiments. As the density is increased eventually the transition ELMs appear and H_{93} drops. The H-mode then disappears at a power level close to that of L-H transition for the same density. The threshold power for the H-L transition is shown in Fig.1 for both methods of obtaining a back transition along with the L-H transition data for a whole series of fields and densities from the present campaign.

3. DEPENDENCE OF τ_E ON THE DIMENSIONLESS PARAMETERS ρ^*, ν^* AND β.

Three separate groups of experiments were carried out to determine the dependence of confinement on ρ^*, ν^* and β. The plasma geometry was the same as in Section 2 and only pulses with Type I ELMs are studied in this paper. To adjust the density, only moderate gas puffing was used, the main particle source being from NBI which was the main heating source also.

The results are compared with the ITERH93-P scaling expression which can be written in dimensionless form:

$$B\tau_{th} \propto \rho^{*-2.7}\, \nu^{*-0.28}\, \beta^{-1.2} \qquad (1)$$

where the parameters ρ^*, ν^* and β are defined in terms of their average values as $\rho^* \equiv W_{th}^{1/2}/n^{1/2}\, a^{3/2}$, $\nu^* \equiv n^3\, a^7/W_{th}^2$ and $\beta \equiv W_{th}/B^2a^3$, with W_{th} being the total thermal stored energy, n the volume averaged density and a the minor radius.

3.1 ρ^* scaling experiments

Three sets of experiments have been completed at different β's and collisionalities, close to those expected in ITER. These are listed in Table I. To keep ν^* and β fixed, the density should be proportional to $B^{4/3}$ and the stored energy proportional to B^2. From Table I it can be seen that this has been approximately achieved and that the resulting dimensionless confinement $B\tau_{th}$ follows the $\rho^{*-2.7}$ scaling of ITERH93-P, that is the scaling is close to gyro-Bohm. The three ρ^* scans are shown against the scaling expression in Fig.3; H_{93} is greater than 0.9 for all of the pulses.

3.2 ν^* scaling experiments

Here β and ρ^* were kept fixed and this means that n = const. and $W_{th} \propto B^2$. The results are shown in Table II. The profiles of ρ^* and β are also well matched for these two pulses as can be seen in Fig.4. From Table II it can be seen that $B\tau_{th}$ scales as $\nu^{*-0.27}$ in close agreement with the ITERH93-P scaling.

Table I ρ^* **scans**

a) $\beta_{nth} \sim 2$ $\quad \nu^*/\nu^*_{ITER} = 2.8$

Pulse No.	B	I	n	P	τ_{th}	$B\tau_{th}/\rho^{*-2.7}$
37380	1	1	2.2	7	0.14	1
37375	2	2	5.6	15	0.26	1.04

b) $\beta_{nth} \sim 1.6$ $\quad \nu^*/\nu^*_{ITER} = 1$

Pulse No.	B	I	n	P	τ_{th}	$B\tau_{th}/\rho^{*-2.7}$
38429	1.5	1.5	2.5	10	0.20	1
38427	2.6	2.6	5.0	21	0.30	0.97

c) $\beta_{nth} \sim 1.5$ $\quad \nu^*/\nu^*_{ITER} = 2.3$

Pulse No.	B	I	n	P	τ_{th}	$B\tau_{th}/\rho^{*-2.7}$
37379	1	1	2	4.4	0.19	1
38047	2	2	4.8	10	0.34	1.03
37944	2.6	2.6	6.8	12.5	0.43	1.05

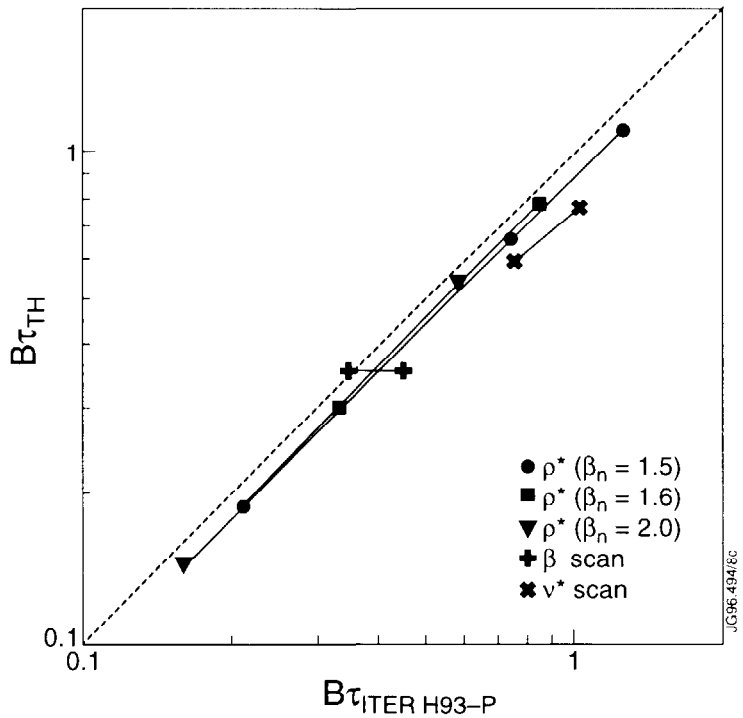

Fig.3 The normalised confinement time $B\tau_{th}$ *versus* $B\tau_{ITERH93\text{-}P}$. *The three* ρ^* *scans are indicated by solid triangles, squares and circles. The* β *scan is indicated by the crosses and the* ν^* *scan by the diagonal crosses.*

Table II ν^* and β scans

	ν^* scan		β scan	
Pulse No.	37718	37728	38407	38415
B (T)	2	2.6	1.5	1.7
I (MA)	2	2.6	1.5	1.7
$\langle n \rangle$ ($10^{19}m^{-3}$)	5	5	2.7	4.1
P (MW)	10	16	6.5	16.5
W_{th} (MJ)	3.0	4.8	1.5	3.4
τ_{th} (s)	0.3	0.3	0.24	0.21
$B\tau_{th}$	0.6	0.78	0.36	0.35
ν^*/ν^*_{ITER}	3.4	1.3	2.1	1.5
β_{nth}	1	1	1.2	2.2

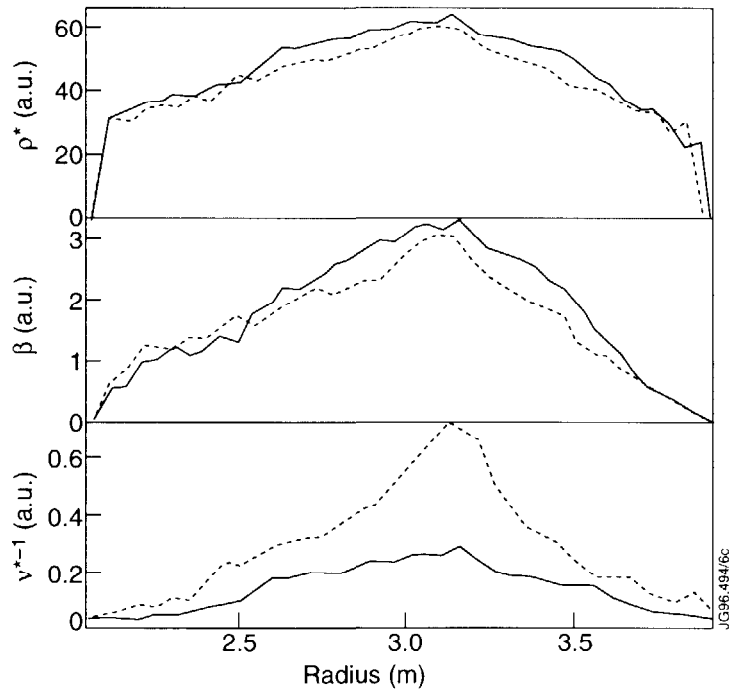

Fig. 4 Radial profiles of ρ^*, β and ν^* for the pulses in the ν^* scan.

3.3 β scaling experiments

Here ρ^* and ν^* were kept fixed. This means that $n \propto B^4$ and $W_{th} \propto B^6$. The results of these experiments are also given in Table II. A preliminary analysis of the data gives a very weak dependence of τ_ε upon β with $B\tau_\varepsilon \propto \beta^{-0.05}$, in marked contrast to the strong dependence of the ITERH93-P scaling expression. A similar result was recently found on DIII-D [7].

A comparison of both the ν^* and β dependence with the ITERH93-P scaling expression is given in Fig.3. The ν^* dependence follows the scaling expression whilst this is clearly not the case for the β dependence.

4. DISCUSSION

The main outcome of the threshold studies is that there are really two power thresholds. The first is the power requirement to reach steady state transition (or threshold) ELMs. There is a second power threshold for steady state periodic type I ELMs. In the transition ELM phase, the confinement improves continuously as the power is increased and the ELM frequency decreases. This phase is completely reversible and there is no hysteresis as the power is reduced. This is very similar to the situation in radiative divertors such as the CDH mode [8] where there is a smooth transition between the L and H states.

In the type I ELM phase, H_{93} reaches a higher value and is constant until the MHD β limit is reached. When the power falls significantly in the type I ELM phase, the transition ELM phase with lower confinement returns. Hence there is apparently no hysteresis in the type I ELM phase either. This latter behaviour may be different in JET to that of other devices due to the high temperature walls and high pumping which are very effective at controlling recycling in JET.

The dimensionless physics parameter scans in ρ^*, ν^* and β confirm the validity of the ITERH93-P scaling expression as far as its ρ^* and ν^* dependence are concerned. However, the β dependence seems not correctly described. There are several possible explanations for this discrepancy and these are currently being investigated. One obvious difference between determining the β scaling as compared with the ρ^* and ν^* scaling is that the range in β is much narrower than either the ρ^* or ν^* range. It is also possible that some data close to the MHD β limit has been included in the ITER data base from which ITERH93-P is derived.

If this lack of β scaling is confirmed by other experiments, the prediction of the ITER confinement time will be increased by about 10% at the β of the ignited ITER.

REFERENCES

[1] RIGHI, E., CAMPBELL, D.J., CORDEY, J.G., et al., in Controlled Fusion and Plasma Physics (Proc. 22nd Eur. Conf. Bournemouth, 1995), Vol. 19C, Part II, European Physical Society, Geneva (1995) II-073.

[2] BALET, B., CAMPBELL, D.J., CHRISTIANSEN, J.P., et al., Ibid., Part I, I-009.

[3] CORDEY, J.G., et al., Proceedings of the H-mode workshop PPPL (1995).

[4] ITER H-MODE DATABASE WORKING GROUP, in Controlled Fusion and Plasma Physics (Proc. 20th Eur. Conf. Lisbon, 1993), Vol. 17C, Part I, European Physical Society, Geneva (1993) 15.

[5] PETTY, C.C., et al., Phys. Plasmas **2** (1995) 2342.

[6] RYTER, F., et al., Nucl. Fusion **36** (1996) 1217.

[7] PETTY, C.C., et al., to be published in Controlled Fusion and Plasma Physics (Proc. 23rd Eur. Conf. Kiev, 1996).

[8] KALLENBACH, A., et al., in Controlled Fusion and Plasma Physics (Proc. 22nd Eur. Conf. Bournemouth, 1995), Vol. 19C, Part II, European Physical Society, Geneva (1995) II-005.

ALFVEN EIGENMODES AND FAST PARTICLE PHYSICS IN JET REACTOR RELEVANT PLASMAS

The JET Team[1]
(presented by D F H Start)

JET Joint Undertaking,
Abingdon, Oxfordshire,
United Kingdom.

Abstract

Alfven eigenmodes have been directly excited by using the JET saddle coils with a system which locks the drive frequency to the mode frequency. The technique has shown that neutral beams do not excite low n modes whereas high n modes are destabilised. Such modes are often generated by NBI alone in hot ion H-mode plasmas when the Alfven speed is about three times the parallel velocity of the beam ions. Kinetic TAE modes have been identified and theoretical calculations predict that these should be destabilised at the fast ion densities present. A new technique for generating TAE modes with ICRH beat waves has been demonstrated. Simulated α-particle heating by ICRH accelerated fast ions has produced electron temperatures of 15keV in hot ion H-modes and in shear reversed plasmas. Third harmonic ICRH has achieved a D-D neutron rate of $9x10^{15}s^{-1}$ which is well simulated by PION code calculations.

1. INTRODUCTION

In a tokamak reactor the slowing down of α-particles will provide the main source of plasma heating. From present day experiments there is evidence that the slowing down is classical. Two important consequences are discussed in this paper. Firstly, the α-particle population is characterised by energies greater than the equipartition energy so that the energy is transferred to the electrons in the core region. A burning plasma will have T_e close to, but higher than T_i. Such plasmas with T_e = 15keV and T_i = 14keV have been achieved in JET with fast particle heating. These values approach the expected temperatures at ignition on ITER (≈20keV), although at lower density. Thus the JET discharges allow electron and ion heat transport to be studied at temperatures relevant to the ignition path and the burn phase in a reactor. Transport analysis results are given for these plasmas and for reversed shear discharges in which T_e and T_i reached 15keV and 32keV, respectively. Secondly, the α-particles generate pressure gradients that can drive collective instabilities such as Alfven eigenmodes. Extensive studies of these modes have been made on JET by both direct and indirect excitation methods.

2. FAST PARTICLE PHYSICS

ICRF heating at the deuterium third harmonic resonance has provided the most stringent test of both fast particle confinement in JET and the accuracy of

---

[1] See Appendix to IAEA-CN-64/O1-4, The JET Team (presented by J Jacquinot), together with R Heeter, Princeton Plasma Physics Laboratory, Princeton, USA, P Lavanchi, J Lister and Y Martin, CRPP, Lausanne, Switzerland, L C Appel and S Pinches, UKAEA, Culham Laboratory, Abingdon, UK, F Nguyen, CEA, Cadarache, France, and J Candy, Institute for Fusion Studies, University of Texas, Texas, USA.

simulation codes such as the PION code [1]. The results of these experiments are given in section 2.1. Minority ICRH provides a good simulation of α-particle heating in ITER since the minority ions might reach MeV energies and fast ion beta can exceed that of the α-particle population in a reactor. Collisional transfer of the fast ion energy takes place to the electrons and this feature is exploited to investigate electron heat transport in a variety of plasma regimes. Such measurements complement ion transport studies with neutral beams which typically transfer 80% of their energy to the majority ions. The results of electron heating experiments, which achieved central temperatures up to 15keV, are described in section 2.2.

2.1 Third harmonic ICRH.

These experiments were carried out with the third harmonic deuterium resonance in the centre of a 2MA plasma with a toroidal field of 2.2T. Transit time magnetic pumping (TTMP) was the main competing damping mechanism to the cyclotron damping. The time evolution of the neutron rate (Fig.1) increases strongly during the high power RF phase and reaches $9x10^{15}s^{-1}$ which is a record

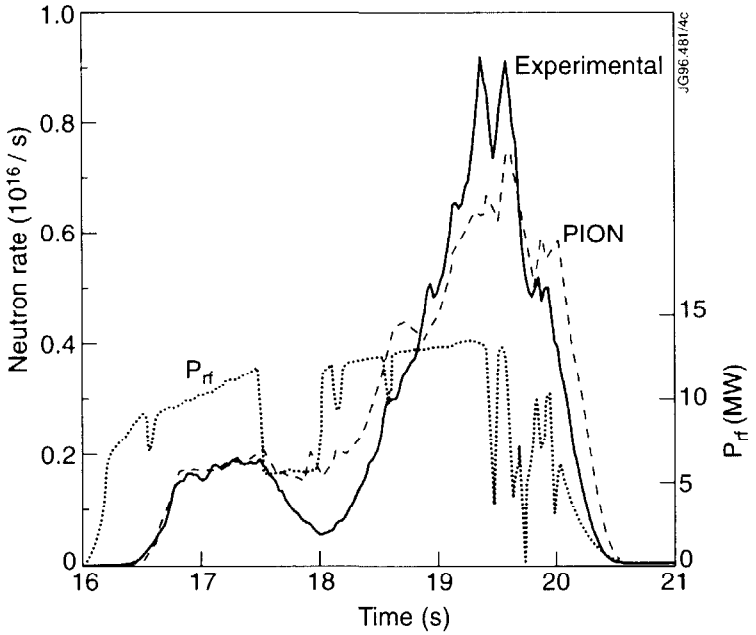

Fig.1 Experimental and PION code neutron rate for $3\omega_{CD}$ ICRH

for ICRH in JET. The neutron rate is the same as that achieved with NBI at the same power level in a similar discharge and is produced by the energetic deuterium tail. A simulation of the time evolution of the D-D neutron rate (Y_{DD}) has been made with the PION code which produces a self-consistent calculation of the power absorption and the deuterium tail. It includes TTMP absorption and effects due to the finite orbit of the fast tail. The result is shown in Fig.1. To achieve the good agreement with experiment it was necessary to include a "parasitic damping" of the order of 4% per pass and a particle loss term that removed particles with energy in excess of 4MeV which were not confined in the plasma. The parasitic damping only played a role at the beginning of the RF pulse when the tail energy was low, and was essential to obtain the time delay between the start of the RF pulse and the rise of Y_{DD}. A similar level of parasitic damping is found in TTMP current drive experiments in DIII-D and could be due to wall loss, RF sheath formation or hydrogen minority damping at the

plasma edge. The strong increase in Y_{DD} at the end of the pulse is due to the density increase which reduces the tail energy and also the number of lost ions so that the fast particle density remains almost constant. Thus the D-D neutron rate due to the interaction between the fast tail and thermal ions increases in proportion to the deuterium density.

2.2 Electron heating and transport.

These experiments have been carried out in hot ion H-modes, central reversed shear discharges and RF-only H-modes. The plasma currents ranged from 2.5MA to 3.5MA and the toroidal fields from 2.6T to 3.4T. The RF frequency was chosen to locate the hydrogen minority resonance layer in the plasma centre. The highest central value of T_e = 15keV was produced in a 3MA/3.1T reversed shear plasma with 14MW of NBI and 5MW of ICRH, but similar temperatures were also achieved in the hot ion H-modes and RF-only H-modes in high triangularity plasmas.

Transport analyses of several of the discharges have been made with the TRANSP code. The results are characterised by the values of χ_e at a minor radius r/a = 0.3. The highest performance discharges have very similar values of χ_e (r/a = 0.3) close to 0.5m^2/s. The 3MA RF-only H-modes have χ_e (r/a = 0.3) $\approx$1m^2/s. For the hot ion H-modes the value of χ_i is about 50% greater than χ_e whereas χ_i is generally less than χ_e inside the confinement barrier of reversed shear plasmas.

3. ALFVEN EIGENMODES

Over the α-particle slowing down time, the fast ion cross field transport, associated with both neo-classical and anomalous effects due to electrostatic or electromagnetic turbulence, is in general negligible. Significant transport and losses of suprathermal particles may take place only in the presence of waves which resonate with them. Of particular importance are weakly damped modes with phase velocities of the order of the α-particle speeds before thermalisation, such as Alfven eigenmodes (AE) which exist within the gaps of the shear Alfven spectrum in magnetically confined toroidal plasmas. It is estimated that if the α-particle losses in ITER are greater than 2% they might damage the first wall and if greater than 20% the fusion reaction will be quenched. Furthermore, Alfven eigenmodes will resonate with the 1MeV neutral beams planned for ITER and might reduce current drive capability. The following sections present studies of the stability of Alfven eigenmodes, excitation by fast particles and ICRF beat waves and the effect on fast ions.

3.1 Stability studies with direct excitation.

The saddle coils in JET are used to excite low n Alfven eigenmodes in the 30kHz to 500kHz range and the modes are detected with a set of toroidal and poloidal synchronous detector coils plus ECE and reflectometer diagnostics. The Alfven character of the modes has been verified by the scaling of the resonant frequency with density and magnetic field [2]. Recently, a system has been installed to lock the drive frequency to that of a single mode and to track this mode in real time. An example is shown in Fig.2 where a mode is detected at 7.3s close to the expected TAE frequency and is tracked until 10.5s. A small sweep is imposed on the resonance frequency to enable the damping to be measured as a function of time. In this case the damping rate (γ) is consistent with radiative damping. The locking gives a powerful technique for studying fast particle effects on mode stability. In a discharge heated by 3MW of 140keV NBI the width of the resonance ($\gamma/\omega \cong 1\%$) of a driven n = 1 mode increased by a factor of two compared with the value in the ohmic phase. Since $\gamma = \gamma_{damping} - \gamma_{drive}$, it appears that the fast ions produce extra damping and do not drive low n modes.

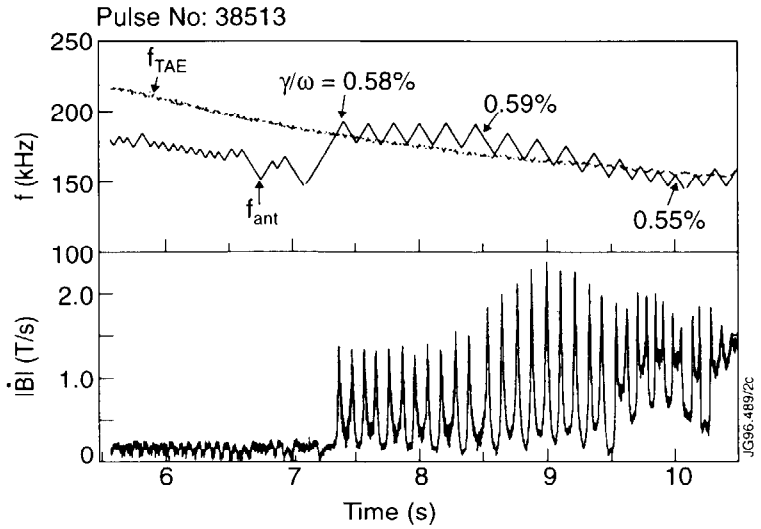

Fig.2 TAE excitation with mode-locked saddle coil drive frequency

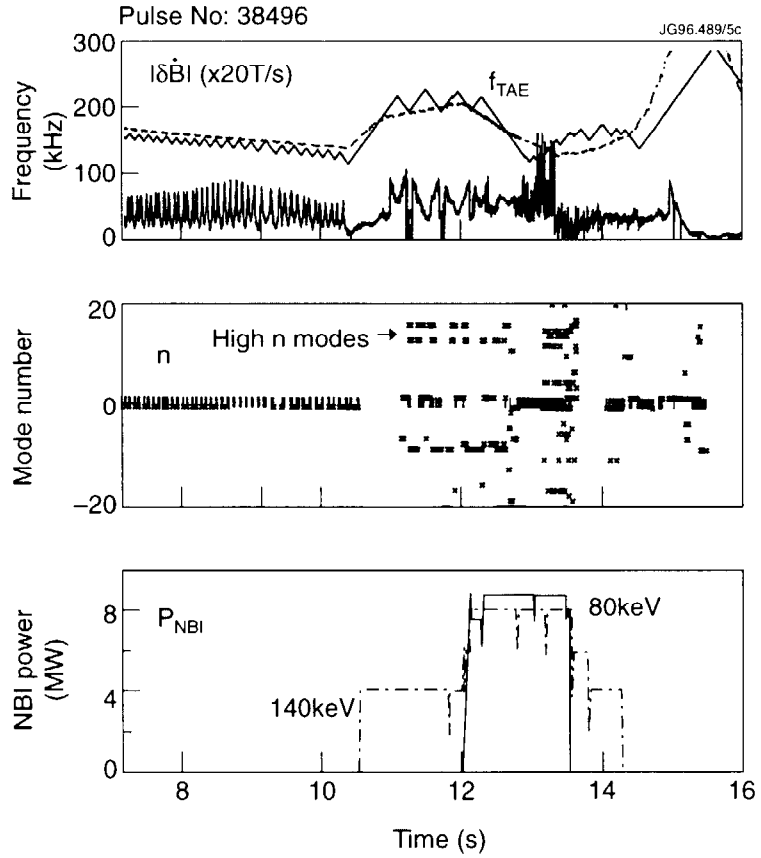

Fig.3 High n TAE modes driven unstable by 140keV NBI

This conclusion is supported by the observations shown in Fig.3. During the ohmic limiter phase the system locks to an n = 1 mode driven by the saddle coils. Then a divertor plasma is formed and the NBI is applied at 10.5s. At this point the driving term is dominated by the fast ions, the mode locking ceases but the system still applies the calculated TAE frequency as reference for the detection

coils. During the NBI phase high n modes are seen and these have similar amplitudes at the edge to the n = 1 mode in the limiter phase ($\delta B/B \cong 10^{-6}$). In the core region the amplitude of the high n modes can be several hundred times greater (for kinetic TAE modes) than the amplitude at the edge; for the n = 1 modes the maximum amplitude is similar to the edge magnetic field. Thus $\delta B/B$ could be higher than 10^{-4} which is approaching the threshold (10^{-3}) for stochasticity and reduced fast ion confinement. The excitation of high n modes by 140keV beams with $v_{//} = v_A/3$, where v_A is the Alfven speed, agrees with calculations using the CASTOR code [3] which predict, for example, an n =14 kinetic TAE (KTAE) to be excited at $\beta_{fast} \geq 1\%$: in Fig.3 the value of β_{fast} was 1.3%.

3.2 Excitation by fast particles.

In JET hot ion H-modes there is invariably Alfven eigenmode excitation when $v_{//}$ of the 140keV beams is close to $v_A/3$. An example is shown in Fig.4. The TAE system was in detection mode (no saddle coil excitation) in which the reference frequency is derived from the calculated Alfven frequency plus a small modulation. The Alfven frequency decreases during beam heating since the density is increased due to both the NBI fuelling and the formation of an ELM-free H-mode at 12.1s. As $v_{//}$ approaches $v_A/3$ there is a strong increase in the Alfven mode activity. There is also a tendency for the neutron rate to saturate and even decrease (roll-over). Such a degradation is often associated with either a sawtooth crash or a giant ELM but this is not the case for the discharge shown in

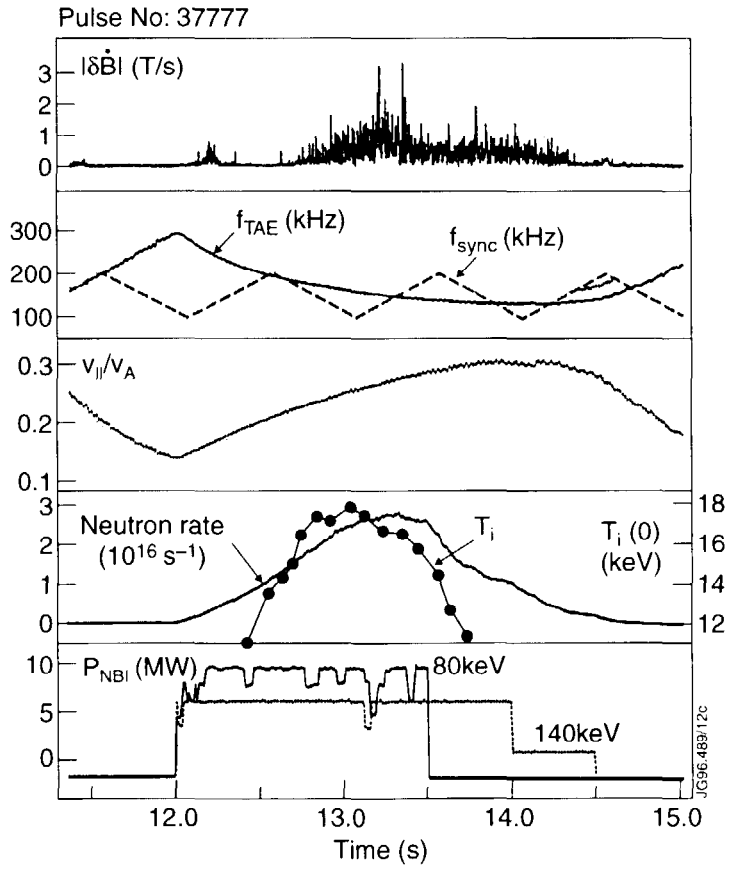

Fig.4 TAE modes excited by NBI at $v_{//} \cong v_A/3$ in a hot ion H-mode.

Fig.4. Some statistics of the resonance condition at the soft roll-over for the 140keV beams are shown in Fig.5. These data were taken for plasma currents ranging from 1.7MA to 5.1MA and for toroidal fields between 2.1T and 3.4T. Almost all the points lie in the range $v_{//}/v_A = 0.3 \pm 0.05$.

Since the signals are of the order of 10^{-6}T the eigenmodes need to be kinetic TAE to possibly affect fast ion confinement. Such KTAE modes [3] have been driven by the saddle coils. An example is shown in Fig.6 for a 3MA, 3.1T plasma heated by 6MW of ICRH and 2.5MW of lower hybrid heating. Figure 6 shows the magnetic field and density oscillation amplitudes. The constant frequency difference between modes for the same mode number and the fact that the frequencies are greater than the TAE frequency are characteristic of KTAE modes.

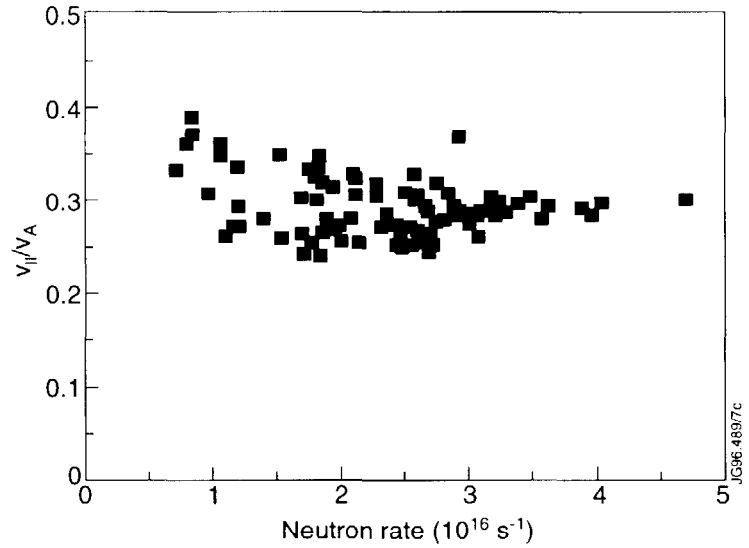

Fig.5 Ratio of $v_{//}/v_A$ for TAE destabilisation in hot ion H-modes

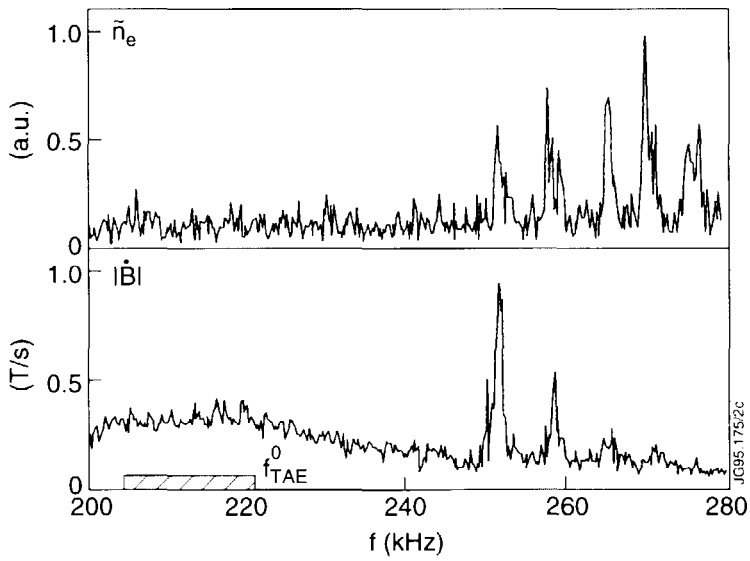

Fig.6 Observation of KTAE modes in an ICRH + LHCD heated plasma

Theoretical calculations of the effect of KTAE modes on the fast ion distribution have been made using the HAGIS code [4] which gives a self-consistent treatment of the wave field and the fast ion distribution. HAGIS is an efficient Monte Carlo code which treats just the perturbation of the fast ions thereby saving a factor of 10^2 in the number of particles required. An example is shown in Fig.7 for α-particles with $<\beta>\sim 10^{-3}$, which is similar to values expected for 10MW of D-T fusion power in JET. The n=6 mode rises with a $\gamma/\omega = 3\%$ to a saturated level $\delta B/B = 10^{-3}$. Such a value is close to the threshold for stochasticity.

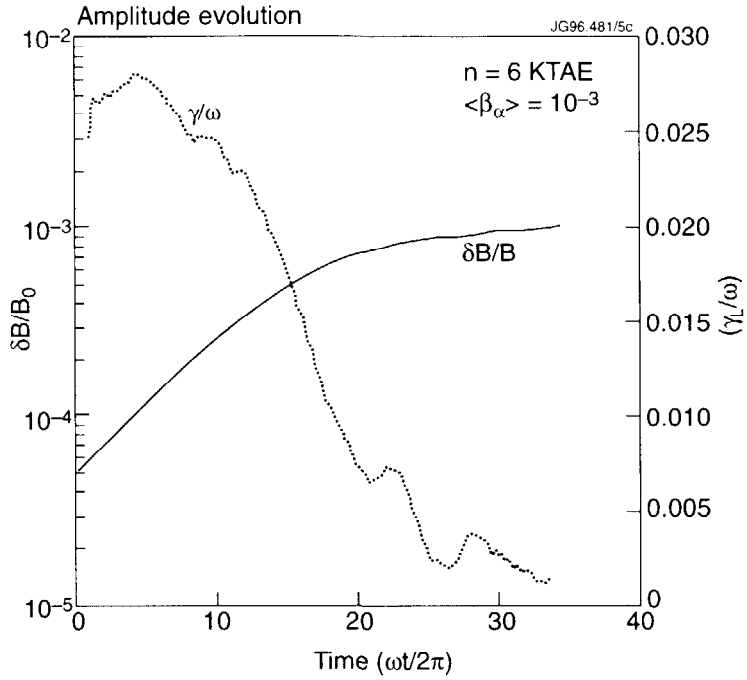

Fig.7 HAGIS prediction of KTAE amplitude and growth rate for 0.1% β_{fast}

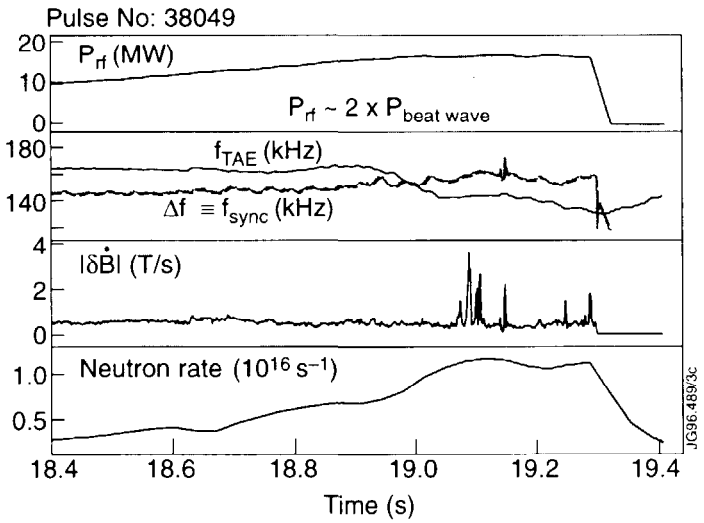

Fig.8 ICRH beat wave drive of TAE modes.

3.3 Excitation by ICRF beat waves.

Figure 8 shows the excitation of n = 3 TAE modes using ICRH beat waves [5]. In this discharge the difference in frequency between two ICRH antennas is around 160kHz and when the TAE frequency is close to this value (140kHz), TAE modes occur with large amplitude. Optimisation experiments have shown that the largest amplitude TAE modes are produced when the antenna phasing is $0\pi0\pi$ and adjacent rather than opposite antennas are used, probably due to the greater overlap of the RF fields.

4. SUMMARY

The JET saddle coils have been used to excite low-n TAE modes with a system which locks to the resonance frequency. The technique has demonstrated that fast neutral beam ions do not excite low n modes but can drive high n-modes unstable in accordance with theoretical expectations. The system will also be used in JET D-T experiments to measure the intrinsic excitation by α-particles. Neutral beam ions produce TAE modes when $v_{//} = v_A/3$ and there is possible evidence of performance limitation by such activity. Kinetic TAE modes have been observed and theoretical calculations suggest that these can be driven unstable at a fast ion beta value of only a few percent. A new method of directly exciting TAE modes using beat waves generated by fast waves has been established. Simulated α-particle heating using MeV fast ions generated by ICRH has produced electron temperatures up to 15keV. Transport analysis of such discharges has shown a factor of two improvement in χ_e in the core of hot-ion H-modes and reversed shear plasmas compared to RF-only ELMy plasmas. A neutron rate of $9 \times 10^{15} s^{-1}$ has been attained by third harmonic deuterium ICRH. This has been successfully reproduced by the PION code which is used extensively to predict D-T performance in JET and ITER.

ACKNOWLEDGEMENT

This work was performed under Task Agreements with CRPP, Lausanne, Switzerland, UKAEA Culham Laboratory, Abingdon, UK and CEA, Cadarache, France, and in collaboration with Princeton Plasma Physics Laboratory, Princeton, USA and Institute for Fusion Studies, University of Texas, Texas, USA.

REFERENCES

[1] ERIKSSON, L.G., et al., Nucl. Fusion **33** (1993) 1037.
[2] FASOLI, A., et al., Nucl. Fusion **35** (1995) 1485.
[3] HUYSMANS, G.T.A., et al., Phys. Fluids **B 5** (1993) 1545.
[4] APPEL, L.C., et al., Nucl. Fusion **35** (1995) 697.
[5] FASOLI, A., et al., Nucl. Fusion **36** (1996) 258.

PERFORMANCE LIMITATIONS IN JET HOT-ION H-MODES

The JET Team[1]
(presented by PR Thomas)

JET Joint Undertaking,
Abingdon, Oxfordshire,
United Kingdom.

Abstract

Hot ion H-modes have produced the highest fusion yields in JET and will play an important role in future DT experiments. The high yield phase of these plasmas is transient and is terminated, usually irreversibly, by a deterioration of confinement associated with a variety of mhd activity. In this paper, the limiting phenomena are described and the identification of the mhd modes made. The connection between the mhd and the confinement deterioration is not entirely clear; several hypotheses are outlined but none has been confirmed unequivocally. The irreversibility is due to a combination of confinement degradation and density increase, which reduces central power deposition by neutral beams and couples the ion and electron temperatures. The prospects for reducing or removing the performance limitations are discussed.

1. INTRODUCTION

Hot-ion H-modes, heated by high power neutral beams and supplemented in some cases by ICRF, have produced the highest fusion yields in JET [1] and will form a cornerstone of the forthcoming DT experiment, DTE1. However, the phase during which high fusion yield is obtained is short-lived and decays, usually irreversibly, to a lower level of performance after 1-2s. This performance deterioration is due to a fall in energy confinement which is associated with a variety of mhd activity. Developing an understanding of the processes which influence the observed behaviour is an essential element of the JET programme as they limit the peak fusion output and its duration. Also, these phenomena introduce variability in the fusion performance which is a concern for DTE1.

This paper will restrict itself to the hot ion H-mode because the reverse shear regime [2] is a relatively new development in JET and the study of the performance limitation mechanisms has only just commenced. Furthermore, disruptions and vertical displacement events either limit performance directly or constrain the operating space to the same effect but these are described elsewhere [3].

2. A DESCRIPTION OF THE PERFORMANCE LIMITATION

High power neutral beam heating is applied to a low recycling, low density divertor plasma. After a period of threshold ELMs, an ELM-free H-mode starts in which the energy, density and fusion power rise continuously until a terminating event occurs; after which the confinement is degraded. Shortly before the terminating event, the plasmas are characterised by energy confinement up to 1.4 times ITERH93-P and central ion temperatures up to 30keV. During the ELM-free phase, the confinement barrier forms a very pronounced edge pedestal, particularly in the ion temperature, and a significant bootstrap current flows at or

[1] See Appendix to IAEA-CN-64/O1-4, The JET Team (presented by J Jacquinot).

near to the separatrix. Pressure gradients approaching $1MPa.m^{-1}$ are found in the barrier region and have a profound effect on plasma stability.

The termination of the high performance phase is often triggered by a global MHD event such as an ELM or a sawtooth collapse plus ELM. Here and in the following, ELM is used unambiguously to mean type I [4] or giant ELMs. Many terminations do not show such global mhd but instead have low m/n activity close to the edge; dubbed "outer modes" [5]. The outer modes are associated with a reduction in confinement and a rapid fall in fusion rate.

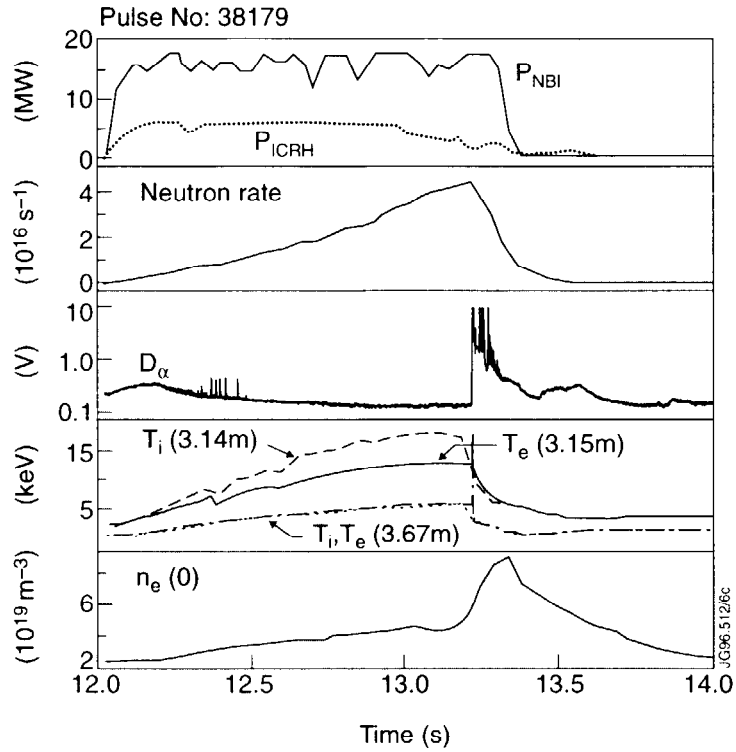

Fig.1 The time history of an hot ion H-mode, heated with NBI and ICRH, which terminates with an ELM. Shown are the heating powers, the neutron rate, the D_α rate, temperatures near the axis and half minor radius and, last, the central electron density.

The distribution between the various kinds of mhd is rather uniform. More than half the terminations involve two or more kinds of mhd instability together. The mhd do not always cause a termination but their ability to do so increase throughout the ELM-free phase. In view of this and the small amplitude of outer modes, compared with the resulting transport, it is supposed that the mhd is coupling to the underlying transport mechanism to trigger a change of state.

A termination which is triggered by an ELM is seen in Fig.1. The D_α spike at the ELM lasts tens to hundreds of ms and corresponds to ionisation of order of the plasma ion inventory; up to 10^{22} ionisations. This is reflected in an increase in plasma density, which can double in a few hundred ms. The outer half of the pressure profile is eaten away by the ELM, as illustrated in Fig.2; after which a cold wave propagates to the core and the central pressure starts to decline. The fusion rate falls because of the propagation of the cold wave to the core and the cooling due to the density increase.

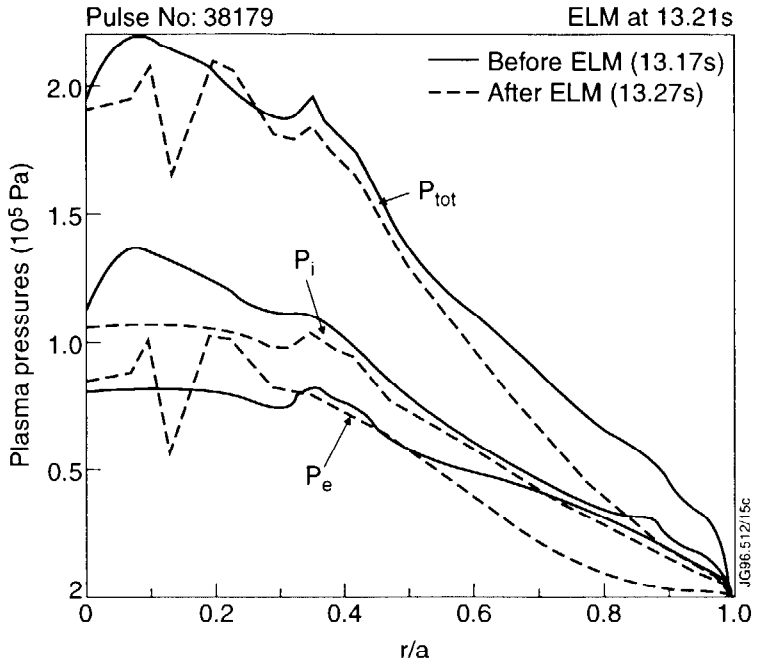

Fig.2: The pressure profiles before and after a terminating giant ELM. P_{tot}, P_i and P_e are the total, ion and electron pressures respectively. Note that the ELM has eaten away the outer half of the electron profile,in particular.

A sawtooth, or other core mhd, becomes an effective cause of confinement limitation above β_N~1.5, or so, because a large proportion of the plasma cross-section is affected and strong coupling to ELMs and outer modes occurs. The core pressure collapses and the energy is distributed in the outer regions of the plasma column. When the core mhd triggers an ELM or outer mode, the decrement of the core energy is able to propagate through the outer regions of the plasma, with little or no change to the pressure or temperature profiles there. This implies that a plasma, in these conditions, must be able to support different levels of transport.

Outer modes are observed in the outer regions of the plasma; typically near the q=3 surface, as shown in Fig.2. Toroidal mode numbers 1-4 and poloidal mode numbers 3-12 are observed. Modes with n=1 typically have a frequency of around 10kHz. A noticable signature of the outer mode is a small, slow increase in the D_α emission which indicates a loss of confinement. As well as an immediate deterioration of core confinement, a cold pulse propagates into the plasma core over tens of ms and together cause the degradation of fusion performance. Evidently, the irreversible performance limitation due to an outer mode alone arises from the particle influxes which are rapidly transported inwards through the region affected by mhd. Note, however, that the plasma can recover from the effects of outer modes which occur early in the ELM-free period.

Prior to the installation of the pumped divertor [6,7], the loss in confinement generated a heat pulse which caused a rise in target tile temperature and generated a carbon bloom. The resultant influx of impurities, coupled with the rise in core transport, prevented any recovery in performance and confused the analysis of the core behaviour. The improved design of the pumped divertor target has eliminated the carbon bloom. However, the link between the mhd instabilities and the loss of core confinement remain unclear and the resulting change in performance continues to be irreversible, for the reasons described above. Even without the carbon bloom, impurity influxes increase during the

terminating mhd activity, as does the main plasma Z_{eff}. It seems, that although impurities might contribute to the performance deterioration, they are not fundamental to the observed behaviour.

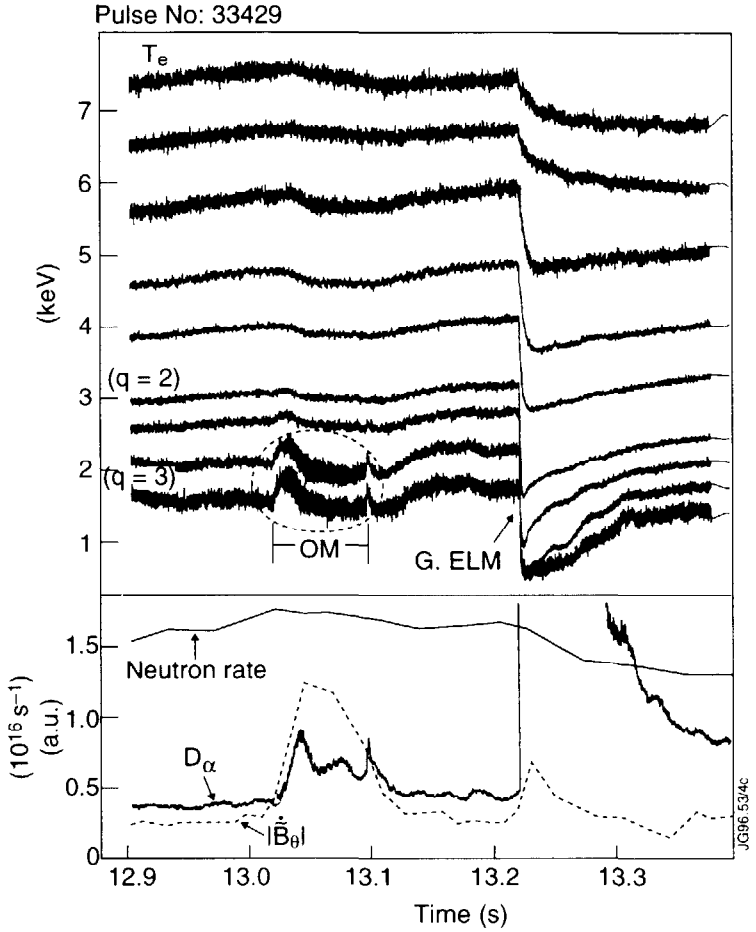

Fig.3 A plasma limited by an outer mode (OM) and a giant ELM (G.ELM). A range of electron temperature traces are shown from the axis to the plasma periphery, together with the neutron rate, D_α and magnetic pick-up coil signals.

Magnetic fluctuations, identified as TAE modes [8], are often observed during performance limitations ascribed to outer modes. It is found that their onset is coincident with the plasma density rising to the point where some of the slowing-down NB particles are resonant with $v_A/3$. Some improvement in the comparison between the measured neutron yield and that estimated from the profiles can be obtained if it is assumed that this resonance causes ejection of the fast ions. However, plasmas have been obtained where TAE modes should have been excited but which have good agreement between experimental and simulated neutron yields. Thus, definitive experiments and measurements will have to be devised before the role of TAEs in these plasmas can be clarified and the fast ion losses demonstrated.

3. MHD STABILITY ANALYSIS

The ideal mhd stability of the hot ion H-modes has been studied; both against low m,n kinks and ballooning modes. It is found that the edge pedestals are very important for determining mhd stability. The pressure gradient is such that, before the terminating events, it is close to or at the ballooning limit. The pressure gradient also drives a bootstrap current which is close enough to the separatrix surface to drive kink instability. This is illustrated in Fig.4 by plotting the trajectory of plasmas in the edge pressure gradient versus normalised edge current density space. The stable region is bound from above by the ballooning limit and on the right by kink instability. Different hot ion H-modes appear to limit at both boundaries and suffer ELMs where the boundaries meet. An important determinant of the trajectory is the recycling level or edge density; when these are high the ballooning boundary is encountered first.

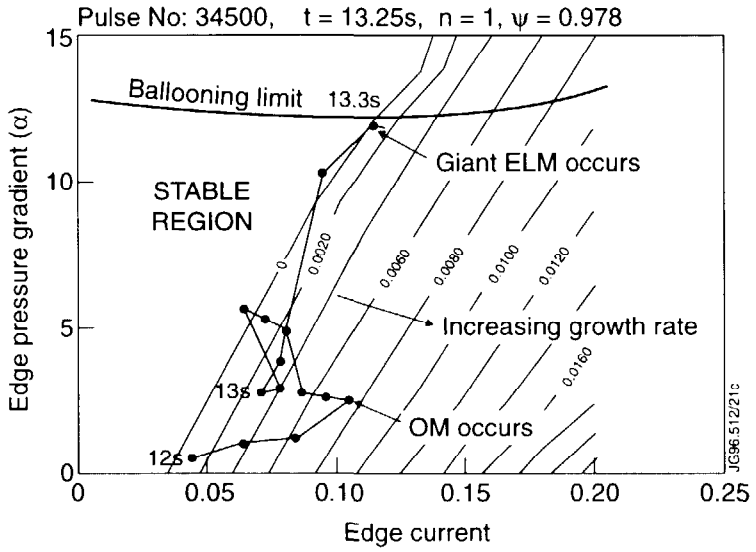

Fig.4 Edge stability diagram of normalised pressure gradient($=2\mu_0 Rq^2 p'/B_T^2$) versus normalised edge current($=J_{edge}/J_0$). The lines to the right of the stable region are contours of the ideal kink growth rate. The trajectory of pulse 34500 (see Fig.7), which showed outer modes and ELMs can be seen.

Analysis, using the CASTOR code [9], shows that ideal external kinks, with n=1-4 are linearly unstable when outer modes are present. The vessel wall in JET is too far from the plasma to have any significant stabilising effect. That outer modes are observed when instability is predicted and with n values from 1 to at least 4, encourages the identification of outer modes with saturated kinks.

The structure of outer modes, measured with the internal soft X-ray cameras, has been compared with the computed kink eigenmodes. This has been done by distorting the equilibrium soft X-ray emission profile by the kink displacements and recomputing the signal which should be seen in the individual detectors. The approach is suited to identifying kink modes because the concentration of lobes around the X-point and the top of the plasma leads to phase inversions in the fluctuations between adjacent detectors. This is in fact what is observed and the observed phases show excellent agreement with the kink mode simulations, as seen in Fig.5. The fluctuating amplitudes are in reasonable agreement. The predicted displacement amplification, of ~1.2cm in the midplane

to ~15cm at the X-point, due to the poloidal flux expansion, is confirmed by the data.

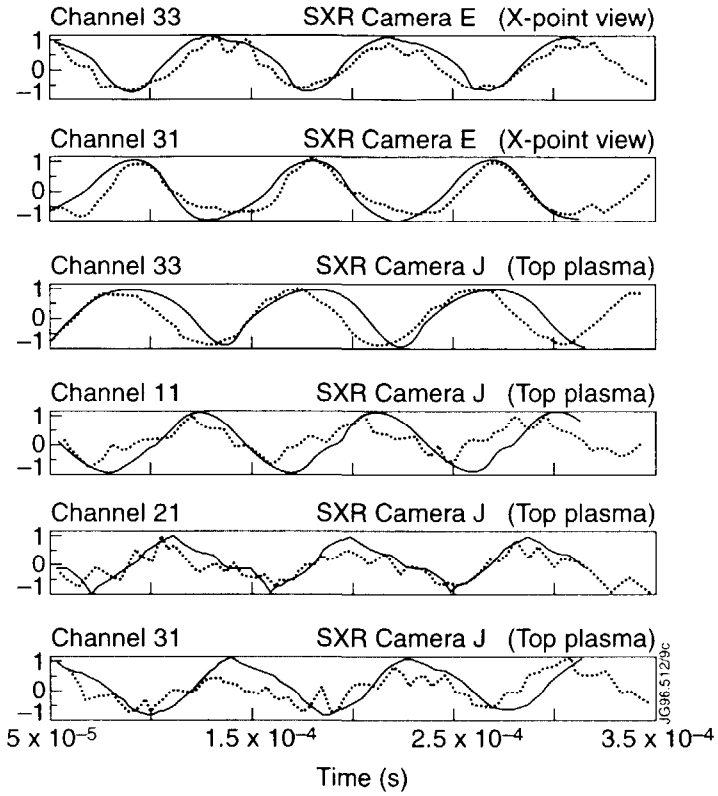

Fig.5 The comparison of the phases of a number of soft X-ray camera signals(·····) with the simulation described in the text(——). The top two panels are particularly significant for showing the 180° phase shift between adjacent channels, looking towards the X-point.

Tearing modes have also been simulated and compared with the outer mode soft X-ray signals, using the same method. Extra structure appears in the simulated signals because of the phase inversion within the resonant surface. The data show no signs of this structure, so securing the identification of the outer mode with ideal kinks.

The β_N at which outer modes appear decreases with increasing plasma current and magnetic field, or equivalently decreasing collisionality. It has been suggested that this is indicative of the importance of neoclassical mhd. There is no evidence to support this conjecture; particularly in respect of the lack of β dependence in the strength of the observed modes and the lack of any signs of tearing. In fact, there is evidence that the fall-off in β_N is an effect of the transport processes operating in this plasma regime, as discussed later.

In discharges limited by an ELM, the edge pressure gradient, evaluated at the 95% flux surface, is at or close to the ideal ballooning limit. A range of different plasma conditions confirm this and the experimental dependence on shear and poloidal field strength correspond to theoretical expectations.

However, there is no direct experimental evidence for ballooning modes at or near the termination of hot ion H-modes in JET. The difficulty of detecting them is probably the determining factor here; not only is the current bandwidth of the data aquisition system smaller than is desirable for this purpose but the predicted unstable region is also in the low emissivity part of the plasma.

However, the pressure profile has been observed to saturate at the ballooning limit for hundreds of ms before the terminating ELM, as seen in Fig.6. Whilst not definitive, this does indicate that ballooning modes are playing a role in ELM terminations.

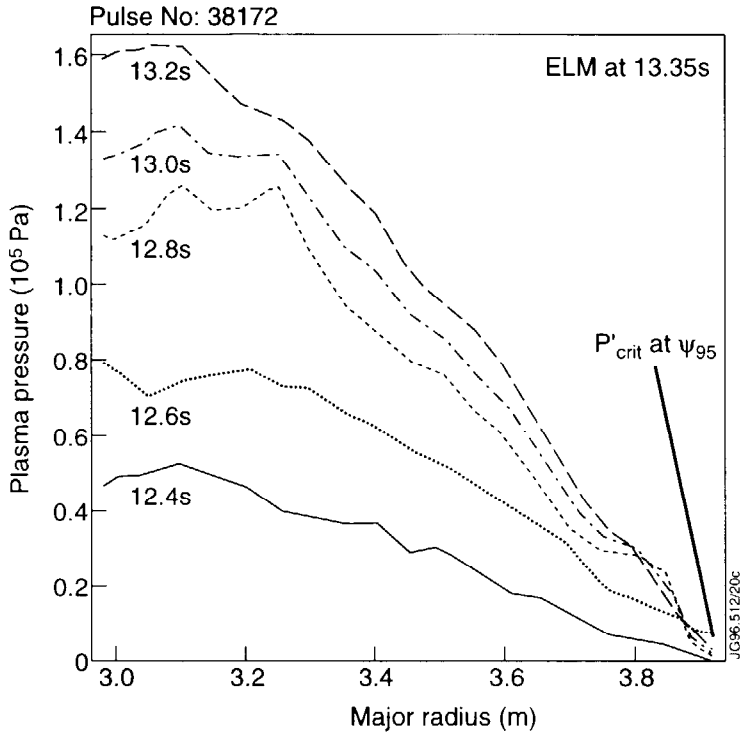

Fig.6 A sequence of pressure profiles, obtained from Thomson scattering and charge exchange recombination spectroscopy, for a pulse which had an ELM at 13.35s. Also shown is the critical pressure gradient for ideal ballooning at the 95% flux surface.

Plasmas limited by ELMs are also predicted to be unstable to kinks. Soft X-ray cameras show precursors to many giant ELMs with the same characteristics as outer modes and lasting tens of ms. In these cases, the degradation of fusion power starts with the outer mode and is not greatly perturbed by the ELM. Given the identification described above, it is likely therefore that kinks are also observed in conjunction with ELMs.

It seems possible that the combination of ballooning and kink instability is needed for ELMs to occur; although it should be stressed that there is no evidence to support this and that there are ELMs with no detectable precursor activity. Nonetheless, the conjunction between predicted instability of both modes and their observation in conjunction with ELMs does seem compelling.

4. TRANSPORT EFFECTS DURING TERMINATION

The relationship between the observed mhd activity and the substantial drop in confinement which occurs is a persistent conundrum. The mhd activity is short lived, with timescales 100μs-100ms. However, the global energy confinement, which usually increases throughout the high performance phase, falls at the termination, by as much as a factor of three, and the neutron yield declines thereafter, usually irreversibly. The irreversibility is likely to be due both to the deteriorated confinement and the density increase, which results from ELMs

particularly, preventing a rebuilding of central pressure and a separation of the ion and electron temperatures.

In cases with a core temperature collapse, the outer temperature and pressure profiles can recover to their pre-termination values. The core losses, which can amount to tens of MW, are transported through the outer region which had been transporting approximately 10MW. This increased heat transport where plasma conditions are unchanged is perhaps indicative of proximity to a turbulent threshold or of super-critical conditions, where a perturbation can trigger a return to degraded transport. Such behaviour is observed during the L-H transition and is the reason why simulations rely on core transport models which depend on edge conditions in order to reproduce the data.

It is clear that outer modes cannot directly cause the associated transport deterioration; there is no sign of tearing and their amplitude is, in any case, too small. Analysis of pulse 34500, shown in Fig.7, indicates that an outer mode increased the effective conductivity from 1.5 to $6m^2s^{-1}$ at the plasma edge. The analysis also shows the outer 25% of the plasma to be exhibiting transport enhanced to the level characteristic of ELMy H-modes. A typical amplitude of $|\delta B/B_\theta| \approx 2.10^{-4}$ would correspond to an island width of 0.025m, if tearing were occurring. In contrast, the island width needed to match the observed change in ion transport is estimated to be 0.2m, assuming ion-ion collisions and a step size equal to the island width. Thus, even were tearing detected, the resulting transport would be smaller than that observed by at least an order of magnitude.

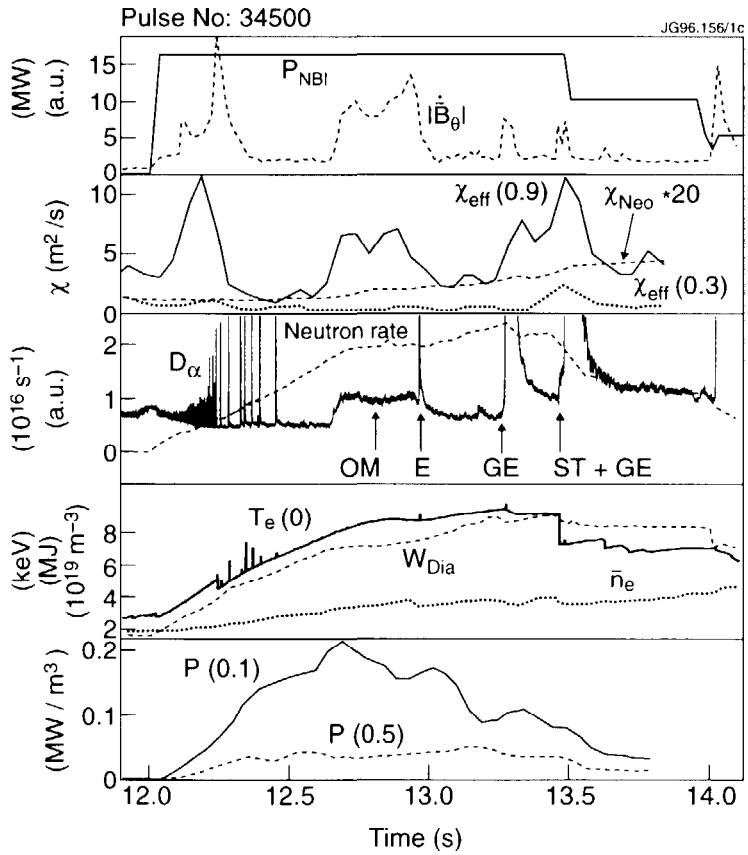

Fig.7 Time history for a pulse which has a range of limiting activity; an outer mode (OM), ELMs (E and GE) and sawtooth plus ELM (ST+GE). The effect on the effective plasma conductivity is shown in the second box.

ELMs have a similar effect on the effective conductivity to outer modes and act over the same outer part of the plasma cross-section. This might not be too surprising if an important component of the ELM is an outer mode.

A number of potential mechanisms for the link between mhd and transport have been investigated:

(i) That mhd induced changes in density profiles lead to poorer NB deposition has been shown to be insufficient of itself. Not only is the deposition profile being both calculated to be continuous across the mhd events but Beam Emission Spectroscopy, monitoring the profile of beam D_α, shows this as well. Thus, whilst there is a degradation of beam deposition from the start of heating to the time of peak performance, the sudden change in energy confinement at termination cannot be ascribed to a corresponding change of power deposition.

(ii) Loss of the confinement barrier alone is not sufficient to reproduce the observed behaviour. The sudden change in confinement at termination, or during an outer mode, clearly encompasses one quarter to one half of the outside of the plasma cross-section and is felt in the core as well.

(iii) ELMs generate as much ionisation in a few tens of ms as the plasma ion content. A hypothesis that the neutral cloud could penetrate to the core and so cause enhanced charge exchange losses there, is not borne out either by modelling or by experiments involving large gas puffs. In these experiments, a gas puff, of 100ms duration and magnitude to match the D_α spikes of terminations in similar pulses, was injected late in the ELM free phase of high performance plasmas. It was found that the edge cooled somewhat and that the cold pulse propagated to the plasma core on a timescale consistent with transport which was not degraded.

(iv) Transport models which connect edge conditions to core transport [10] give a satisfactory account of most termination events. Further evidence for these models is found in their ability to reproduce the gas puff experiments, described in the previous paragraph, and ability of laser ablation injection of impurities to cause changes in transport which propagate rapidly to the core. Also, the propagation of the L-H transition is reproduced. These observations encourage the belief that the transport mechanism is in some way extensive and that edge conditions are able to affect core transport.

(v) As described at the end of Section 2, magnetic activity, identified as TAE modes, is seen during fusion rate roll-over associated with outer modes. Unlike the other mechanisms, (i)-(iv), TAE modes would cause confinement degradation by reducing the input power density, rather than acting on the plasma losses. The TAE modes could be triggered by the outer mode induced density rise dropping the Alfven velocity to match the resonance condition with the beam ions. Instability requires sufficient fast ion pressure gradient. It might be that this lies behind the variablity in the observation of shortfalls in fusion yield which could be ascribed to TAE modes and underwrites the need to verify that TAEs cause fast ion losses at all.

The data might be interpreted as showing that mhd can directly modulate the turbulence causing transport. Except for TAE modes, as described in (v) above, there do not seem to be any candidates for interactions of this kind. Since there is other evidence which indicates that the edge temperature can affect the core plasma transport, this seems the most natural mechanism for connecting mhd with the loss of confinement in the terminating events. Success in simulations encourages this view. However, unambiguous corroboration of this model is likely to be very difficult to obtain and will have to await further progress in understanding transport in general.

5. PERFORMANCE IMPROVEMENT

In principle, substantial improvements in fusion performance can be obtained by increasing the magnetic field at constant q. If it is assumed that the β limit is independent of field strength, the fusion yield should improve roughly as the fourth power of the field. For example, hot-ion H-modes at 1.7MA/1.5T are able to reach the Troyon limit and profile analysis shows that they approach 60% of the ballooning limit across the entire plasma, as seen in Fig.8(a). In contrast, their 3.8MA/3.4T counterparts Fig.8(b) achieve only β_N~1.7 or so and are far from the ballooning limit, except in the outer region of the plasma. This seems to be a transport effect and modelling has been able to reproduce the difference.

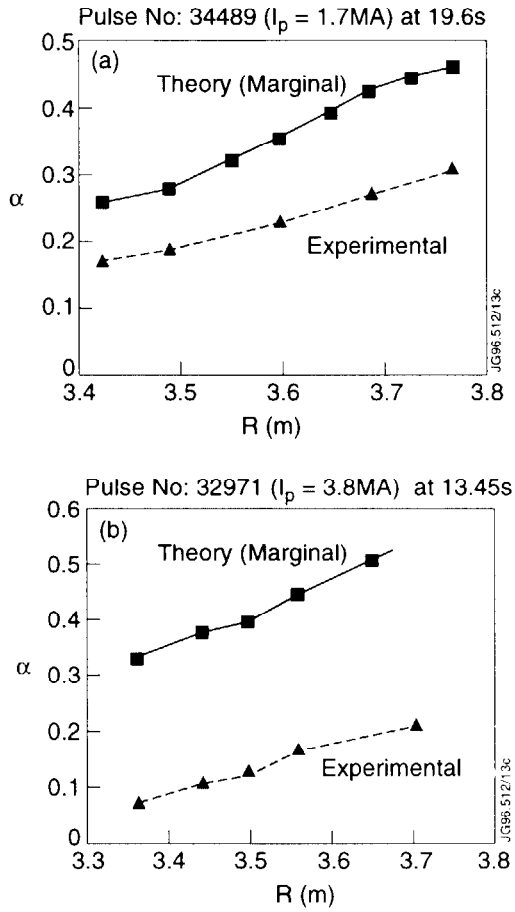

Fig.8 A comparison of the experimental profile of plasma pressure gradient compared with the ballooning threshold for (a) 1.7MA/1.5T and (b) 3.8MA/3.4T.

The mixed Bohm/gyro-Bohm transport model, coupled to the neoclassical barrier model, has successfully simulated the 1.7MA and 3.8MA pulses. The termination of the high performance phase was represented by ideal ballooning and a limit on the edge bootstrap current, as a proportion of the plasma current, to reproduce the kink instability. It is a feature of the two components of the confinement model that the barrier improves more rapidly with magnetic field than the core confinement. Thus, in the 3.8MA pulses the ratio of the edge pressure gradient to that in the core is such that the mhd limits are encountered in the edge region long before the core. In contrast, the 1.7MA pulses limit more or

less uniformly across the plasma cross-section. The density scale length in the barrier region has so far proven to be smaller than JET's diagnostics have been able to resolve. Thus it has not been possible to confirm the modelling results directly. However, the model edge pressure profiles are consistent with experiment, particularly in respect of the magnitude of the pedestal, so it is feasible that the relatively poor performance at high current is due to a transport effect. The only clear way forward is to increase the central power density at the start of the high power heating, in order that more energy is placed in the core before the heat wave arrives at the boundary and triggers the observed mhd instabilities.

Since the trigger appears to be mhd instability, it must be possible to ameliorate the behaviour, and so improve JET's fusion performance, by modification of pressure and current density profiles. A modest success in profile control has been achieved by ramping down the plasma current during the ELM-free phase. This has the effect of reducing the edge current density and so stabilising outer modes. Unfortunately, the other forms of mhd limitation replace the outer modes sooner or later and this technique does not offer any prospects for steady state!

6. CONCLUSIONS

The high performance phase of hot-ion H-modes is terminated by a loss of confinement which appears to be triggered by mhd instabilities.

The mhd instabilities concerned are giant ELMs, sawteeth and outer modes, either individually or in combination. Theory and experiment are in quite good accord as to the identity and occurrence of the offending modes. The so-called outer modes have been identified as saturated low n/m external kink modes. Giant ELMs occur when the plasma is calculated to be unstable against kinks and ballooning modes simultaneously. Outer modes are observed as precursors to many ELMs. Ballooning modes have not been detected for these conditions but this is thought to be due to the diagnostic difficulty. However, the edge pressure gradient is observed to saturate at the ballooning limit for many hundreds of ms before some ELMs thus lending credence to their importance.

The most likely mechanism to connect the mhd instability with the loss of confinement is that which connects core transport with edge plasma conditions. Heuristic models based on this idea account for a range of phenomena observed in tokamaks, including the L-H transition, the propogation of cold waves following gas puffs or laser ablation impurity injection and, in combination with a neoclassical model for the barrier losses, the time delay to terminating ELMs. The detection of TAE modes during fusion rate roll-overs has led to the conjecture that the TAEs are ejecting slowing-down NB ions but this has not been proven.

If it is assumed that the mhd instability triggers the termination of the high performance phase, it should be possible to improve the fusion yield of these plasmas. However, the most destabilising features, the pressure pedestal and the resulting bootstrap current, are fundamental to the regime and amelioration might not be possible. Thus, the profile modifications which are most likely to succeed are those which peak up the core pressure relative to the pedestal: increased neutral beam power, to boost the core energy content before the heat pulse arrives at the confinement barrier; shear reversal to establish an internal confinement barrier and sawtooth suppression. All of these will be tried at JET in the near future.

REFERENCES

[1] THE JET TEAM (presented by P. Lomas), IAEA-CN-64/A1-1, this Conference.
[2] THE JET TEAM (presented by C. Gormezano), IAEA-CN-64/A5-5, this Conference.
[3] THE JET TEAM (presented by A. Tanga), IAEA-CN-64/AP1-18, this Conference.
[4] ZOHM, H. et al., in Controlled Fusion and Plasma Physics (Proc. 19th Eur. Conf. Innsbruck, 1992), Vol. I, European Physical Society, Geneva (1992) 243.
[5] NAVE, F. et al., JET Report JET-P(96)14, submitted to Nuclear Fusion.
[6] THE JET TEAM (presented by G. Vlases), IAEA-CN-64/A4-1, this conference.
[7] THE JET TEAM (presented by J. Jacquinot), IAEA-CN-64/O1-4, this Conference.
[8] THE JET TEAM (presented by D. Start), IAEA-CN-64/A2-6, this Conference.
[9] HUYSMANS, G., GOEDBLOED, J. and KERNER, W., Phys. Fluids B **5** (1993) 1545.
[10] THE JET TEAM (presented by A. Taroni), IAEA-CN-64/D3-3, this Conference.

DISRUPTIONS AND VERTICAL DISPLACEMENT EVENTS IN JET

The JET Team[1]
(Presented by A Tanga)

JET Joint Undertaking,
Abingdon, Oxfordshire,
United Kingdom.

Abstract

Major disruptions and vertical displacement events (VDE's) represent a serious problem for the integrity of large devices such as ITER and a reactor. This arises from the localised power deposition on the divertor target and first wall, the production of runaway electrons in the post-disruptive plasma and the substantial forces transmitted to the vacuum vessel by eddy and halo currents. Extensive experiments have been performed in JET to characterise the phenomena associated with disruptions and VDE's and to investigate the underlying physics. In addition, the installation of a disruption feedback stabilisation system based on a set of 4 internal saddle coils driven by high power (3kA/1.5kV), high frequency (0-10kHz) amplifiers has allowed initial experiments on the control of disruptions by suppression of the n=1 mhd precursor. This system has also been used to study fundamental aspects of the physics of error field induced modes, which is of direct application to ITER.

1. VERTICAL DISPLACEMENT EVENT (VDE)

For the Pumped Divertor phase of JET, an improved vertical stabilisation system, designed to stabilise vertical instability growth rates of up to $1000s^{-1}$ was installed. Under quiescent conditions, this has proven capable of stabilising all plasma equilibria used at elongations of up to 1.9. Whilst disruptions are rather frequent, (40 - 60% of the total pulses) high current disruptions and VDE events are relatively rare occurrences (< 10%) of the total number of disruptions. However these kind of disruptions, which produce the largest forces and halo current, are of the highest interest. A major problem relating to control of the vertical position was encountered at disruptions, as was observed in the original JET configuration, and at edge localised modes (ELM's). This loss of control was generally experienced at singular giant ELM's in highly shaped plasmas, which often terminated the long ELM-free H-modes in high fusion performance experiments. At such ELM's, a rapid displacement of the plasma occurred, generally inwards and upwards, and as a result, the plasma usually made contact with the upper inner wall region. The sudden plasma movement led to a rapid rise in the radial field current to the limiting value of 2.5kA on a timescale of ~ 5ms, the upper level of the radial field amplifier was exceeded, and a VDE resulted. Typical traces for a VDE event are shown in Fig.1.

Within a timescale of ~ 100μs the thermal energy is deposited on the target plates as shown by infrared fast camera observations and the plasma moves vertically as shown by magnetic signals (n=0). Langmuir probe observations support the hypothesis of a toroidal SOL current of the order of 10kA, intercepted by the divertor target during ELM's.

[1] See Appendix to IAEA-CN-64/O1-4, The JET Team (presented by J Jacquinot).

Using a simplified model of the vertical stabilisation it can be shown that such SOL current could produce a sufficiently large amplitude impulse to cause the loss of control with the subsequent VDE.

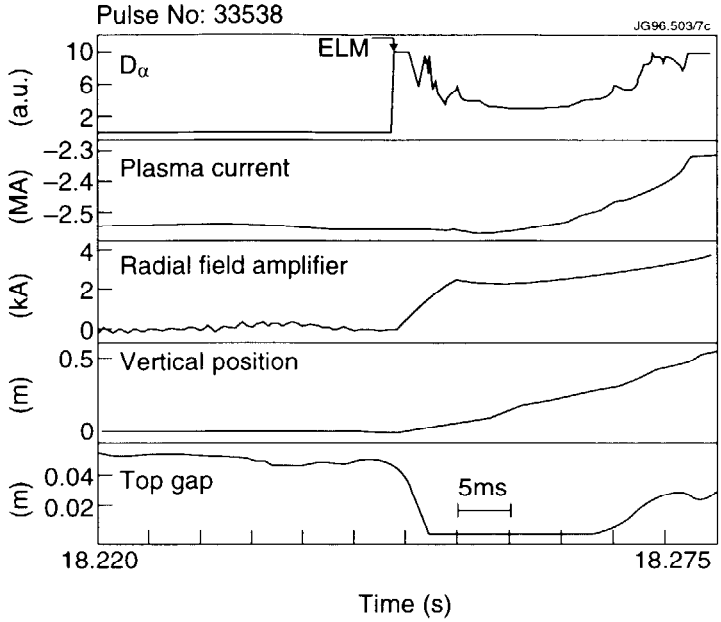

Fig.1 Time evolution of an upward VDE event following a giant ELM. Pulse number 33538.

2. DISRUPTION FORCES

Plasma disruptions produce forces primarily on the vacuum vessel. The study of the dynamic stresses on the vessel for a plasma disruption is performed by a FE shell model representing 180° of the vessel. The input for a disruption is obtained from the strain gauge data taking into account the plasma position signals.

In order to evaluate the forces produced by the plasma in a given configuration an estimate of the disruption dynamics is necessary. However, for the same plasma configuration the disruption dynamics changes considerably leading to a large variation of the forces produced.

2.1 Vertical forces

The vertical forces are generated by the plasma vertical movement during a disruption. They scale with the square of the plasma current as shown in Fig.2. The value of the vertical force therefore depends on the plasma configuration, on the plasma current and on the plasma dynamics. An empirical estimate of the maximum vertical force which can be generated in a given configuration (F number) is calibrated against the forces measured in disruptive plasma pulses [1].

At a comparable plasma current the disruptions which produce the large vertical forces are those caused by VDE, with loss of the vertical stabilisation in which the current movement product $I_p.\Delta Z$ is larger. On the other hand, disruptions in which the control of the vertical position is maintained during the decay of the plasma current, produce small or negligible vertical forces.

The frequency distribution of the vessel forces in the last 2 years of JET operations is shown in Fig.3. The distribution shows the higher forces produced by the downward disruptions despite the stabilisation effects of the currents induced in the divertor coils.

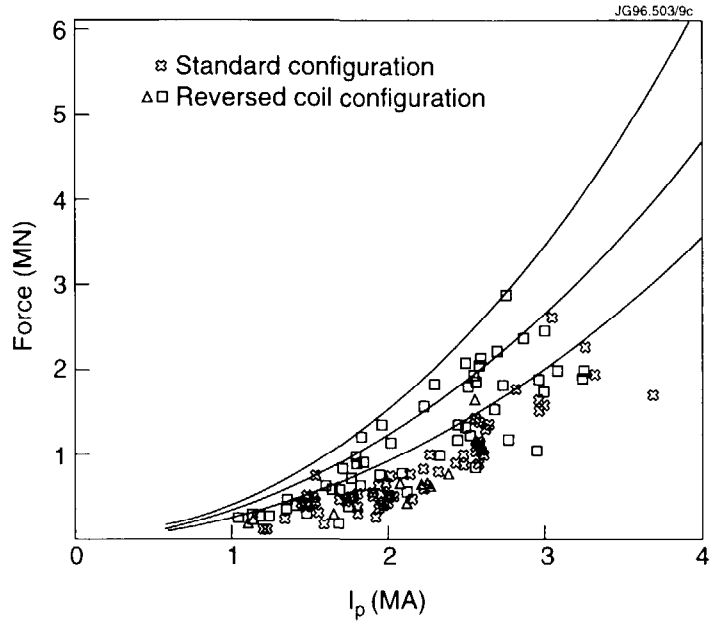

Fig.2 Measured vertical vessel force versus the plasma current prior to disruption.

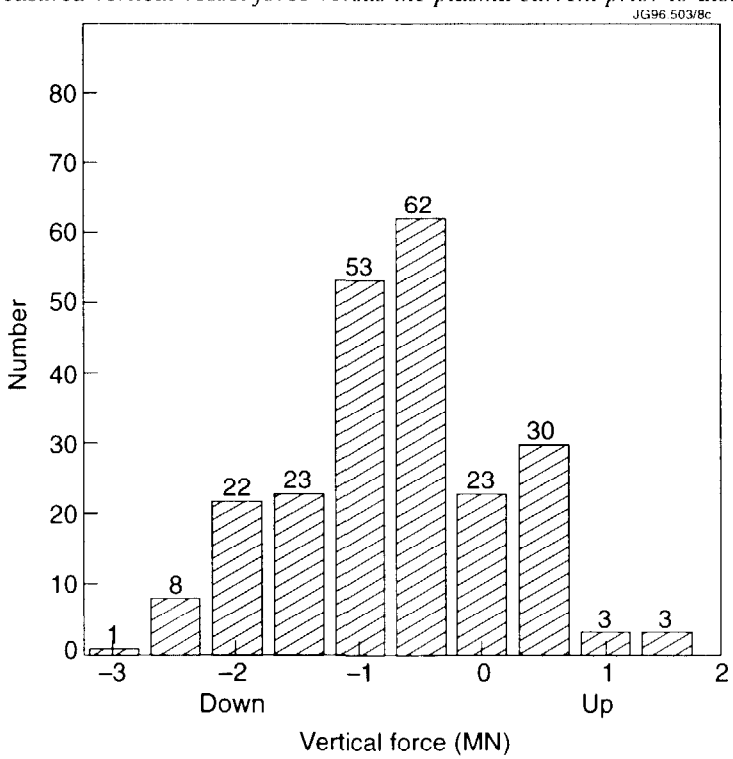

Fig.3 Distribution of the measured vertical vessel force for all the disruptions which occurred in 1996 (up to September 1996).

2.2 Halo currents

The halo currents sensitive diagnostics have been installed in the vacuum vessel: a pair of toroidal field pick up coils located on the top and bottom of the vessel, poloidal current shunts at 2 toroidal positions, a number of poloidally and

toroidally distributed shunts on the earthing connections of certain in-vessel components [2]. It has been found that the integrated estimated halo current scales with the measured vertical force.

The total average halo currents was found to be ≤ 20% of the initial plasma current, as shown in Fig.4.

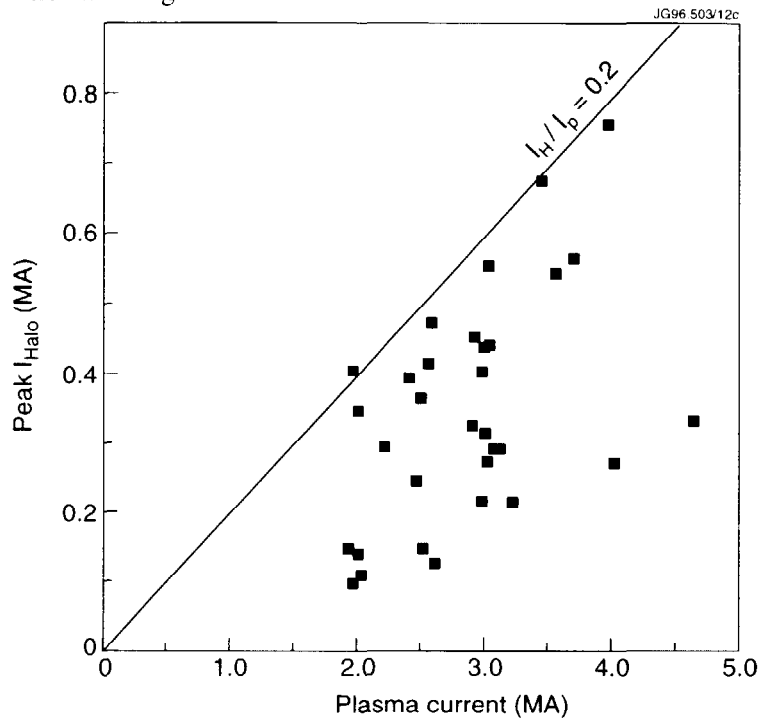

Fig.4 Integrated halo current versus plasma current prior to the disruption.

3. LATERAL DISPLACEMENTS

The vacuum vessel displacements are measured at the ports and the radial displacements are available on four octants at the upper and lower main vertical ports (MVP's) and all eight octants at the main horizontal port (MHP), where also the tangential displacements are measured.

The toroidal distribution of the halo current is given only for upwards disruptions.

Local measurements of intercepted halo currents and measurements of forces on the vessel supports indicate large time fluctuations and toroidal asymmetries of the halo current density in the presence of toroidal asymmetries of the global vertical forces acting on the JET vessel as measured from the 8 instrumented tiles in 8 locations at the top of the vessel. The typical trends are shown in Fig.5.

In the presence of the measured toroidally asymmetric halo currents a net lateral movement of the vacuum vessel was observed. The toroidal distribution of the time integrated halo currents peak was as high as twice the average as shown in Fig.6. The observed lateral movement of the vessel is associated with an apparent asymmetry of the measured plasma current centred at two different toroidal locations. The inferred m=1, n=1 island would be equivalent to a tilting of the plasma with a resulting force which needs to be balanced by other asymmetric toroidal forces such as induced or halo current forces. From the movement of the position of the plasma current centroid the apparent edge safety factor could be evaluated. A correlation has been found between large sideways movements and an estimated value of the safety factor between 1.0 and 1.3. From

the vector sums of the average octant displacements, it appears the whole vessel moved approximately by 5.6mm in the direction between octant 5 and 6.

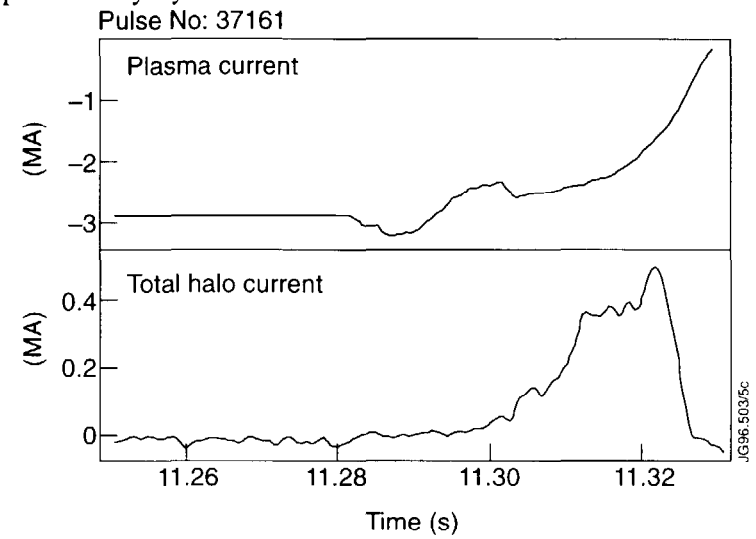

Fig.5 Time evolution of VDE and measured halo current for pulse 37161.

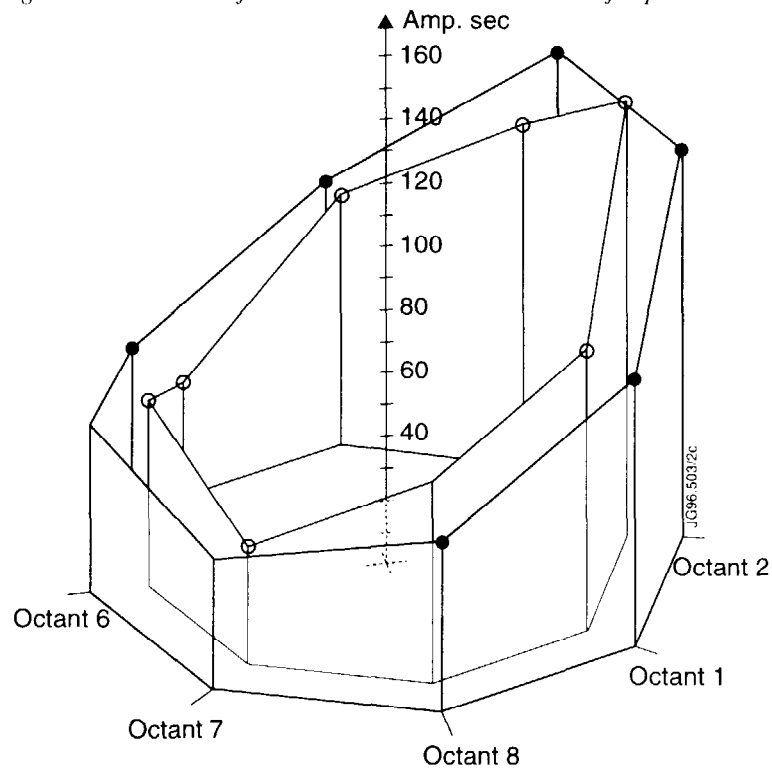

Fig.6 Time integrated mushroom tile current for pulse 34078 highly asymmetric disruption.

4. SADDLE COILS

Experiments on the influence of external error fields on mhd stability have been pursued using the internal saddle coil set [3]. n=1 'locked' modes induced by intrinsic error fields are considered to be significant for ITER since the critical error field threshold is predicted to be very low, $B_r/B_t \sim 2 \times 10^{-5}$.

Initial experiments have investigated the threshold for the static error field modes. In JET n=1 fields B_r as small as 0.12 mT (B_r/B_t~5 10^{-5}) are sufficient to penetrate (with n_e=1-1.4$10^{19}$m^{-3} q_{95}~3, I_p=1-1.5MA) and generate tearing modes. Figure 7 shows the linear dependence of the penetration threshold with the plasma electron density.

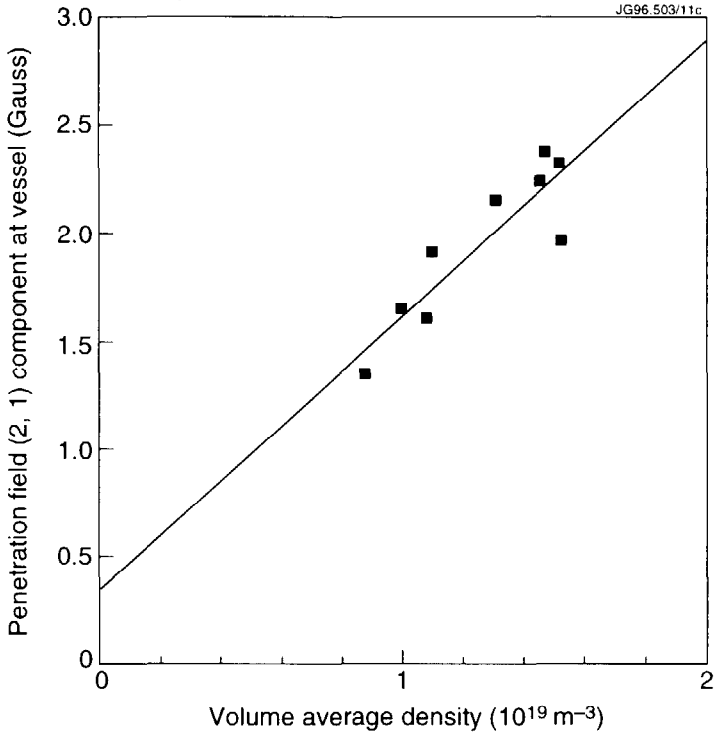

Fig.7 Penetration threshold (I_{SC}·B_{r21}) as a function of the average electron density n_e.

Rotating tearing modes have also been generated with the application of a small n=1 field rotating at a frequency close to the plasma rotation frequency.

The considerable scatter of the data shown in Fig.7 appears to depend on the details of the plasma equilibrium.

Magnetic feedback control has been applied in JET to saturated tearing modes. The amplitude and the position of the modes have been measured by four fast pickup coils. The spurious pickup due to the feedback vacuum field and to the ideal MHD plasma response to this field has been measured and compensated in the digital controller. The plasma ideal response is independent of the field frequency and strongly dependent on the plasma configuration and q value. Upon the application of the feedback AC field a modification of the growth rate of the tearing mode has been observed in a few pulses as shown in Fig.8.

It has not yet proved possible to stabilise tearing modes precursors of density limit disruptions because their high instability parameter Δ' and the low feedback gain applied.

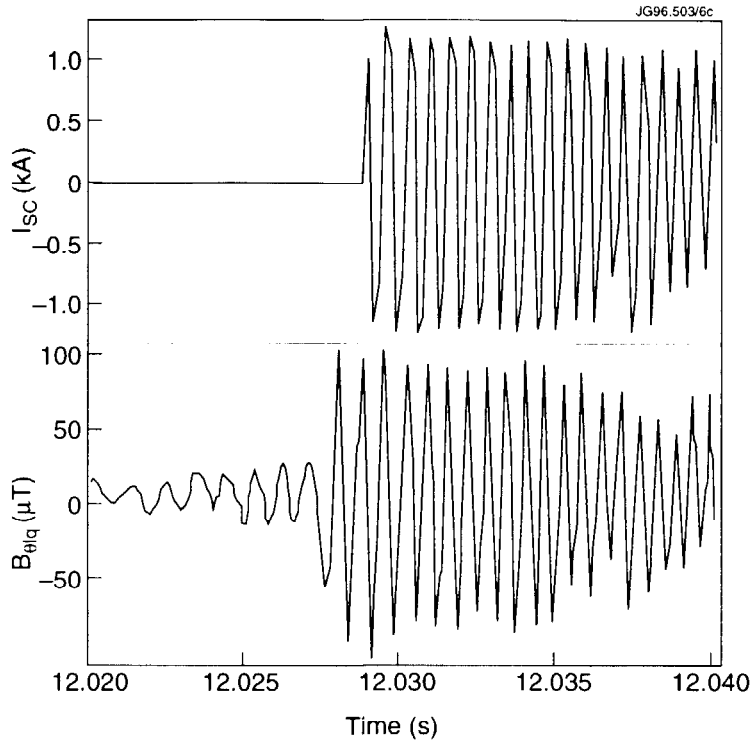

Fig.8 Modification of a tearing mode growth rate at the sudden application of the feedback current (I_{SC}). Feedback started by a trigger on mode amplitude at a field level of ~ 50μT. $B_{\theta lq}$= field at the poloidal limiter (n=1).

CONCLUSIONS

The analysis of the disruption dynamics and vessel forces in JET has shown that the large vertical forces produced by the elongated plasma cause both halo current forces localized on in-vessel components and stresses on the main vacuum vessel. VDE events producing the highest vertical forces cause sideways vessel displacements associated with a tilting of the plasma column. Experimental evidence shows that this event occurs when the limit q is in the region 1-1.3. Loss of control of vertical stabilisation associated with ELM's in shaped plasma produce upward VDE's. Experiments with the lower saddle coils set have measured the threshold for the static error field mode and have been applied to the saturated tearing modes. Systematic measurements of vessel displacements and forces have been carried out.

REFERENCES

[1] NOLL, P., et al., Fusion Technology **15** (1989) 259.
[2] ANDREW, P., et al., in Proc. 16th IEEE/NPSS Symposium on Fusion Engineering **1** (1995) 770.
[3] SANTAGIUSTINA, A., et al., in Controlled Fusion and Plasma Physics (Proc. 22nd Eur. Conf. Bournemouth, 1995), Vol. 19C, Part IV, IV-461.

EFFECT OF DIVERTOR CONFIGURATION ON PLASMA PERFORMANCE IN JET

The JET Team[1]
(presented by G. Vlases)

JET Joint Undertaking,
Abingdon, Oxfordshire,
United Kingdom.

Abstract

JET has been operating with a new divertor, Mk IIA, since April 1996. Mk IIA is geometrically more closed than Mk I and has better power handling capacity. Pumping performance is improved, and access to high recycling and detached regimes is facilitated. Quasi-steady ELMy H-modes with $H_{89} \sim 2.0$ are produced with moderate gas puffing. The Type I ELM frequency depends primarily on triangularity and the gas puff rate at fixed power, and not strongly on target orientation or divertor magnetic flux expansion. The stored energy loss per ELM decreases with increasing frequency, but can only be reduced below 4% by strong gas puffing, with loss of confinement quality. Highly radiating, detached divertor plasmas can be produced by impurity seeding, but at the expense of confinement degradation and increased Z_{eff} (similar to Mk I results).

1. INTRODUCTION

The JET divertor programme is designed to investigate the effect of divertor geometry on plasma performance in a series of progressively more closed configurations. The programme began with Mark I (1994 - 1995, Fig.1a), presently uses a somewhat more closed divertor (Mark IIA, 1996-1997, Fig.1b), and will conclude with an ITER-specific "Gas Box" configuration (Mark II GB, 1997-1998). In addition to examining the effects of the geometrical positioning of various divertor components, the programme explores the effect of target orientation, X-point height, and flux expansion. Each of the divertors uses a cryopump with a nominal pumping speed of 240 m^3s^{-1}.

The term "closure" in this context refers to the degree to which neutrals recyling from the target plates escape from the divertor region. Closure depends on the divertor plasma temperature, density, and equilibrium geometry as well as on the geometry of the divertor components. In general, a "geometrically closed" divertor will have a larger effect on closure in the low recycling and detached plasma limits, where the ionisation mean free path becomes larger, than in the intermediate high recycling regime. The reasons for increasing closure are (a) to provide easier access to the regime of high volumetric losses in the divertor, thus reducing the target heat loading, (b) to reduce the neutral density in the main chamber, which improves main plasma confinement quality and reduces sputtering of impurities, and (c) to increase neutral pressure in the divertor chamber, thus facilitating pumping. At the same time, improved closure generally leads to reduced flow in the scrape-off-layer (SOL), which results in poorer flushing out of impurities and ash from the main chamber; this can be partly offset by increased pumping. The problem of choosing the correct geometrical closure for a divertor which must operate with Type I ELMs is particularly

[1] See Appendix to IAEA-CN-64/O1-4, The JET Team (presented by J Jacquinot).

difficult because of the great disparity in effective SOL width between and during ELMs. Finally, closure does not prevent the escape of ionized impurities from the divertor region, as they are driven up the field lines by the parallel ion temperature gradient, and are only retained in regions of high SOL flow. Thus, improved closure, per se, will not generally improve impurity retention for seeded divertors.

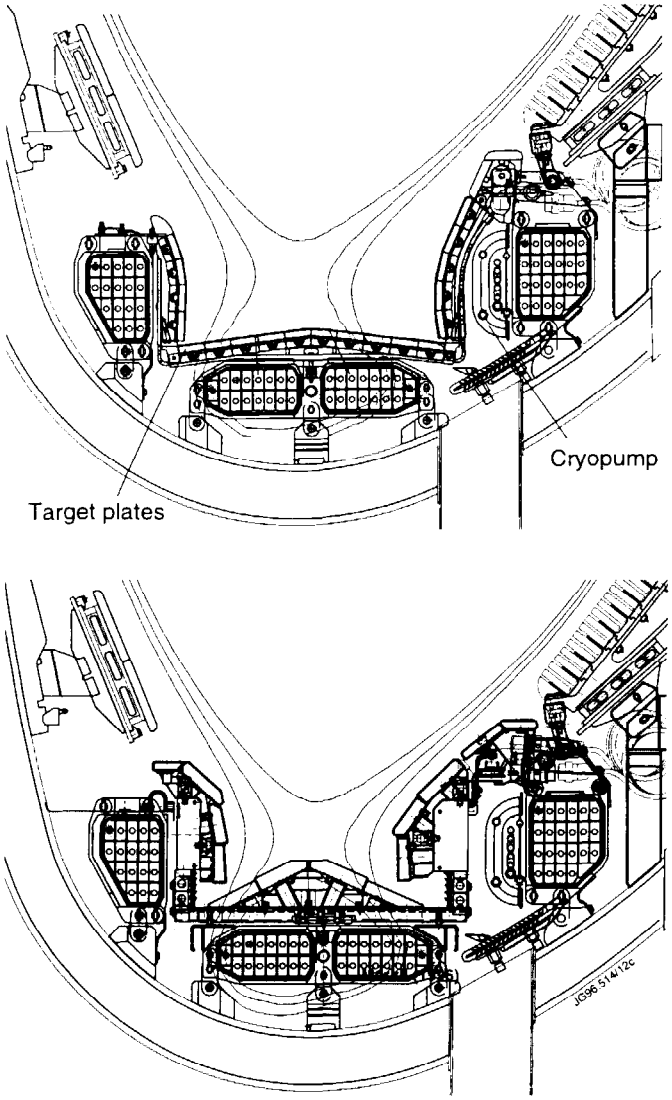

Fig.1 Poloidal cross sectional view of Mark I (top) and Mark II A (bottom).

Much attention was given in the JET Mk I campaign to the study of highly detached, highly radiating seeded divertor plasmas, where it was found possible to reduce the heat flow to the targets to very low levels. However, the confinement quality (H_{89}) was low and Z_{eff} was relatively high at high radiated power fractions with fully detached divertor plasmas [1]. Similar results have been found in other tokamaks [2-4]. Thus the use of this operating scenario for ITER is perceived to be difficult. On the other hand, it has been suggested that time-averaged power loading in ITER operating with divertor plasmas detached only near the separatrix strike points (semi-detached) and Type I ELMy H-modes, which

improves confinement and Z_{eff}, may prove to be satisfactory [5]. In this scenario, the interaction of the Type I ELMs with the target becomes the main concern for the divertor design. In the Mk IIA campaign the study of seeded, radiating divertors has continued, but heavy emphasis has also been placed on the investigation of Type I ELMy H-mode discharges, and the effect of divertor configuration on them.

2. GLOBAL COMPARISON OF MK I AND MK II A

In this section the relative performance of Mk I and Mk IIA is discussed with respect to the principal divertor performance criteria: power handling capacity, approach to detachment, pumping effectiveness, and control of impurities. Mk IIA has a much larger wetted area than Mk I due to the use of large tiles and inclined target plates, and was predicted to have power handling capacity in the non-swept mode 2 - 5 times greater than that of (unswept) Mk I, depending on equilibria used. Infrared measurements of tile temperature show that Mk IIA has exceeded its design goals, and that the overheating of the tiles is not encountered in any normal JET operating scenario.

Increasing divertor geometrical closure should result in access to the high recycling-detachment regime at lower main plasma densities for a fixed power input. Figure 2 shows Langmuir probe measurements of the degree of detachment, defined as midplane SOL electron pressure divided by twice the measured divertor electron pressure [6], for equivalent L-mode density ramp discharges in the two divertors. It is seen that detachment begins at a lower density in Mk IIA than in Mk I, as expected. The "Super Fat" Mk IIA configuration has reduced divertor flux expansion and thus greater leakage than the "Standard Fat", while the HFE of Mk I is even more open. Each of these pulses ended in a density limit disruption, and the density attained decreased as the degree of closure increased. It appears that in general, the "detachment window" between onset of

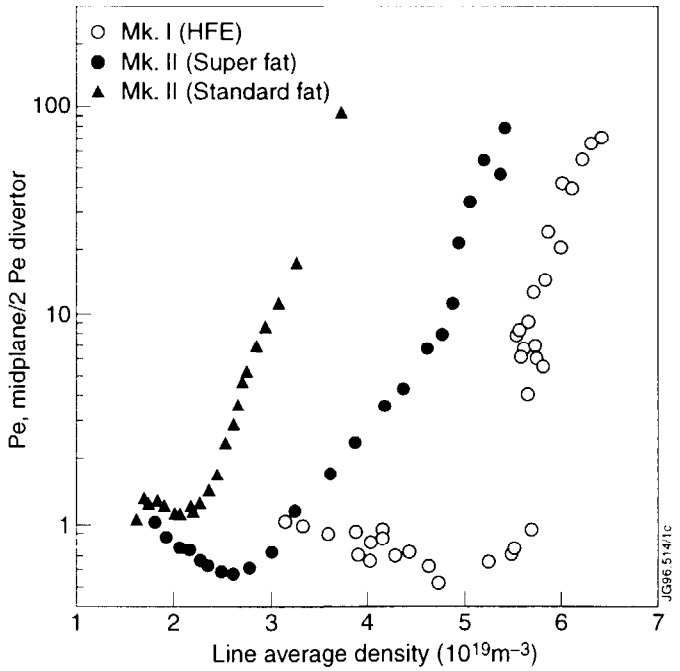

Fig.2 Degree of detachment vs. line averaged density for 3 MW L-mode discharges in Mk I and Mk IIA, showing the effect of increasing closure on the onset of detachment and the density limit.

I_{sat} rollover and disruption is smaller in Mk IIA than in Mk I for ohmic and low power L-mode pulses. (The density limit in H-mode operation is not disruptive and lies near the Greenwald limit in both divertors [7]).

The rate of pumping in Mk IIA is generally higher than in Mk I for equivalent Ohmic [8], L-mode, and ELM-free H-mode discharges, and is less sensitive to strike point position. EDGE2D/NIMBUS simulations indicate that Mk IIA is functioning as a moderate slot divertor and trapping the neutrals near the pumping ports in the lower corners.

Figure 3 shows measured Z_{eff} for Mk I and Mk IIA ELMy H-mode pulses as a function of volume averaged density, and indicates that they are quite comparable. The same statement can be made about the radiated power fraction and main plasma carbon densities. Carbon is the predominant impurity, with beryllium the next largest contributor. Improved closure in Mk IIA should lead to reduced intrinsic impurity content, if most of the sputtering is caused by neutrals originating at the target plates, rather than by direct interaction of plasma with the main chamber walls. The lack of improvement is believed to be due, at least in part, to bypass leakage of neutrals out of the divertor region, which has been increased by the higher divertor neutral pressure. The bypass leaks will be reduced by about 80% during a shutdown in October 1996.

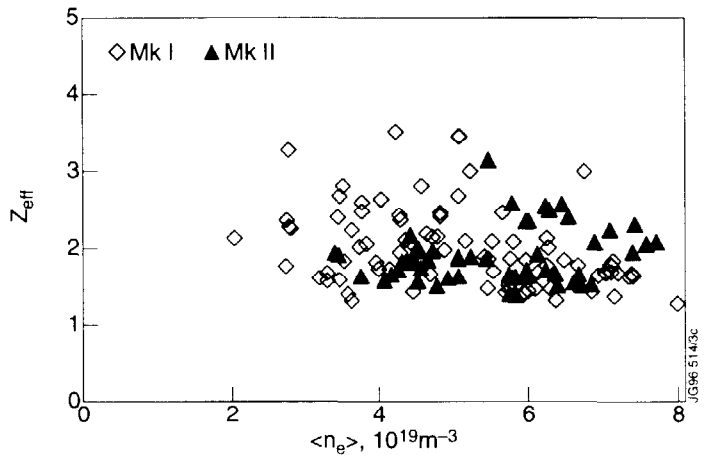

Fig.3 Measured values of Z_{eff} in Mk I and Mk IIA vs <n_e> for Type I ELMy H-mode pulses with total power input ≥ 12 MW.

3. CONFIGURATIONAL EFFECTS ON STEADY STATE ELMY H-MODE DISCHARGES IN MK IIA

3.1 Discharges with beam fuelling only

In order to isolate the effects arising from configurational changes, a series of discharges was carried out with fixed plasma current, magnetic field, and neutral beam power (2.5 MA, 2.5 T, and 12 MW, respectively), in which the target orientation, flux expansion (horizontal target only), and main plasma triangularity were varied. Equilibrium reconstructions (EFIT) of the poloidal flux surfaces in the divertor region are illustrated in Fig.4 for the low triangularity cases. The high triangularity equilibria are nearly identical in the divertor, but differ in the main plasma. It was found that these discharges reached nearly steady state conditions within about 3 seconds of applying the beam power, and that this state was characterized by regularly spaced Type I ELMs. The ELM frequency depends most strongly on triangularity, without reproducible

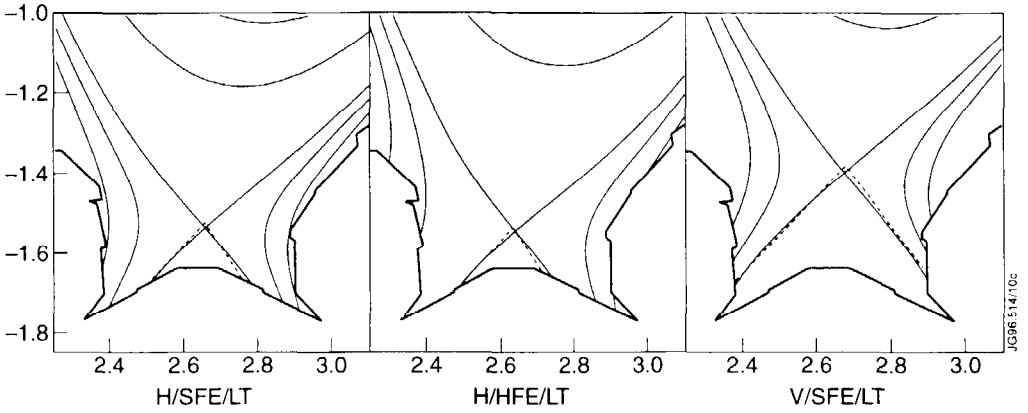

Fig.4 EFIT reconstructions of horizontal standard flux expansion, horizontal high flux expansion, and vertical standard flux expansion equilibria used in the configuration experiments. Flux surfaces shown are 1 and 2 cm distant from the separatrix at the outer midplane.

dependencies on target orientation or flux expansion, as shown in Fig.5. Although the ELM frequency f_E varies by a factor of about 6 for these pulses, the confinement quality, as measured by H_{89}, was independent of both f_E and configuration, as shown in Fig.6. However, the "natural density" at which these beam-fuelled discharges run decreases with increasing f_E. Z_{eff} also drops as f_E

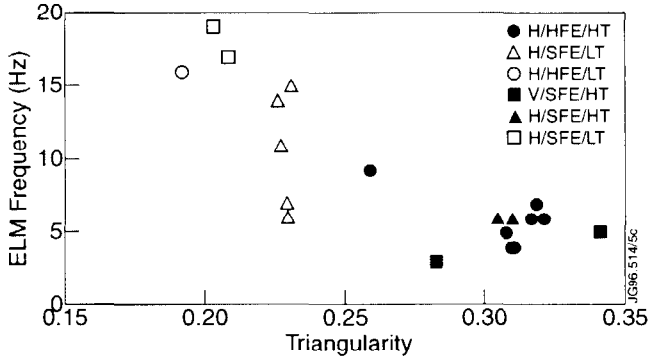

Fig.5 ELM frequency vs. triangularity for pulses with beam fuelling only. The designation of the equilibria A/BBB/CC indicates target orientation, flux expansion (high or standard), and triangularity (high or low), respectively. All of the pulses were run at 2.5 MA, 2.5 T, and 12 MW NB power.

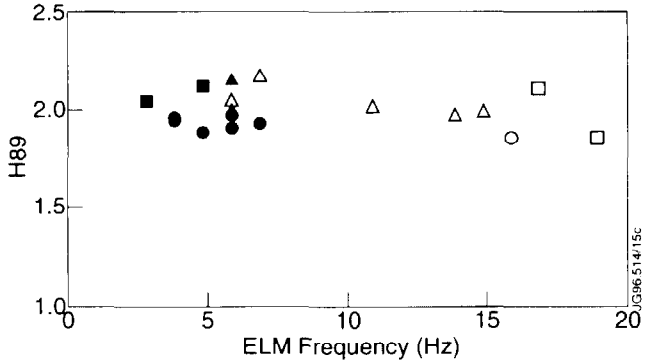

Fig.6 Variation of confinement quality, H_{89}, with ELM frequency, beam-fuelled pulses. The ITERH93-P ELM-free confinement scaling factor, H_{93}, is approximately $0.46xH_{89}$ for the pulses described in this paper.

increases, illustrating the importance of ELMs in purging the edge plasma of impurities. The radiated power fraction in these discharges was quite low for the high ELM frequency configurations, around 25%, increasing at lower ELM frequencies to about 40%.

A set of simulations has been carried out to model the quiescent periods between ELMs of the standard flux expansion horizontal and vertical 12 MW ELMy H-mode pulses described above, using the EDGE2D/NIMBUS code system and a variety of models for the perpendicular SOL transport. It was found that a pinch term gave satisfactory agreement with measured divertor profiles, whereas the customary constant diffusion coefficient model did not. The values used were $\chi_E = 0.2\ m^2s^{-1}$, $D = 0.1\ m^2s^{-1}$, and $V_{pinch} = 4.5\ ms^{-1}$. The present version of the code models the neutral particle behaviour, including the effects of the bypass leaks, more accurately than earlier versions. With this transport model and the bypass leaks included, differences between results for the horizontal and vertical targets are greatly reduced. The target ion saturation current profiles are nearly identical, while the electron temperature profile on the vertical target is flatter than on the horizontal, but not inverted, as shown in Fig.7. The midplane profiles are essentially identical for horizontal and vertical targets, and are quite narrow, with $\lambda_n = 9$ mm, $\lambda_{Te} = 7$ mm, and $\lambda_{Ti} = 12$ mm. These code results are in qualitative agreement with Langmuir probe measurements.

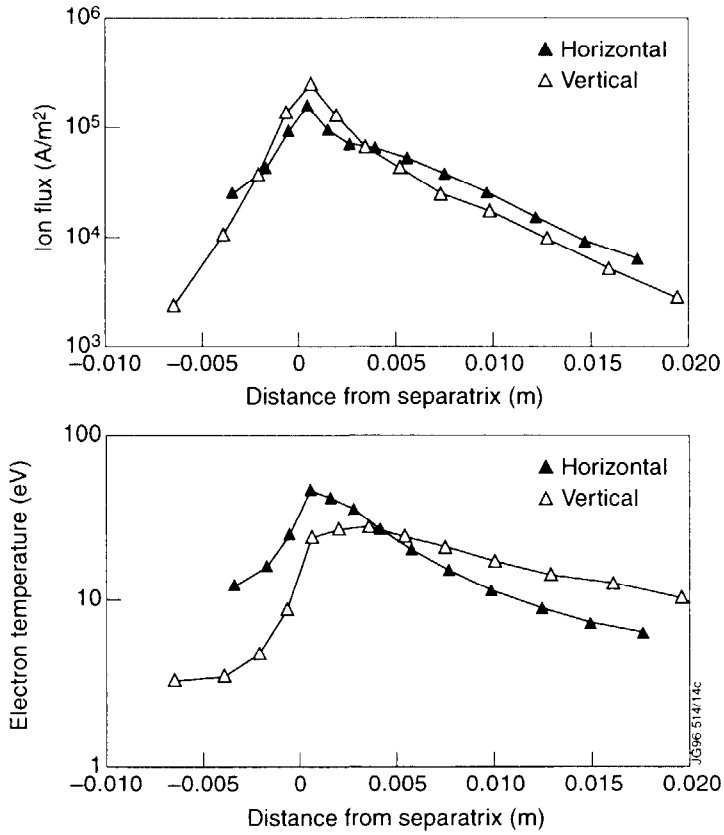

Fig.7 EDGE2D/NIMBUS simulations of target profiles of ion flux (above) and electron temperature (below) for horizontal and vertical pulses corresponding to the experiments. The distance from the separatrix has been mapped to the midplane.

3.2 Discharges with beam fuelling plus D_2 gas puffing

The above series of discharges was systematically repeated with D_2 puffing, which was varied in strength and location. It was found that the ELM frequency was increased by adding heavy fuelling (> 2 x 10^{22} s^{-1}). As puffing is added, the radiated power fraction initially stays the same or decreases slightly. As puffing increases further, the radiated power fraction also increases to a maximum of about 50%, with most of the increased radiation appearing in the divertor/X-point region. The mid-plane neutral pressure rises and the confinement quality declines, with these two variables being clearly correlated, as shown in Fig.8. In this figure the high triangularity standard flux expansion horizontal and vertical configurations appear to be the best, but there may be too few points to be statistically significant. However, as for the beam fuelled cases, the high triangularity discharges have lower ELM frequencies and higher Z_{eff} (Fig.9). The response of the main plasma density to the puffing is described in reference [7].

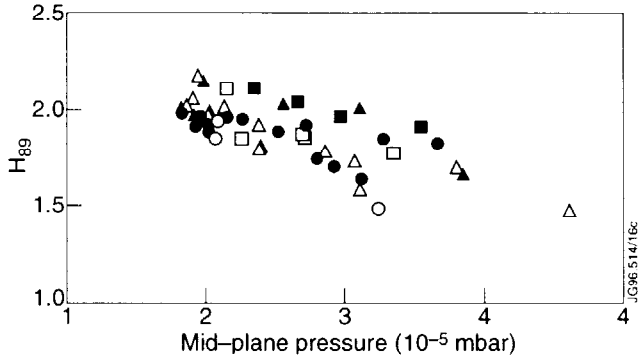

Fig.8 Variation of confinement quality, H_{89} with mid-plane neutral pressure for beam fuelled and D_2-puffed discharges.

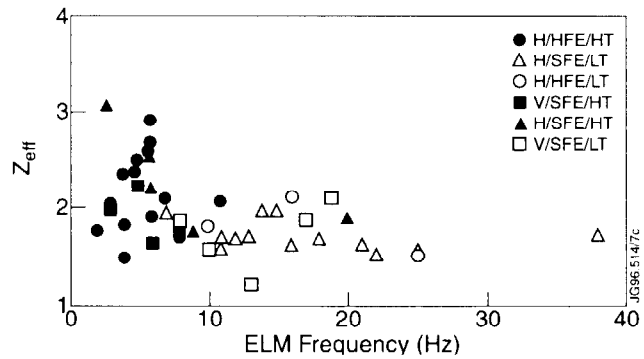

Fig.9 Variation of Z_{eff} with ELM frequency for beam fuelled and puffed discharges.

3.3 Discharges with beam fuelling plus D_2 and N_2 puffing

In order to increase the radiated power fraction beyond the 0.5 available with D_2 puffing, a series of discharges with N_2 seeding was carried out, again in a variety configurations. These discharges attained total radiated power fractions up to about 0.75, and were broadly similar to those carried out with Mk I [1]. As the N_2 puff rate is increased, the character of the ELMs changes and the confinement decreases steadily and makes a gradual transition back to enhanced L-mode levels of H_{89} ~ 1.4, as shown in Fig.10. For these discharges, it appears that the decline of H_{89} with f_{rad} is less severe for the horizontal targets than for the vertical. It was shown by Matthews et. al. [9] that the Z_{eff} values for highly radiating divertor

operation from several tokamaks can be described by a scaling law which can be written approximately as:

$$P_{rad} \sim (Z_{eff} - 1)\langle n_e \rangle^2 S,$$

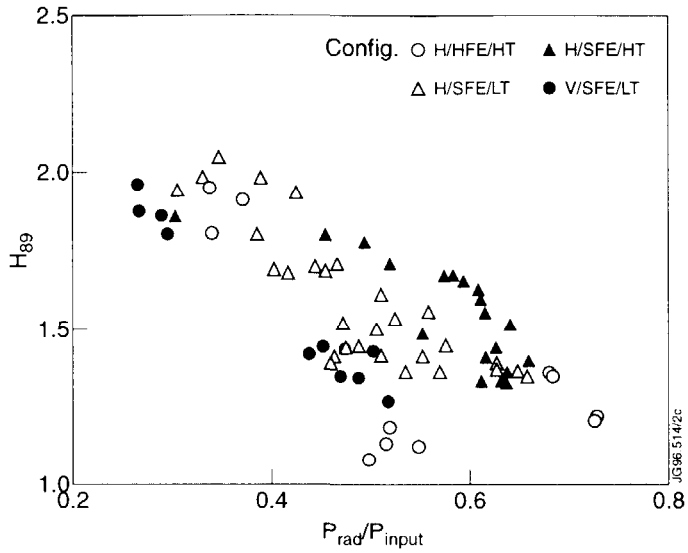

Fig.10 Confinement quality H_{89} vs. radiated power fraction in Mk IIA, for four configurations, with D_2 puffing only ($f_{rad} \leq 0.45$) and D_2 + N_2 puffing.

This scaling is not consistent with the scaling which would be observed if the bulk of the impurities were retained in the divertor. The Mk IIA data for highly radiating pulses fits the same scaling as was found for Mk I, as shown in Fig.11, indicating no improvement of seeded impurity retention, probably for the reason stated in Section 1 of this paper. Neon seeded discharges behave similarly with respect to Z_{eff} scaling, although they display a tendency to radiate more in the main plasma edge than in the X-point region, which reflects the tendency of neon to radiate less than N_2 at low T_e.

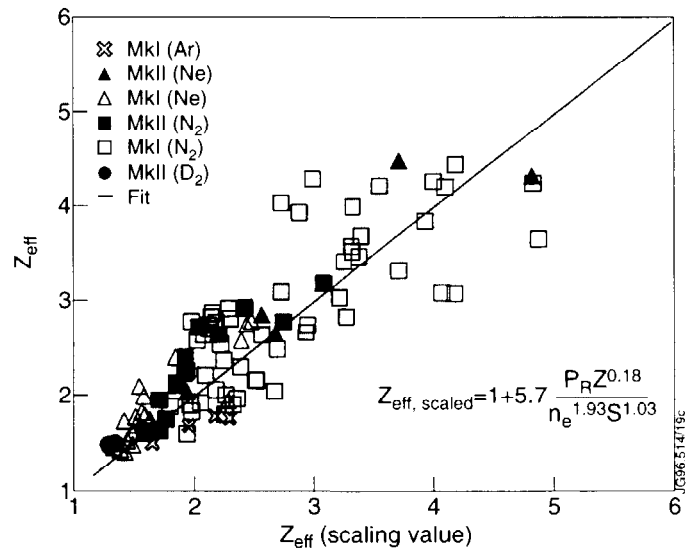

Fig.11 Measured Z_{eff} vs. $Z_{eff,scaled}$ for JET radiative discharges in Mk I and Mk IIA for a variety of seed gases.

4. DETAILED STUDIES OF TYPE I ELMS

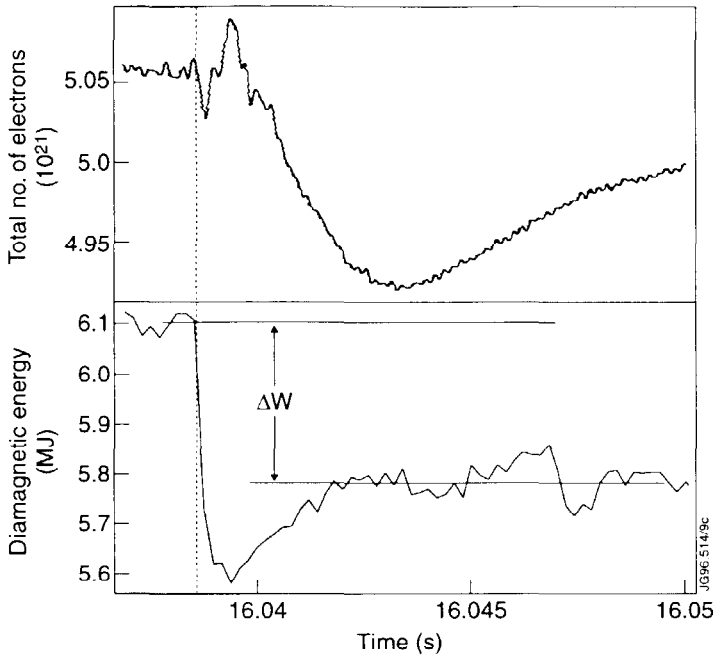

Fig.12 Traces of total particle inventory and stored energy vs. time for a typical ELM from the configuration study described in Section 3. The overshoot in ΔW is due to vessel shielding effects.

It was shown in Section 3 that Type I ELMs are inherent to non-seeded discharges well above threshold, where good confinement and low Z_{eff} are obtained. It is thus important to understand the energy and particle loss per ELM, and the timescales associated with them, in order to assess their impact on divertor components. Figure 12 shows the total particle inventory and stored energy on a fast time scale for a typical isolated ELM. The stored energy drops extremely rapidly, on a time scale of 100-200 μsec, characteristic of parallel heat conduction. The particle inventory drop occurs more slowly, on the scale of a few milliseconds, characteristic of particle flow times in the SOL. It appears thus that the energy is conducted very quickly along the field lines to the target, with the particle efflux following the primary conduction-dominated energy dump. Figure 13 shows the percentage drop in density and energy, respectively, for 10 pulses from the database described in Section 3.2. Five of the pulses, representing five of the configurations studied, had no puffing, with a corresponding set for pulses with a moderate puff rate of 1 x 10^{22} s^{-1}, which is sufficiently low to have only a small effect on the ELM frequency. It can be seen that there is a general trend for the percentage energy and density drops to decrease with increasing frequency, although the time averaged energy and particle loss from ELMs, obtained by multiplying the frequency times the drops, increases with ELM frequency. Thus the low frequency, higher triangularity discharges lose less energy through ELMs in a time-averaged sense, but the individual ELMs are larger and thus potentially more damaging to the divertor plates. By increasing the puffing rate, the ELM frequency can be made larger, and the fractional energy loss per ELM can be reduced further, to about 2% in our discharges. This comes, however, at the expense of confinement, as illustrated in Fig.14. Even higher puffing causes a transition from Type I to grassy ELMs, with a further decrease in confinement to enhanced L-mode values.

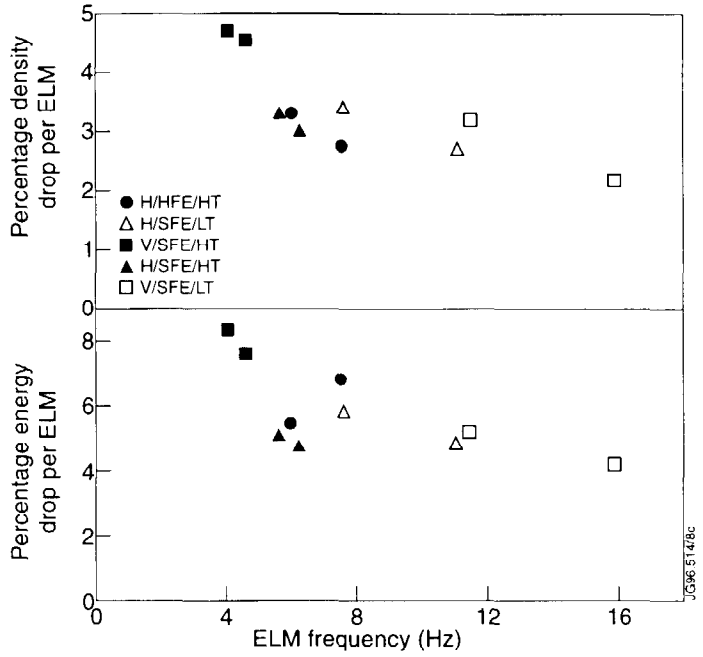

Fig.13 Percentage density drop (top) and energy drop (bottom) per ELM vs. ELM frequency for pulses from the configuration study of Section 3.

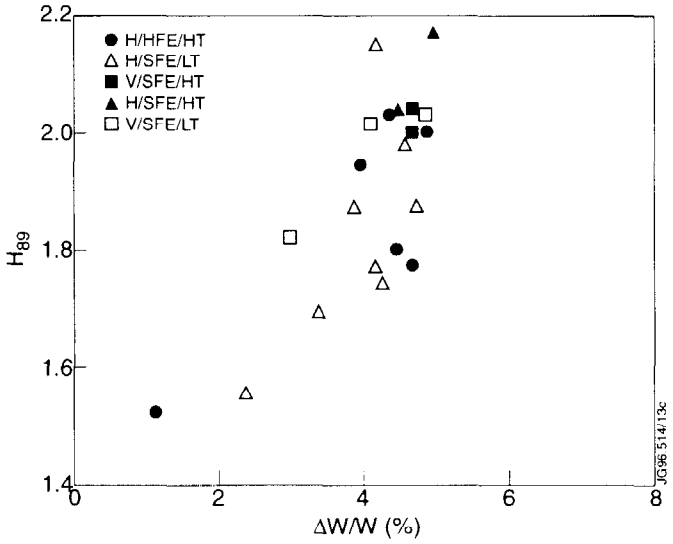

Fig.14 The confinement quality H_{89} vs. percentage energy drop per ELM, ΔW/W, for the beam fuelled and D_2 puffed pulses of the configuration study.

Energy deposition on the ITER target plates of greater than about 1% of the stored energy is expected to cause severe erosion [10]. Fast Langmuir probe studies in JET show a very fast, short lived deposition of particles displaced by up to 20 cm from the pre-ELM strike point position, followed by a high-recycling deposition of particles at the original strike zones which lasts a few milliseconds, as shown in Fig.15 for an ELM on the vertical plates. Full cross section CCD views indicate that the ELM also produces a great deal of D_α radiation at the main chamber limiters and upper dump plates. Because of the relatively slow time resolution of the JET infrared cameras and bolometers, however, it is not possible to determine precisely the fraction of the energy leaving the main plasma which

reaches the plates. It is known, however, that the ELM energy which does reach the plates is shifted and distributed over a larger area than that arriving between ELMs. More detailed quantification of the deposition of the ELM energy in JET must thus await more refined measurements and further analysis.

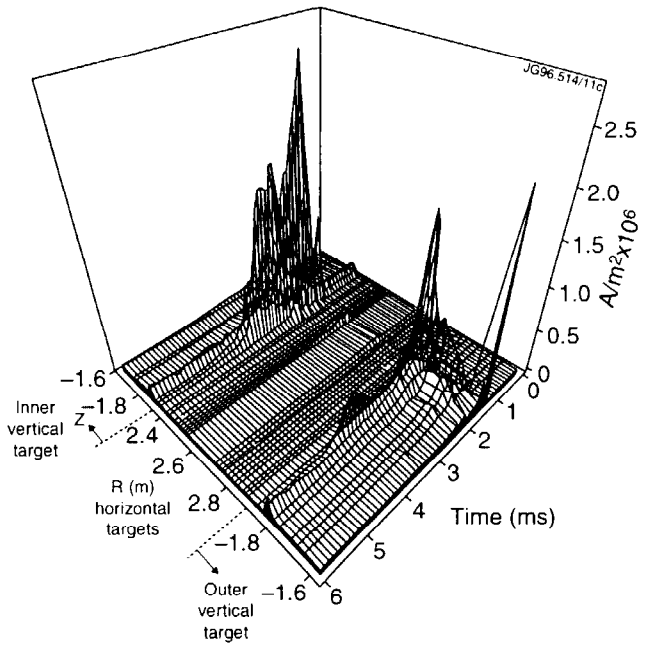

Fig.15 Unfolded 3-D plot of fast Langmuir probe ion saturation current measurement during an ELM on the vertical target.

5. CONCLUSIONS AND IMPLICATIONS FOR ITER

Compared with Mk I, the geometrically more closed Mark IIA configuration produces higher neutral pressures with correspondingly higher pumping rates, and facilitates access to the high recycling and detached plasma regimes. Although the density limit in Mk IIA is lower in ohmic and low power L-mode plasmas, it remains, as in Mk I, at roughly the Greenwald limit for H-mode pulses. The expected reduction in intrinsic impurity level in Mark IIA has not been observed, and this is believed to be due, at least in part, to bypass leakages.

For fixed power, field, and current, the ELM frequency in Type I ELMy H-mode discharges can be increased by a factor of several by decreasing the triangularity from 0.32 to 0.19, with no loss in confinement quality. The energy loss per ELM varies from about 8% to 4% as the triangularity is reduced. Further increase of the ELM frequency and decrease of amplitude, down to about 1%, was obtained by heavy D_2 puffing, but at the expense of confinement. However, ELMs somewhat larger than 1% may be acceptable to ITER, as the fraction of the ELM-expelled energy which reaches the plates is not yet well known in JET.

Differences which arise from target orientation (vertical vs. horizontal) at fixed flux expansion and triangularity appear to be quite small; both offer good confinement and plasma purity in the Type I ELMy H-mode operating regime. On the horizontal plate, large flux expansion resulted in slightly higher achievable main plasma densities, but poorer confinement and higher contamination by the intrinsic impurities. This may be due to the ELMs extending beyond the edge of the divertor.

Mark IIA operation with radiative power fractions greater than 0.5, achieved by seeding with N_2 or Neon, produced confinement degraded to a level

probably not acceptable for ITER, with high Z_{eff}, as had been found in Mk I. In this series of pulses, the vertical targets showed poorer confinement at a given f_{rad}, and were not capable of going to as high values of f_{rad}.

In summary, if the L→H power threshold in ITER is such that the Type I ELMy H-mode regime can be achieved, it appears to offer high confinement and low Z_{eff}, relative to the high radiated power fraction regime. The energy deposited on the plates between ELMs for the oberved radiated power fractions would be acceptable for ITER, but the deposition pattern of the ELM energy needs further study.

REFERENCES

[1] THE JET TEAM (presented by G.F. Matthews) Plasma Phys. Control. Fusion **37** (1995) A227.
[2] NEUHAUSER, J., et. al., ibid., A37.
[3] ITAMI, K., and THE JT-60 TEAM, ibid., A255.
[4] ALLEN, S.L., et. al., ibid., A191.
[5] VLASES, G.C., et. al., to be published in J. Nucl. Mater. (Proc. 12th Int. Conf. on Plasma Surface Interactions, San Raphael, 1996).
[6] LOARTE, A., and MONK, R., to be published
[7] THE JET TEAM (presented by D. Stork), IAEA-CN-64/A1-1, this Conference.
[8] THE JET TEAM (presented by L.D. Horton), paper presented at 23rd Eur. Conf. Kiev, 1996 (to be published in Plasma Phys. and Control. Fusion).
[9] MATTHEWS, G., et. al., to be published in J. Nucl. Mater. (Proc. 12th Int. Conf. on Plasma Surface Interactions, San Raphael, 1996).
[10] ITER-JCT AND HOME TEAMS (presented by G. Janeschitz) Plasma Phys. Control. Fusion **37** (1995) A19.

ENERGY AND PARTICLE TRANSPORT MODELLING WITH A TIME DEPENDENT COMBINED CORE AND EDGE TRANSPORT CODE

The JET Team[1]
(presented by A. Taroni)

JET Joint Undertaking,
Abingdon, Oxfordshire,
United Kingdom.

Abstract

A new time dependent code has been developed by linking the $1^1/_2$ D core plasma transport code JETTO to the 2D edge plasma transport code EDGE2D/NIMBUS. The code includes a combined Bohm-gyro-Bohm type transport model for energy transport in the plasma core and this has been extended to include particle transport and a neoclassical transport barrier at the plasma edge for the simulation of JET hot ion H-modes. Outside the separatrix the transport coefficients extrapolated from the model are assumed to be constant. It is shown that the code gives a completely consistent time dependent simulation of the measured plasma profiles across the entire cross section of hot-ion ELM free discharges, including the scrape-off layer and divertor regions. The code also predicts that the ballooning stability limit is reached when a giant type I ELM appears in experiments.

1. INTRODUCTION

The importance of a global approach to transport studies, modelling simultaneously the entire plasma from the centre to the scrape-off layer (SOL) and divertor regions has been stressed recently by the development of transport models [1-2], relating the overall plasma performance to the behaviour of plasma in the boundary region.

As an example a model developed for the simulation of hot-ion H-mode plasmas in JET is considered. The model is based on the formation of a neoclassical transport barrier just inside the separatrix. The strength of the barrier depends on recycling. In the absence of accurate measurements of all the quantities relevant for an accurate evaluation of particle and energy sources and sinks just inside the separatrix, the assumptions made require to be validated by the proper modelling of experimental observations outside the separatrix.

At JET such a global approach to transport studies is now possible [3] thanks to the combination in a single code of the $1^1/_2$ D core plasma transport code JETTO and the 2D edge plasma transport code EDGE2D/NIMBUS, as described in section 2. The transport model presently used in the code is given in section 3, while in section 4 results of the simulation of a typical JET hot-ion H-mode are presented.

2. THE COMBINED CODE

The stand alone versions of the codes that have been combined into a global time dependent code are among the most advanced of their kind and are extensively used for the analysis and prediction of JET results. A link between JETTO and the impurity transport code SANCO, allowing a full multi-species

[1] See Appendix to IAEA-CN-64/O1-4, The JET Team (presented by J Jacquinot).

treatment of impurities in the plasma core, has recently been completed. Coupling between SANCO and the multi-species impurity package in EDGE2D/NIMBUS is in progress.

EDGE2D has been upgraded to include all components of the classical particle drifts in the equations and boundary conditions for all plasma species. Another recent upgrade of EDGE2D is the implementation of a 21 moment description of parallel transport. The transport coefficients are calculated using the reduced charge state (RCS) method [4], with no assumption on impurity density or atomic mass.

In linking the codes at a prescribed interface inside the separatrix continuity of densities and temperatures and of the corresponding total particle and energy fluxes at a chosen interface is enforced. This is achieved by imposing proper boundary conditions into each code at each time step. Poloidal averages of the quantities in EDGE2D/NIMBUS are used at the interface. Continuity of neutral profiles and fluxes is also enforced in order to have a consistent evaluation of particle sources.

An important point is that at the interface one code receives a variable or flux from the other and returns the corresponding flux or variable. This procedure ensures continuity of all relevant quantities with sufficient accuracy, even for fast transients, by simply running both codes with time steps typical of EDGE2D/NIMBUS, avoiding extra iterations at each time step. As a result the coupled code is very robust and requires less than 10% additional computer time with respect to the stand alone EDGE2D/NIMBUS code [3].

3. ENERGY AND PARTICLE TRANSPORT MODELS

The transport models used in the code are mainly empirical. Their derivation and justification can be found in [5].

The transport model for energy is a combination of Bohm and gyro-Bohm-like terms. The corresponding thermal conductivities are:

$$\chi_e = \chi_B + \chi_{gB}$$
$$\chi_i = 2\chi_B + \chi_{gB} + \chi_{neo,i} \qquad \text{for} \quad 0<r<r_I$$

The model includes a region of finite width at the plasma edge from a radius r_I to the plasma boundary $r=a$ ($\rho_I<\rho<1$ in a normalised radial flux surface co-ordinate) where transport is close to neoclassical. A neoclassical barrier for impurity transport in JET ELM free H-mode discharges was previously considered in the SANCO code [6] and taken into account as a boundary condition of the energy equations in JETTO [1].

The Bohm and gyro-Bohm parts of the model, used for $\rho< \rho_I$, are given by:

$$\chi_{gB} = c_{gB}\sqrt{T_e}\,\frac{\nabla T_e}{B_T^2}$$

$$\chi_B = c_B\,\frac{\nabla P_e}{nB_T}\,q^2 a^2 L_{T1}^{-1}$$

where to compute the average of the inverse of the characteristic length of the temperature variation:

$$L_{T1}^{-1} \equiv < \nabla T_e/T_e >_{0.8<\rho<\rho_1}$$

the first order approximation is taken: $L_{T1}^{-1} \sim \left(T_{e,\rho=0.8} - T_{e,\rho=\rho_1}\right)/T_{e,\rho=\rho_1}$. c_{gB} and c_B have been chosen by calibrating the model in a number of JET L-mode discharges and are kept constant [1].

The Bohm-like term is non local, via its dependence upon L_{T1}^{-1}. This dependence allows the use of the model in both H- and L-mode, by reducing the Bohm-like term in H-mode. In L-mode the transport barrier is switched off.

In the same region particle transport is given by an effective diffusion coefficient:

$$D_{eff} = \alpha_D(r)\frac{\bar{\chi}}{\langle n_e \rangle} \text{ with: } \bar{\chi} = \frac{\chi_e \chi_i}{\chi_e + \chi_i}$$

where $<n_e>$ is the volume average density and $\alpha_D(r)$ is a shape factor (including a normalising constant density) that reduces D_{eff} with respect to χ as ρ increases (Fig.1). Such an empirical dependence of D_{eff} seems to be required to match at the same time:

a) the experimental density profiles;
b) the neutral fluxes computed by EDGE2D (which match experimental values of D_α emission); and
c) the lack of strong variation with time of the ion saturation current density at the divertor targets in low recycling ohmic and hot ion H-mode discharges.

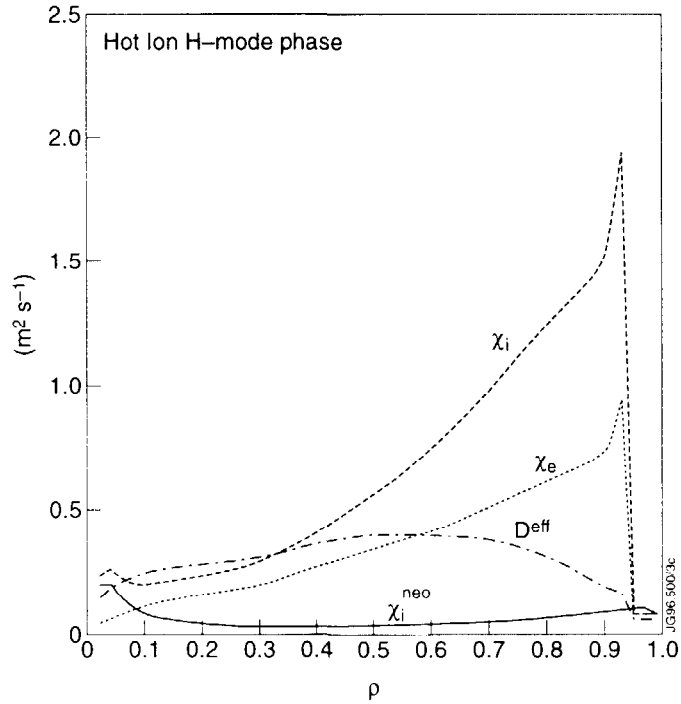

Fig.1 Radial dependence of the transport coefficients in the hot ion H-mode.

The shaping factor $\alpha_D(r)$ and the inverse dependence upon $<n>$ are to be considered as an indication of the existence of an inward particle pinch velocity term increasing strongly towards the boundary and increasing with density. Work is in progress to include explicitly such a term in the model.

In the present version of the code the width of the neoclassical boundary transport barrier $\Delta = a - r_l$ is imposed and kept constant in time. Typically $\Delta \approx 5$ *cm*,

which for the JET hot ion H-modes with plasma current $I \approx 3$ *MA* simulated so far corresponds to a few ion banana orbit radii ρ_b. The main effect of the barrier is to act as a 'plug' which at low collisionality provides thermal fluxes essentially independent of temperature but directly proportional to $n^2 Z_{eff}$ [1]. Such plugging is obtained by assuming within the barrier region:

$$\chi_i = \chi_e = D \propto \frac{\Delta}{\rho_b} \chi_i^{neo}$$

where χ_i^{neo} is the neoclassical ion thermal diffusivity. This corresponds in first approximation to assuming $\chi_i = \chi_e = D_{eff} \approx \chi_i^{neo}$ and $\Delta \propto \rho_b$.

For the simulations shown in the next section, the transport coefficients in the SOL region are assumed to be the same as the transport coefficients computed at the JETTO/EDGE2D interface (≈ 2 *mm* inside the separatrix) from the core transport model. However better agreement with measurements in the divertor region is obtained by including an explicit inward pinch velocity term $V \approx 15\ D/a$ in the SOL particle flux (even if the particle diffusion coefficient is rather small as shown in Fig.1).

4. SIMULATION OF HOT ION H-MODES

The hot ion H-mode is a very interesting plasma regime in JET, and has provided record values of energy confinement and fusion reaction rate. This regime is usually entered directly from a low recycling ohmic regime following the formation of the separatrix X-point, soon after ($\approx 100\text{-}150$*ms*) the application of vigorous neutral beam injection (NBI) heating. The good, ELM-free, confinement phase is characterised by an almost linear increase of the energy content lasting for about one second, and usually terminates as a result of some MHD activity (sawtooth, giant type I ELM, "outer" mode) [7]. These pulses have been extensively studied by means of the JET transport codes. In the following results will be presented of the simulation of a typical representative of these pulses, the *3MA, 3.4T* Pulse Number 32919 obtained with the Mark I divertor configuration.

The simulation has been carried out assuming a pure plasma but including Z_{eff} and impurity radiation from the experimental data base. NBI power deposition profiles computed by the TRANSP code as a function of time have been used, assuming that the injected particles (and corresponding energy) lost via shine-through and direct charge exchange losses at the plasma periphery are promptly lost at the vessel wall. This assumption might have to be reviewed, if necessary,when an accurate experimental evaluation of the SOL power balance will becomes available.

The results presented here refer mainly to the time evolution of the discharge from the ohmic phase ($11.6\text{s-}12\text{s}$) into the ELM-free high performance phase ($t < 13s$). Some results for the so called roll-over phase preceding a giant ELM at $t \approx 13.3s$ will also be briefly referred to. The transition to H-mode is simulated by switching on the neoclassical boundary barrier $0.125s$ after NBI is switched on at $t \approx 12.0s$. The benign ELMs at the beginning of the H-mode are ignored (Fig.2).

The density decrease during the ohmic phase is simulated by assuming that the target recycling coefficient R_t is less than unity during this phase (see Table I, showing typical values of the quantities that characterise particle recycling during the ohmic and H-mode phases). The rate of increase of the total plasma particle content dN/dt during the NBI phase exceeds the NBI fuelling source S_n^{NBI}. The extra influx of neutrals Φ_0^{ex} necessary to simulate the plasma density increase, without any external puff being activated, has been assumed to be released

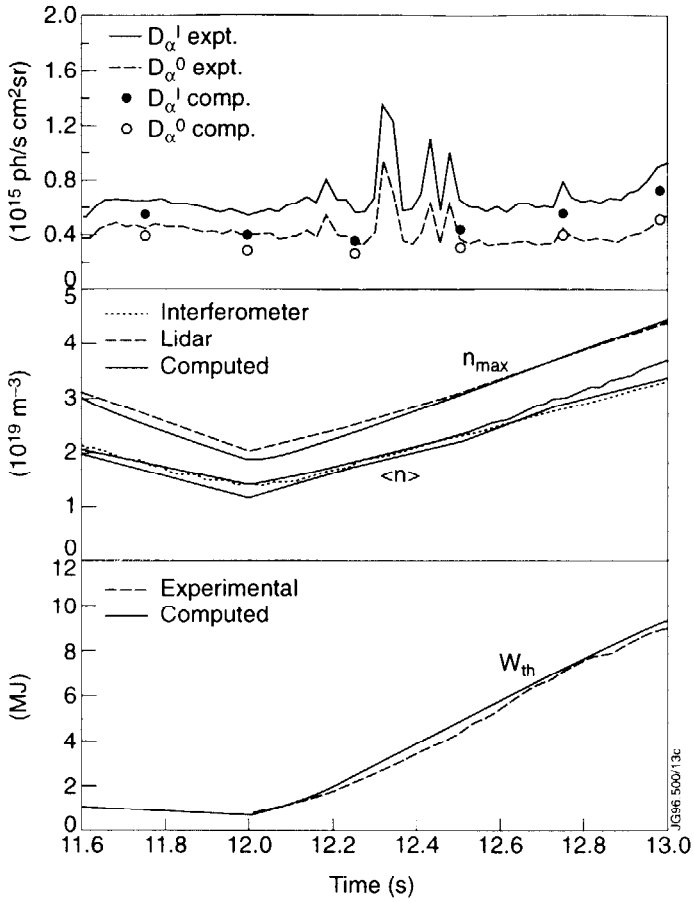

Fig.2 Experimental and computed time evolution of D_α emissivities (see text), averaged and peak core plasma densities, and thermal energy content.

Table I

	dN/dt	S_n^{NBI}	F_0^{ex}	F_0^c	F_i^c	F_i^t	F_0^{pump}	F_0^{leak}	R_t
OH	*-1.35*	*0.0*	*0.0*	*3.3*	*4.65*	*30*	*0.14*	*0.4*	*0.96*
H	*1.75*	*1.4*	*0.5*	*3.2*	*2.85*	*30*	*0.15*	*0.5*	*1.0*

from the divertor or from different regions along the vessel walls without significant variations of the computed core plasma performance. The numerical results shown in this paper refer to divertor release. Table I shows for comparison also values, computed by the code, of the influx of neutrals into the core Φ_0^c, the outflux of ions from the core Φ_i^c, the total flux of ions to the target Φ_i^t, the pumped flux of neutrals Φ_0^{pump} and the flux of neutrals through the bypass leaks [8] in the sub-divertor region Φ_0^{leak}. Units are 10^{21} s^{-1}.

The temporal evolution of the computed and experimental averaged and peak core plasma density in the ohmic and H-regime is shown in Fig.2. The same figure compares the evolution of the D_α emission integrated along lines of view looking at the inner (D_α^I) and outer (D_α^O) divertor plates, and of the thermal energy content.

Figure 2 indicates, in particular, that the distribution of neutrals in the SOL and divertor regions, their influx into the plasma core, and the particle transport in both regions are all consistent with experimental observations. The resulting charge exchange loss terms computed by the code reach a maximum in excess of *2.5 MW* at *t≈13 s*. Their profiles are strongly peaked at the separatrix being negligible at the plasma centre.

Figure 3 compares experimental and computed profiles of the ion saturation current density in the ohmic and H-mode phases, showing little variation of this quantity, consistent with recycling being very low in both phases.

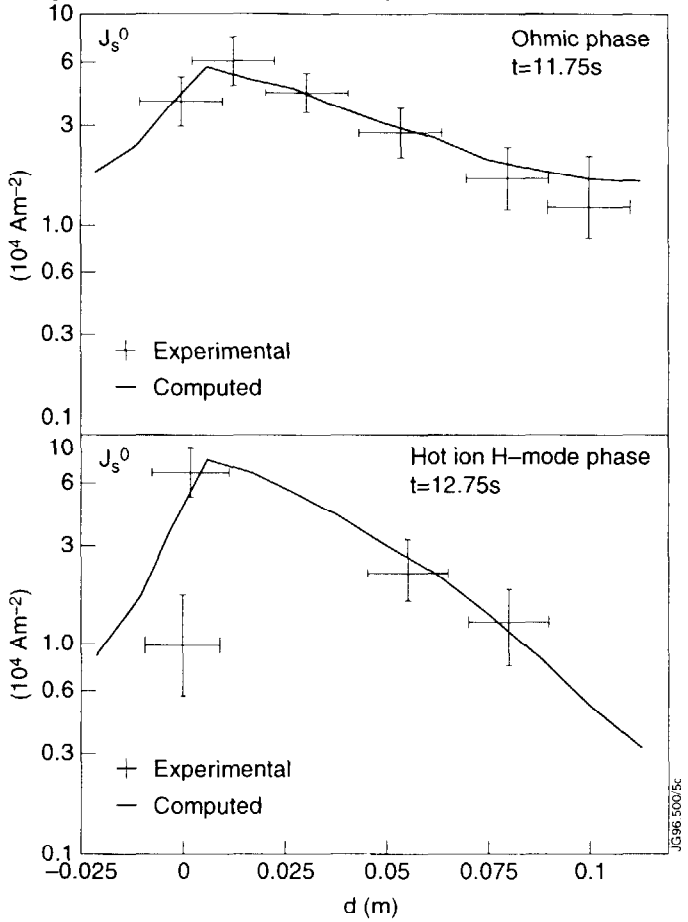

Fig.3 Computed and experimental spatial variation of the ion saturation current density at the outer target as a function of distance from the separatrix.

The simulated and predicted evolution of the ion temperature and of the total neutron rate is given in Fig.4. It can be seen that a natural saturation of the ion temperature is predicted by the model as a consequence of the density increase. It can also be seen that the model somewhat underestimates the central ion temperature towards the end of the good performance phase, while the neutron rate is slightly overestimated. This seems to indicate a small inconsistency in the experimental data, which is confirmed by TRANSP analysis of this kind of pulse.

A number of code runs have been dedicated to the simulation of the roll-over phase by increasing the core fuelling from the SOL and Z_{eff} before the roll-over takes place. While some features of the roll-over, such as the saturation of the energy content, are correctly represented in these simulations, others are not. For

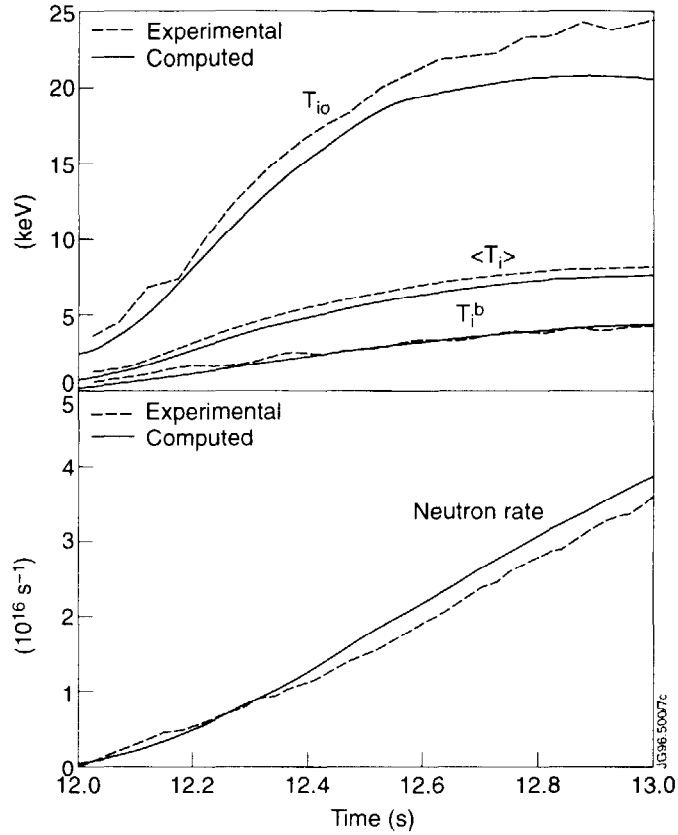

Fig.4 Experimental and computed time evolution of the ion temperature at the plasma centre and at the top of the transport barrier. The average ion temperature and the neutron rate are also shown.

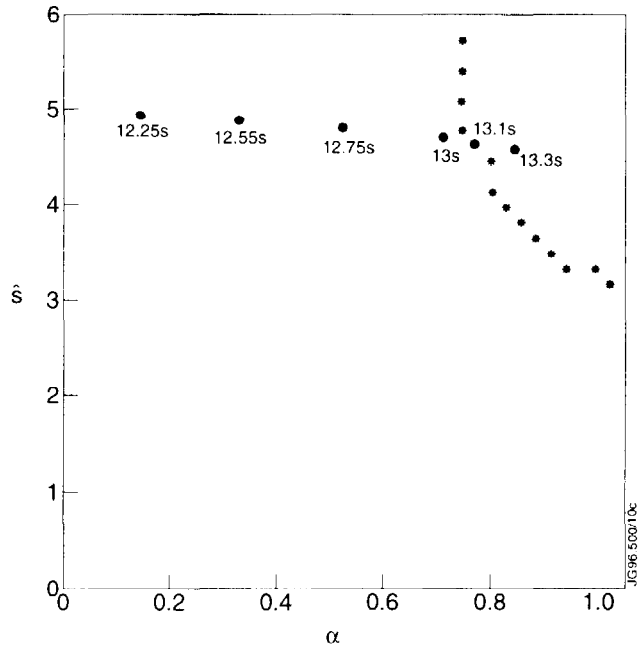

Fig.5 Trajectory of the discharge in the ballooning stability diagram of s (the normalised shear) versus α (the normalised pressure gradient).

example, the predicted decrease of the central ion temperature is generally underestimated while the increase in the ion saturation current is overestimated. Clearly more work is required for a complete modelling of the roll-over phase.

An interesting result is found by computing at the core plasma boundary the trajectory of the discharge in the ballooning stability diagram. This is done using the simulated plasma profiles in the IDBALL package [9] linked to the combined code. This trajectory approaches and hits the stability limit at approximately the time when first a roll-over, that practically does not modify the neoclassical transport barrier ($t \approx 13.1$), and then a giant ELM that strongly reduces it ($t \approx 13.3$), take place (Fig.5).

5. CONCLUSION

The combined code for core and edge transport studies developed at JET, together with the availability of measurements in the two regions is a powerful tool to simulate tokamak discharges in a time dependent way.

By eliminating ad hoc (and sometimes convenient) assumptions at the interface between core and boundary region this code provides a very tough and complete test for transport models, including the effect on the SOL of transport assumptions in the core and vice versa. Results from the combined code can be used to improve modelling in the stand alone core and edge transport codes.

The transport model used in the code, although not fully predictive and essentially empirical, has proven to be useful to clarify some important aspects of the evolution of hot-ion H-modes. In particular it supports the hypothesis that type I giant ELMs might be caused by ballooning instability in the edge transport barrier region.

ACKNOWLEDGEMENTS

Particularly grateful acknowledgement is due to the following for their contribution in developing the code and the transport models, for discussion of the results, and for providing experimental information:

B.Balet, A.V.Chankin, A.Cherubini, G.Corrigan, M.Erba, M.Fichtmueller, H.Guo, L.Lauro-Taroni, G.K.McCormick, V.V.Parail, G.Radford, R.Simonini, J.Spence, E.Springmann.

REFERENCES

[1] CHERUBINI, A., et al., Plasma Phys. Control. Fus. **38** (1996) 1421-1425.
[2] KOTSCHENREUTHER M., et al., Phys. Plasmas **2** (1995) 2381.
[3] TARONI, A., et al., to appear in Controlled Fusion and Plasma Physics (Proc. 23rd Eur. Conf. Kiev, 1996).
[4] BOLEY, C.D., et al., Phys. Fluids **22** (1979) 1280.
[5] ERBA, M., et al., to appear in Plasma Phys. Control. Fus.
[6] LAURO-TARONI, L., et al., in Controlled Fusion and Plasma Physics (Proc. 17th Eur. Conf. Amsterdam, 1990), Vol. 14B, Part I, European Physical Society, Geneva (1990) 247.
[7] THE JET TEAM (presented by P. J. Lomas), IAEA-CN-64/A1-5, this Conference.
[8] THE JET TEAM (presented by G. C. Vlases), IAEA-CN-64/A4-1, this Conference.
[9] HENDER, T., private communication.

OPTIMISATION OF JET PLASMAS WITH CURRENT PROFILE CONTROL

The JET Team[1]
(Presented by C Gormezano)

JET Joint Undertaking,
Abingdon, Oxfordshire,
United Kingdom.

Abstract

Internal transport barriers extending up to r/a = 0.55 have been achieved on JET by tailoring the plasma current profile by proper current ramps up to 3MA, with or without heating. The best performing discharges are produced when a long L-mode phase with high core confinement can develop before the onset of an H-mode. High central ion temperatures (32keV) and electron temperatures (15keV) are simultaneously produced resulting in neutron rates comparable to the best Hot Ion H-mode in JET with a time duration (0.5s) in excess of the energy confinement time.

1. INTRODUCTION

Operating a tokamak with higher confinement than predicted by the usual confinement scaling laws [1] has several advantages. One of them is to increase the fusion yield for a given input power allowing access in JET to regimes in DT operation where the alpha power can play a significant role. Another advantage is to operate a fusion reactor at lower plasma current. This opens the possibility of steady state operation, especially at high poloidal beta, high bootstrap current, by reducing the demand on non-inductive current drive. These so-called advanced tokamak scenarios require the demonstration of improved confinement not only transiently but for long duration.

Current profile control has proved to be an important technique to optimise confinement of tokamak plasmas. For example, in JET, current profile modification has produced high confinement with a reversed shear magnetic configuration in the pellet enhanced H-mode (PEP + H-mode) [2] and also in high β_p, high bootstrap current plasmas [3]. Ion minority current drive has been used to stabilise or destabilise sawteeth by local modifications of the current profile [4]. Lower Hybrid Current Drive (LHCD) has been used to modify the current profile before the formation of a Hot Ion H-mode [5], to raise the safety factor on axis q(o) above unity and provide sawtooth suppression during the high power heating phase resulting in an increase of the overall neutron rate. This technique has also allowed the addition of Ion Cyclotron Resonance Heating (ICRH) and Neutral Beam Injection (NBI) at high power levels in the Hot Ion H-mode which, in the absence of sawteeth, benefits from increased power deposition in the plasma core and a 30% increase in confinement [6].

Large efforts have been made to develop discharges with reversed shear either by using LHCD (Tore Supra) [7] achieving high confinement quasi steady-state discharges or by making use of heating in the current ramp phase to freeze

[1] See Appendix to IAEA-CN-64/O1-4. The JET Team (presented by J Jacquinot), with the collaboration of the DIII-D Team.

the current profile to achieve an optimised q profile resulting in good central confinement [8-10].

In current ramp experiments in JET in the 1994/95 campaign, a few MW of LHCD power was applied during a fast current ramp (1MA/s). A substantial increase of the electron temperature (up to 10keV) was observed during the initial phase of the reversed shear. Transport analysis has shown that the electron thermal diffusivity during this phase was reduced by one order of magnitude to values close to the level of the neo-classical thermal conductivity. This phase of enhanced confinement was not maintained when heavy gas puffing was used to raise the density in order to allow NBI with low shine-through. A broad density profile resulted and an ELMy H-mode was produced with 12MW of NBI power.

New hardware has allowed operation of the JET NBI system at lower density. With proper current ramp and power waveforms, large Internal Transport Barriers (ITB) have been obtained with a combination of NBI and of ICRF resulting in high performance plasmas.

2. INTERNAL TRANSPORT BARRIER

In JET, the ITB is established when the main power waveform is applied during the current ramp phase of the plasma, with or without a preheating phase. The main evidence of an internal barrier can be seen from the evolution of the ion temperature profile as shown in Figs.1 and 2 for two different timings of the power application. With early power application (Fig.1), a barrier is formed very close to the plasma core, about 1.2 s after the start of the heating. This barrier then moves outwards to r/a = 0.45. The discharge remains in an L-mode during the whole development of the ITB and is generally terminated by a disruption, following high frequency core MHD.

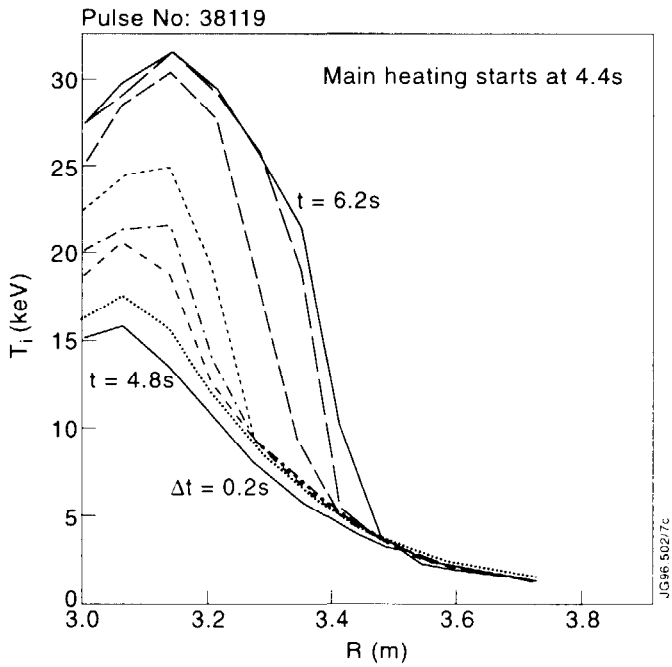

Fig.1 Evolution of ion temperature profile from charge exchange recombination (B_t = 3.4T; 2.5 < I_p < 3MA) with early power waveform and 1MW (ICRH) of preheating.

ITBs have also been established when power is applied later in time and with no preheating as shown in Fig.2. The barrier is established almost immediately with a slow expansion up to r/a ~ 0.55. In this case, the L-mode

phase is followed by an H-mode with central pressure up to 2.5 bar. It can be noted that a pedestal is formed at the plasma periphery and the whole ion temperature profile is raised by about 2 keV. These profiles are quite different from profiles of equivalent Hot Ion H-modes with similar power and neutron yield which shows significantly lower central temperature and much higher edge temperature. Similar transport barriers can be seen on the electron temperature profiles and to a lesser extent on the density profiles.

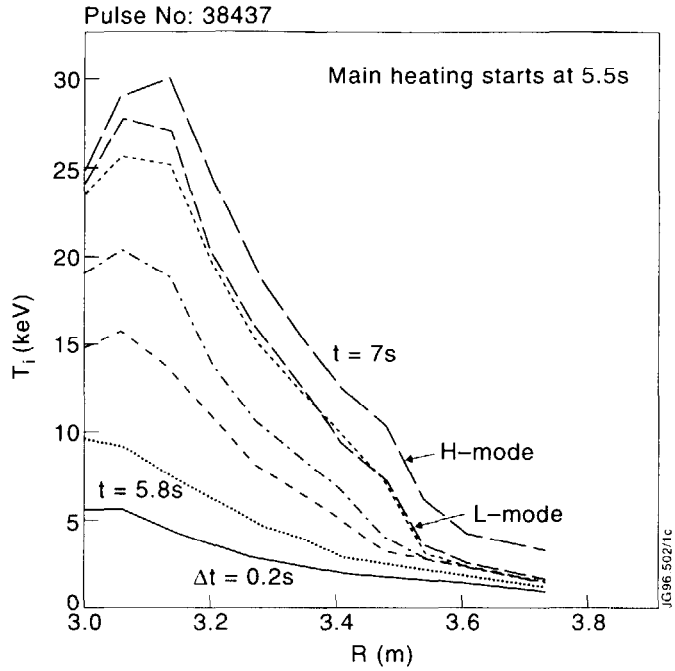

Fig.2 Evolution of ion temperature profile from charge exchange recombination (B_t = 3.4T; 2.5<I_p < 3MA) with late power waveform and no preheat.

ITBs are very sensitive to the timing of the high power waveform as illustrated in Fig.3. The ramp rate of the discharge to 2.5MA is adjusted to the highest rate compatible with the absence of MHD activity during the ramp. The second ramp in current is used to delay the onset of the H-mode. If H-modes appear too early, the L-mode peaked pressure profile is not yet fully established and NBI penetration is compromised by the formation of the edge pedestal. In addition, the strike points of the last closed surface are maintained close to the divertor pump entrance to prevent the edge density from forming quickly. This also delays the onset of the H-mode. The present configuration has low triangularity due to the mode of operation used for this campaign. As shown in Fig.4, early heating results in a late core transition. Late heating leads to an early H-mode which prevents the establishment of an ITB. The best performance (without disruption) has been obtained when the power is applied 5.5 s after the beginning of the discharge. Note that discharges with an ELMy H-mode obtained with late heating still have peaked density profiles because q(o) remains above unity and sawteeth are absent. The neutron yield is about 2 times higher than corresponding sawteething discharges with similar power. An optimisation of this mode of operation for high performance steady operation is still outstanding.

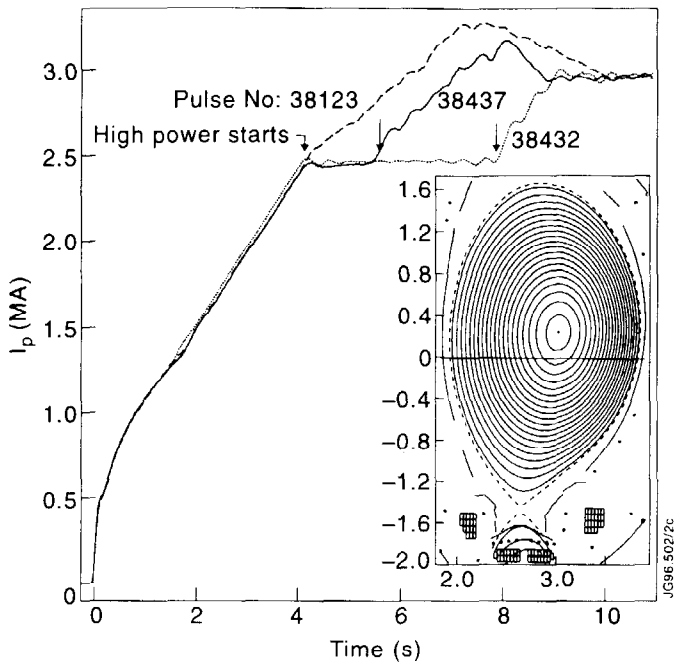

Fig.3 Typical current waveforms and flux contours for ITB. In the absence of heating, sawteeth appear at about t = 9 s.

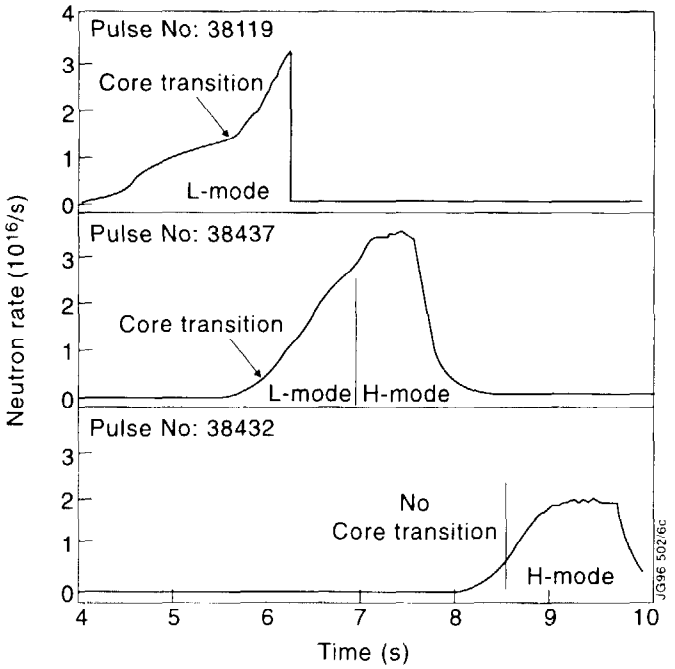

Fig.4 Time evolution of the neutron yield for different timing of the power waveform with a total power of 25MW. No ITB is observed when power is injected after 6 s from the start of the discharge.

3. HIGH PERFORMANCE DISCHARGES WITH SHEAR OPTIMISATION

An example of a high performance discharge where the L-mode phase is followed by an H-mode is shown in Fig.5. The H_{89} factor reaches 2 during the L-mode phase and 2.5 during the H-mode phase. These discharges have about 30% less stored energy than a comparable Hot Ion H-mode but a similar neutron yield because of the peaked profiles. There is no evidence of impurity accumulation on this time scale, Z_{eff} remaining constant at about 1.7. It is to be noted that in the case shown in Fig.5 the neutron yield remains about constant during the ELMs for as long as the power was applied, i.e. for times longer than the energy confinement time (0.4 s). However, in similar pulses a giant ELM often leads to a degradation of performance. The largest neutron yield which has been achieved in such discharges equals the highest yield in the Hot Ion H-mode achieved on JET in the present campaign.

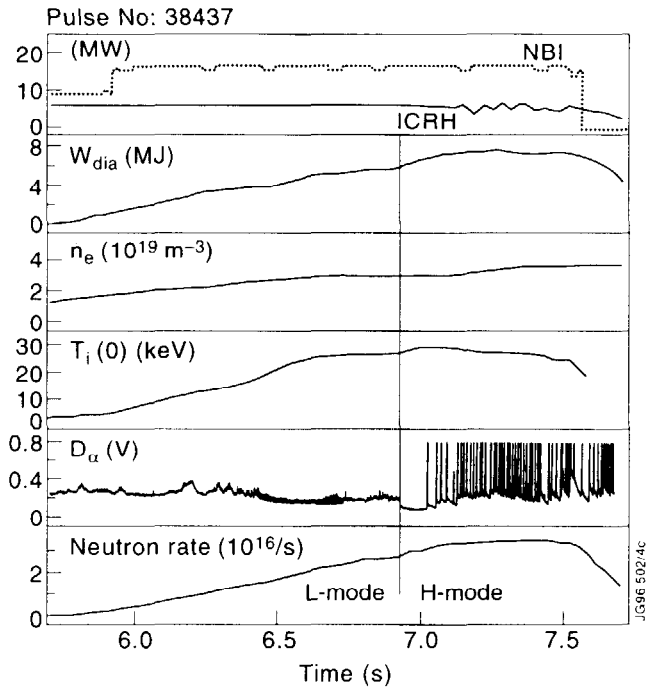

Fig.5 Time history of a high fusion yield pulse with shear optimisation (B_t = 3.4T; 2.5 < I_p 3MA). ICRH frequency (51MHz) corresponds to a resonance (H minority or 2nd harmonic D) close to the centre.

Several experimental observations (such as: no significant flux of gamma radiation, an increase of only 2 to 3 keV in electron temperature when comparing NBI only and combined heating shear optimised discharges), together with numerical simulations indicate that a substantial part of the Ion Cyclotron wave is coupled to fast deuterons at energies lower than a few hundred keV leading to ion heating, especially at high electron temperature.

In the absence of a proper simulation of the damping and heating of the Ion Cyclotron wave in such plasmas, a TRANSP simulation has been made for a discharge with shear optimisation where the ICRH power was off for 1 s. As shown in Fig.6, good agreement between experimental values and simulation is obtained with a significant thermal yield reaching more than 50% of the total yield. The current profile in JET can only be measured through a combination of polarimetry and magnetic measurements to reconstruct the equilibrium (EFIT).

Unfortunately, only one polarimeter channel can reasonably be used. Consistency checks have been made between the equilibrium reconstruction and the calculated current profile in TRANSP. It is not yet possible to have a reliable q profile, but it appears that a strong reversed shear is not necessary to trigger an ITB, in agreement with observations on DIII-D. The location of the barrier at the onset of the H-mode appears to be in the vicinity of a q=2 surface.

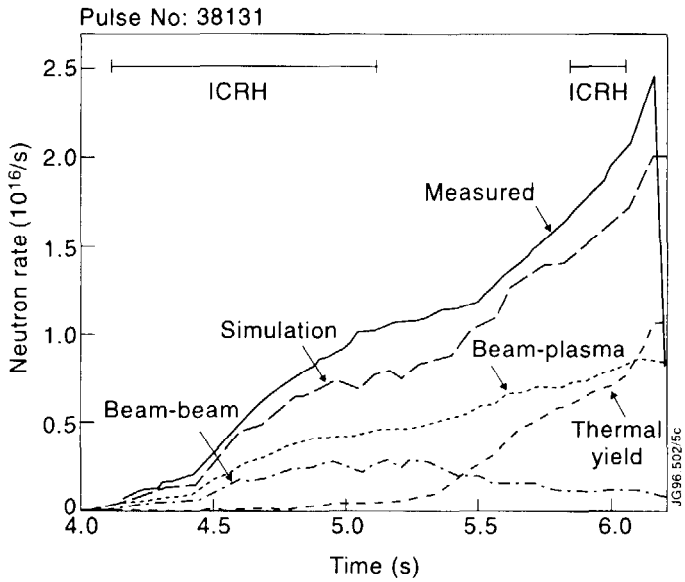

Fig.6 TRANSP simulation of pulse 38131. NBI (14MW) is on from 4 s ICRH (7MW) is off for 1 s.

4. POWER DEPENDENCE AND LIMITATIONS

A minimum power is required to obtain ITB in JET, as shown in Fig.7 where the data base of neutron rate versus total injected power is given for all discharges where a sustained core transition has been achieved. A substantial part of the data scattering is due to the large range of power, density and configuration waveforms investigated for shear optimisation, in particular neutron rate is very sensitive to target density. The low range of power corresponds to power step-down experiments, similar to Fig.6, where 6 to 8MW of ICRH power was switched off after about 1s when an ITB was already established. The dependence of this minimum power versus various parameters such as magnetic field and plasma current has not been done yet. The performance during the L-mode phase was often limited by low frequency, n =1 modes hardly rotating, sometimes locked, located near the q = 2 surface. These modes are very different from the modes appearing during pulses with early heating with an n = 1 structure rotating at very high frequency and leading to a disruption. The low frequency modes shown in Fig.8 are not disruptive, but limit the increase of neutron yield especially when these modes are locked. Their amplitude is variable which contributes to the scatter in the data and their dependence on plasma parameters is under investigation.

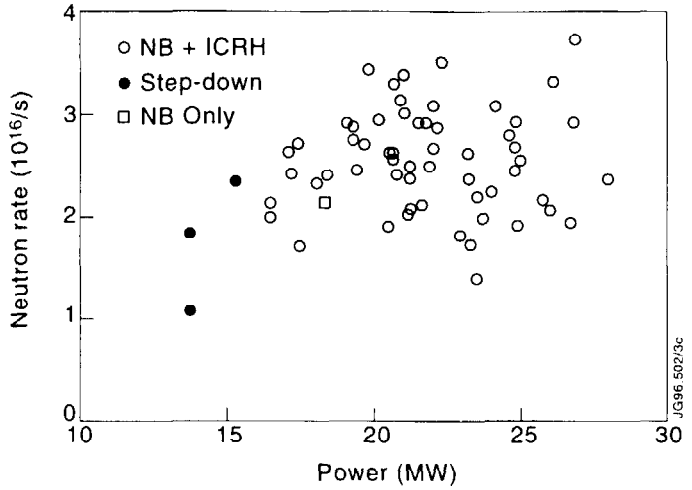

Fig.7 Neutron rate versus power for discharges with sustained core transitions .

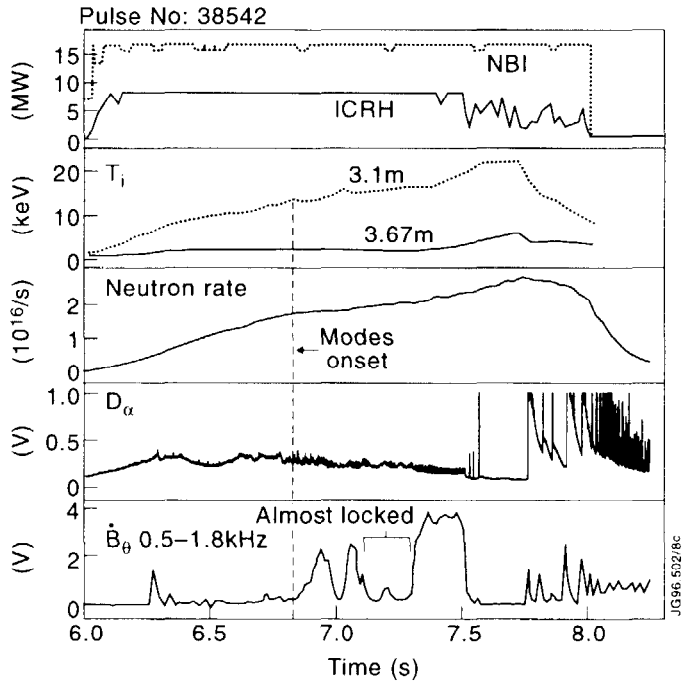

Fig.8 Time history of a discharge where low frequency MHD limits L-mode performance.

5. SUMMARY AND CONCLUSIONS

Internal Transport Barriers have been obtained on JET in low triangularity discharges with shear optimisation. The best performing discharges have a long L-mode phase followed by an H-mode phase which is deliberately delayed by a second current ramp. Up to 28MW of combined power has been used for discharges with I_p from 2.5 to 3MA and B_t = 3.4T with low target density. Internal barriers with r/a = 0.55 have been achieved, resulting in:

- high confinement L-modes (H_{89} = 2)
- simultaneous high T_i (32keV) and T_e (15keV)

- an ITB is only formed above a power level of about 17MW in these conditions
- high neutron yield (3.9 10^{16}/s) comparable to the best Hot Ion H-modes for times longer than an energy confinement time
- no apparent accumulation of impurities
- a high ratio of neutron yield to stored energy.

It should be noted that these are still early experiments. More development, including optimisation of pre-heat techniques, use of non-inductive current drive (LHCD and phased ICRH), use of higher triangularity, together with further optimisation of the ELMy H-mode phase, might lead to higher performance and/or extended duration. Extending the duration of the high performance phase is of obvious importance for reactor application.

6. REFERENCES AND ACKNOWLEDGEMENTS

[1] THE JET TEAM (presented by J.G. Cordey), IAEA-CN-64/AP1-2 this conference.
[2] TUBBING, B., et al., Nucl. Fusion, **31** (1991) 839.
[3] CHALLIS, C., et al., Nucl. Fusion, **33** (1993) 1097.
[4] BHATNAGAR, V.P., et al., Nucl. Fusion, **34** (1994) 1579.
[5] EKEDAHL, A., et al., to appear in Controlled Fusion and Plasma Physics (Proc. 23rd Eur. Conf. Kiev, 1996).
[6] COTTRELL, G., et al., ibid.
[7] LITAUDON, X., et al., ibid.
[8] JET TEAM (presented by C. Gormezano), in Plasma Physics and Controlled Nuclear Fusion Research (1994) (Proc. 15th Int. Conf. Seville, 1994) Vol. 1, IAEA, Vienna (1996) 633.
[9] LEVINGTON, F.M., et al., Phys. Rev. Letters (1995) 417.
[10] STRAIT, E.J., et al., Phys. Rev. Letters (1995) 4421.

Specific contributions from C Greenfield, E Lazarus, T Luce, B Rice, E Strait (GA), M Zarnstorff, G Schmidt (PPPL) and from B Lloyd, C Warwick, and C Hunt are gratefully acknowledged.